JAERI 1308

JAERI 1308

A Computer Code 'BEAM' for the Ion Optics Calculation of the JAERI Tandem Accelerator System

November 1987

日 本 原 子 力 研 究 所

Japan Atomic Energy Research Institute

JAERIレポートは，日本原子力研究所が研究成果編集委員会の審査を経て不定期に公刊している研究報告書です。

入手の問合わせは，日本原子力研究所技術情報部情報資料課（〒319-11茨城県那珂郡東海村）あて，お申しこしください。なお，このほかに財団法人原子力弘済会資料センター（〒319-11 茨城県那珂郡東海村日本原子力研究所内）で複写による実費頒布をおこなっております。

JAERI reports are reviewed by the Board of Editors and issued irregularly.

Inquiries about availability of the reports should be addressed to Information Division Department of Technical Information, Japan Atomic Energy Research Institute, Tokai-mura, Naka-gun, Ibaraki-ken 319-11, Japan.

編集兼発行　日本原子力研究所
印　　刷　いばらき印刷㈱

A Computer Code 'BEAM' for the Ion Optics Calculation of the JAERI Tandem Accelerator System

Shiroh KIKUCHI and Suehiro TAKEUCHI

Department of Physics
Tokai Research Establishment
Japan Atomic Energy Research Institute
Tokai-mura, Naka-gun, Ibaraki-ken

(Received August 29, 1987)

Abstract

The computer code BEAM is described, together with an outline of the formalism used for the ion optics calculation. The purpose of the code is to obtain the optimum parameters of devices, with which the ion beam is transported through the system without losses. The procedures of the calculation, especially those of searching for the parameters of quadrupole lenses, are discussed in detail. The flow of the code is illustrated as a whole and its constituent subroutines are explained individually. A few resultant beam trajectories and the parameters used to obtain them are shown as examples.

Keywords: Computer Code, Ion Optics Calculation, Tandem Accelerator, Beam Trajectory, Quadrupole Lens Parameter, Parameter Search Procedure

原研タンデム加速器のためのイオン光学計算コード'BEAM'

日本原子力研究所東海研究所物理部

菊池　士郎・竹内　末広

1987年7月29日受理

要　　旨

タンデム加速器の運転にさいして，イオン源からひき出されたイオン・ビームを，標的のおかれた所定の位置まで無駄なく運ぶためには，ビーム輸送管に装着された数多くの光学機器のパラメーターをどのようにえらべばよいかを計算するコードである．最初に，イオン光学の計算の方法についてのべたのち，特に問題となる四重極レンズのパラメーター・サーチについて詳述した．コード全体を見渡してから，ひとつひとつのサブルーチンについて説明し，最後にいくつかの計算例を示してある．

Contents

目　　次

List of Tables

List of Figures

表 説 明

図 説 明

第 1 図　本レポートで使われる座標系。

第 2 図　扇形偏向電磁石。

第 3 図　ビーム軸と直交しない出入口面を持つ偏向電磁石。

第 4 図　単一開口レンズ。(a)レンズ附近の電場　(b)レンズの収束性。

第 5 図　二重開口レンズの概念図。

第 6 図　電場内におけるビーム軸方向のポテンシャルの近似曲線。真のポテンシャル曲線が破線で近似されている。

第 7 図　二重開口レンズ内のイオンの収束軌道。

第 8 図　位相空間楕円。参考文献 1 より。

第 9 図　ストリッパーによるイオンの散乱に関する(a)座標系と(b)変数。変位 r は x または z を意味する。参考文献 17 より。

第 10 図　長さ L のストリッパー通過後のビームの位相空間楕円。入射ビームには，ゼロ・エミッタンスが仮定されている。参考文献 17 より。

第 11 図　Q－レンズによるビームの収束。Q－レンズとウェイストの間に他の装置が(a)ない場合と(b)ある場合。

第 12 図　パラメーター k_1 によるウェイストの変化。もう 1 つのパラメーター k_2 は固定されている。$W=W_0$ における直線は，W_0 にウェイストを作ることを示す。この直線とウェイスト曲線の交点にある数字は，IWX_SELECT と IWZ_SELECT のためのもの。(本文参照)。

第 13 図　パラメーター k_1-k_2 対の表示。$x-s$ および $z-s$ で示された曲線の交点から得られる k_1-k_2 対が，両面で同じ場所にウェイストを作る。

第 14 図　ウェイスト近辺でのビームの形。k_1-k_2 対のえらび方で，4 種類の形がとられる。

第 15 図　パラメーター・サーチの場合の k_1 と k_2 の動き方。

第 16 図　原研タンデム加速器システム。ビーム軸に沿って装着されているイオン光学装置は，便宜上下記のような文字を頭につけて分類されている。

BM －：偏向電磁石
DS －：二重スリット
EQ －：電気 Q－レンズ
MQ －：磁気 Q－レンズ
ST －：ストリッパー
VA －：アパーチャー

第 17 図　計算の流れのアウトライン。太線枠はターミナル・キーボードからの入力を示し，二重枠はディスク内のファイルからのデータの読み込みを示す。

第 18 図　サブルーチン CHARGE_EXCHANGE の計算の流れ。ストリッパーによるイオンの荷電変換後の荷電分布の計算，および計算のモードにしたがって加速器の端子電圧あるいはイオンの最終エネルギーの計算を行う。太線枠はターミナル・キーボードからの入力

パーチャー・システム。ここでは便宜上，ウェイストも「装置」として処理する。二重枠はディスクのファイルからのデータの読み込みを示す。これらの流れは，すべて第17図の9°に挿入されるものである。

第35図　このCodeによる計算の最終段階の流れ。太線枠はターミナル・キーボードからの入力を示す。この流れは第17図の10°に挿入されるものである。

第36図　ターミナル・キーボードからのデータの入力例。アンダーラインの引かれた文字および数字が入力データである。この例は，最終エネルギー40 MeVの^{10}Bイオンを得るための入力である。

第37図　第36図の入力例によって得られた，ビーム軌道。

第38図　最終エネルギー120 MeVの^{127}Iイオンのビーム軌道。

第39図　タンデム加速器の端子電圧と個々のQ－レンズのパラメーターを入力データとして与える場合の入力例。

1. Introduction

An accelerator system is equipped with a number of optical devices, such as deflection magnets and electrostatic or magnetic quadrupole lenses, in order to transport ions without losses from an ion source to a target. Ion optics calculation can be utilized to obtain the optimum parameters of those equipments for such an operation. Because of some assumptions, on which the calculation is based, the results are not always fitted strictly to the actual operating conditions. However, it gives approximate values helpful and sufficient to operate the system with slight adjustments by the operators.

The computer code BEAM has been developed for the ion optics calculation of the JAERI tandem accelerator system. One of the aims of the code is to examine the optimum parameters of the optical devices, especially those for the quadrupole lenses, for the suitable transport of ions at the accelerator operation time. The other is to observe the aspect of the ion beam trajectories on a picture display system, through which their realistic appearances are recognized more distinctly.

This report describes the code BEAM and its associated problems somewhat in detail. Sections 2 and 3 summarize the basic preliminaries for the ion optics calculation, section 4 presents their extention to the acceleration tube, and section 5 outlines the beam envelope optics. In section 6 the effects of the charge exchange processes are shown, and in section 7 the parameter search procedures are discussed. Section 8 explains the constitution of the code and illustrates the individual subroutines included, and the examples of calculation are also shown. Finally, the report is concluded in section 9.

2. Basic preliminaries

2.1 Basic assumptions

In the present calculation, the following assumptions are made.

(1) The ions move close to the beam axis, namely, the ion beam is paraxial. Therefore, the higher order terms of the field expansion can be neglected.

(2) The ion velocities are assumed to be low enough, so that the relativistic corrections can be neglected.

(3) The space charge effect can be neglected.

Practically, the assumption (2) is concerned with the calculation for the acceleration tubes. To make more extensive calculation, the relativistic ray equation should be solved. Since the space charge effect cannot be ignored where the current density is high and/or the ions are moving with considerably low velocities, the assumption (3) is not applicable to the situation in the region of ion sources. Thus, such a region should be avoided in the calculation by means of the present code.

2.2 Coordinate system

A coordinate system[1] of $\{z, x, s\}$, shown in **Fig. 1**, is used. The axes z and x are associated with the vertical and horizontal directions, respectively, at the starting point of the traveling of the ions. These axes move together with the ion, without rotating around the beam direction. The axis s is so chosen that it always coincides with the beam direction.

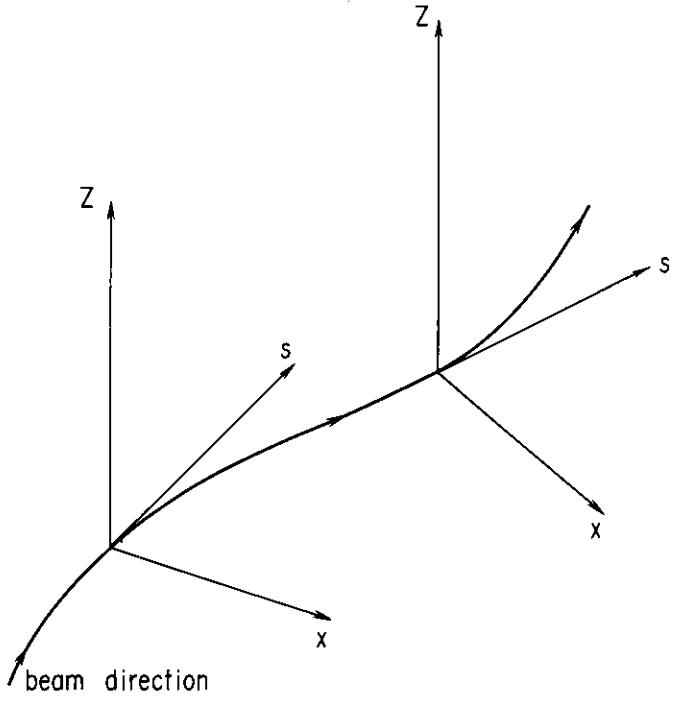

Fig. 1 The coordinate system used in the present formalism.

2.3 Matrix representation

The transformation of each ion passing through an optical device is represented by a transfer matrix, as

$$\begin{pmatrix} r_2 \\ p_2 \end{pmatrix} = \begin{pmatrix} a_p & b_p \\ c_p & d_p \end{pmatrix} \begin{pmatrix} r_1 \\ p_1 \end{pmatrix}, \tag{2.3.1}$$

where, r denotes the transverse position coordinate, x or z, of the ion, p is its canonical conjugate momentum, and the subscripts 1 and 2 refer to the entrance and exit of the device, respectively. The determinant of the transfer matrix is

$$D_p = a_p d_p - b_p c_p = 1, \tag{2.3.2}$$

since the system is a Hamiltonian system[2].

The transverse momentum p is expressed, in the paraxial ion optics, by using the axial momentum p_s and the slope r' of the ion trajectory to the beam axis as

$$p = p_s \cdot r' . \tag{2.3.3}$$

Substituting into Eq.(2.3.1),

$$\begin{pmatrix} r_2 \\ r_2' \end{pmatrix} = \begin{pmatrix} a & b \\ c & d \end{pmatrix} \begin{pmatrix} r_1 \\ r_1' \end{pmatrix}, \tag{2.3.4}$$

where

$$a = a_p,\ b = b_p \cdot p_{s1},\ c = c_p / p_{s2},\ d = d_p \cdot p_{s1} / p_{s2}. \tag{2.3.5}$$

The subscripts 1 and 2 are the same as for Eq.(2.3.1), and the determinant of the matrix is

$$D = ad - bc = \frac{p_{s1}}{p_{s2}}. \tag{2.3.6}$$

If the space on both sides of the device is at the same potential, p_s is constant in paraxial beam optics and the determinant D is unity.

In case that the system is composite of optical devices, the total transfer matrix between the entrance and the exit of the system is given as the product of the transfer matrices for the individual devices multiplied in the reverse order of application,

$$M_{total} = M_n \cdot M_{n-1} \cdots\cdots M_2 \cdot M_1 . \tag{2.3.7}$$

3. Transfer matrices

This section presents the transfer matrices[1),3),4)] for the fundamental optical devices. Usually, they are given in the from of Eq.(2.3.4) rather than of Eq.(2.3.1).

The matrix for the acceleration tube is described in the next section. In this case the ion energies at both sides of the device are different, and accordingly the determinant of the transfer matrix is not unity.

3.1 Matrix for a field free drift space

A field free region limited by two planes perpendicular to the beam axis is called a field free drift space. The matrix for the drift space is expressed by

$$M_{drift}=\begin{pmatrix}1 & \ell\\ 0 & 1\end{pmatrix}, \tag{3.1.1}$$

where ℓ is the drift length.

3.2 Matrix for a quadrupole lens

In both the electrostatic and the magnetic quadrupole lenses, the field in a single element is provided by four poles, and has a converging effect on the ions in one plane, for example $x-s$ plane, and a diverging effect in the other, $z-s$ plane. The transfer properties of a single quadrupole element are expressed in the matrix form

$$M_c=\begin{pmatrix}\cos kL & \frac{1}{k}\sin kL\\ -k\sin kL & \cos kL\end{pmatrix} \tag{3.2.1}$$

for the converging plane, and

$$M_d=\begin{pmatrix}\cosh kL & \frac{1}{k}\sinh kL\\ k\sinh kL & \cosh kL\end{pmatrix} \tag{3.2.2}$$

for the diverging plane. Here, L is the effective length of the quadrupole. The field parameter k is

$$k=\frac{2}{d}\left(\frac{n\cdot V}{E}\right)^{1/2} \quad \mathrm{cm}^{-1} \tag{3.2.3}$$

for the electrostatic lens, and

$$k=\frac{1}{d}\left(\frac{3.2\pi IN}{B\rho}\right)^{1/2} \quad \mathrm{cm}^{-1} \tag{3.2.4}$$

for the magnetic lens. Where d is the aperture diameter of the lens in cm, V is the potential on the poles in volts, n is the number of elementary charges carried by the ions, E is the energy of the ions in electron volts, $B\rho$ is the magnetic regidity of the ions in gauss·cm, and IN is the number of ampere-turns per pole.

A quadruple doublet is a set of two quadrupoles of opposite polarity separated by a

drift space. The total transfer matrix is given as

$$M_{cd}=M_d \cdot M_{drift} \cdot M_c \tag{3.2.5}$$

in one plane and

$$M_{dc}=M_c \cdot M_{drift} \cdot M_d \tag{3.2.6}$$

in the other.

A quadrupole triplet consists of three quadrupoles, the polarities of which are opposite by turns. Individual quadrupoles are separated by the drift spaces usually with equal lengths. The total matrix is

$$M_{cdc}=M_c \cdot M_{drift} \cdot M_d \cdot M_{drift} \cdot M_c \tag{3.2.7}$$

in one plane and

$$M_{dcd}=M_d \cdot M_{drift} \cdot M_c \cdot M_{drift} \cdot M_d \tag{3.2.8}$$

in the other.

3.3 Matrix for a thin lens

The idealized concept of a thin lens describes that the action of the localized field at the principal plane of the lens is represented by a discontinuous change of the direction of the trajectory, with no change in its position r. Its thickness is assumed to be infinitely thin and the transfer matrix is obtained as

$$M_{thin\ lens}=\begin{pmatrix} 1 & 0 \\ -\frac{1}{f} & 1 \end{pmatrix}, \tag{3.3.1}$$

f being the focal length.

3.4 Matrix for a bending magnet

Among various types of bending magnets, the simplest is the sector magnet with uniform field, which has straight entry and exit faces orthogonal to the incoming and outgoing trajectories, respectively. As is shown in **Fig. 2**, the central ray of an ion beam draws a circular trajectory of radius ρ through an angle φ in the magnet. The direction of the uniform magnetic field is perpendicular to the paper upward.

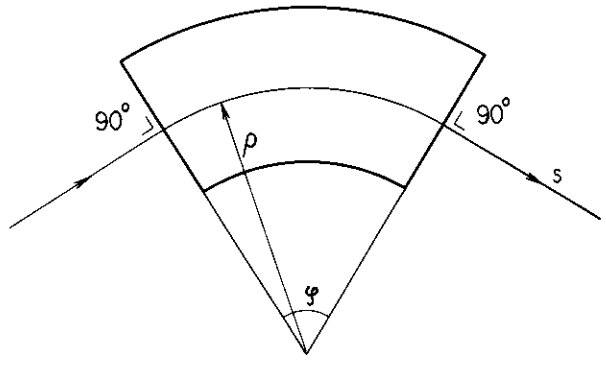

Fig. 2 Sector magnet.

The transfer properties are represented in matrix form as

$$M_{bending}=\begin{pmatrix} \cos\varphi & \rho\sin\varphi \\ -\frac{1}{\rho}\sin\varphi & \cos\varphi \end{pmatrix} \tag{3.4.1}$$

for the bending plane, and

$$M_{vertical}=\begin{pmatrix} 1 & \rho\varphi \\ 0 & 1 \end{pmatrix} \tag{3.4.2}$$

for the plane vartical to the bending plane.

For the bending plane, a dispersion term for momentum p should be taken into account. The dispersion vector is given as

$$\begin{pmatrix} D \\ D' \end{pmatrix}=-\begin{pmatrix} \rho(1-\cos\varphi) \\ \sin\varphi \end{pmatrix} \tag{3.4.3}$$

and the resultant transfer properties are given by the following two terms,

$$\begin{pmatrix} r_2 \\ r_2' \end{pmatrix}=M_{bending}\begin{pmatrix} r_1 \\ r_1' \end{pmatrix}+\frac{\Delta p_1}{p_1}\begin{pmatrix} D \\ D' \end{pmatrix} \tag{3.4.4}$$

The bending magnet of uniform field with arbitrary entry and exit angles of ε and γ is shown in **Fig. 3**. These angles are taken to be positive if the center of curvature and the trajectory outside the magnet lie on the same side of the normals to the magnet faces. Such a magnet can be regarded as a sector magnet with magnet wedges at both ends. The magnet wedges act as thin lenses, as described below[1),3)], so that the resultant transfer matrices are

$$\begin{aligned} M_{bending}&=\begin{pmatrix} 1 & 0 \\ \frac{\tan\gamma}{\rho} & 1 \end{pmatrix}\begin{pmatrix} \cos\varphi & \rho\sin\varphi \\ -\frac{1}{\rho}\sin\varphi & \cos\varphi \end{pmatrix}\begin{pmatrix} 1 & 0 \\ \frac{\tan\varepsilon}{\rho} & 1 \end{pmatrix} \\ &=\begin{pmatrix} \frac{\cos(\varphi-\varepsilon)}{\cos\varepsilon} & \rho\sin\varphi \\ -\frac{1}{\rho}\frac{\sin(\varphi-\varepsilon-\gamma)}{\cos\varepsilon\cdot\cos\gamma} & \frac{\cos(\varphi-\gamma)}{\cos\gamma} \end{pmatrix} \end{aligned} \tag{3.4.5}$$

and

$$\begin{aligned} M_{vertical}&=\begin{pmatrix} 1 & 0 \\ -\frac{\tan\gamma}{\rho} & 1 \end{pmatrix}\begin{pmatrix} 1 & \rho\varphi \\ 0 & 1 \end{pmatrix}\begin{pmatrix} 1 & 0 \\ -\frac{\tan\varepsilon}{\rho} & 1 \end{pmatrix} \\ &=\begin{pmatrix} 1-\varphi\tan\varepsilon & \rho\varphi \\ \frac{-\tan\varepsilon-\tan\gamma+\varphi\tan\varepsilon\cdot\tan\gamma}{\varphi} & 1-\varphi\tan\gamma \end{pmatrix}. \end{aligned} \tag{3.4.6}$$

The dispersion vector is modified to

$$-\begin{pmatrix} \rho(1-\cos\varphi) \\ \tan\gamma(1-\cos\varphi)+\sin\varphi \end{pmatrix} \tag{3.4.7}$$

and should be added to Eq.(3.4.5) in the same manner as Eq.(3.4.4). Since, however, $\Delta p/p$ is small enough to be neglected in the present tandem accelerator, this term is not included in the present calculation.

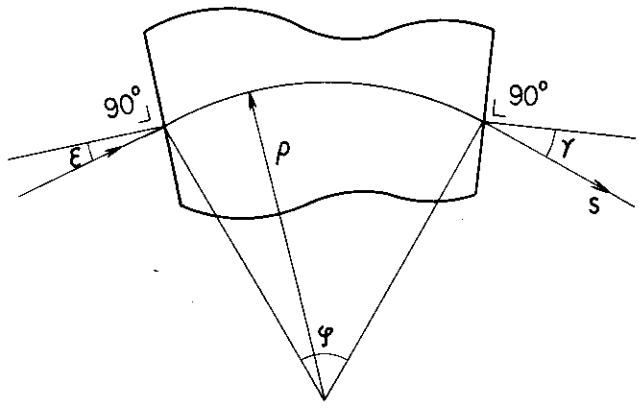

Fig. 3 Uniform field bending magnet with non-orthogonal entry and exit.

4. Acceleration tube

4.1 Double aperture lens

In principle, the acceleration tube can be regarded as a double aperture lens, which consists of two single aperture lenses separated by a certain distance. The single aperture lens is a single circular aperture in a plane electrode separating the space into two regions of different fields. The aspect of the field around the aperture, and its focusing properties for ions passing through it are shown in **Fig. 4**.

Fig. 5 depicts the double aperture lens. Two single aperture lenses are set with a distance of $d\ell$ and at potentials V_1 and V_2. The potentials outside both lenses are constant, and the space between them is that of the uniform field.

In general, trajectories of ions in an electrostatic field are given by solving the ray equation. Zworykin et al.[5] have simplified the ray equation to that for the non-relativistic and paraxial ray, and have expressed the field potential function in a power series of r and the axial potential $\varphi(s)$. Neglecting the terms of higher order than the first in r and r', the ray equation becomes

$$r''+\frac{\varphi'(s)}{2\varphi(s)}r'+\frac{\varphi''(s)}{4\varphi(s)}r=0. \tag{4.1.1}$$

This equation has been integrated[5] by replacing the continuous axial potential $\varphi(s)$ with a number of uniform field segments, Gan's method, as shown in **Fig. 6**. In the figure, the actual potential (solid line) is approximated by the straight line (broken line) in each segment. The integration has been performed separately over the uniform field segments and over the infinitesimal breaking point regions between the neighboring uniform field segments.

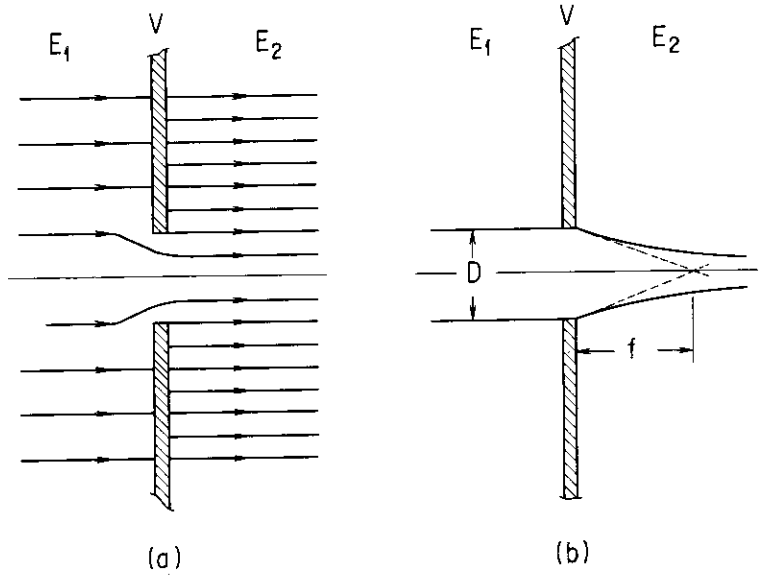

Fig. 4 Schematic views for the single apertures lens. (a) The lines of force around the lens, and (b) the focusing properties of the lens.

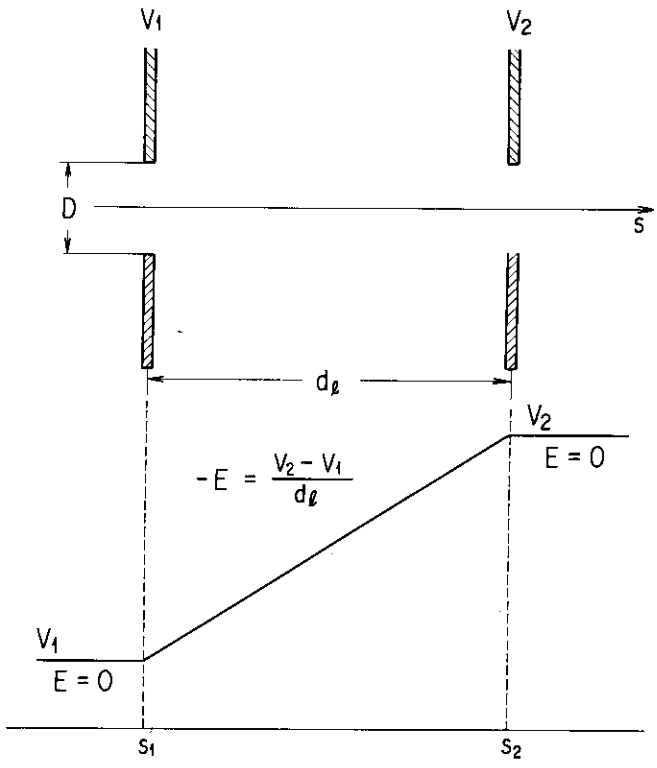

Fig. 5 Schematic diagram of double aperture lens.

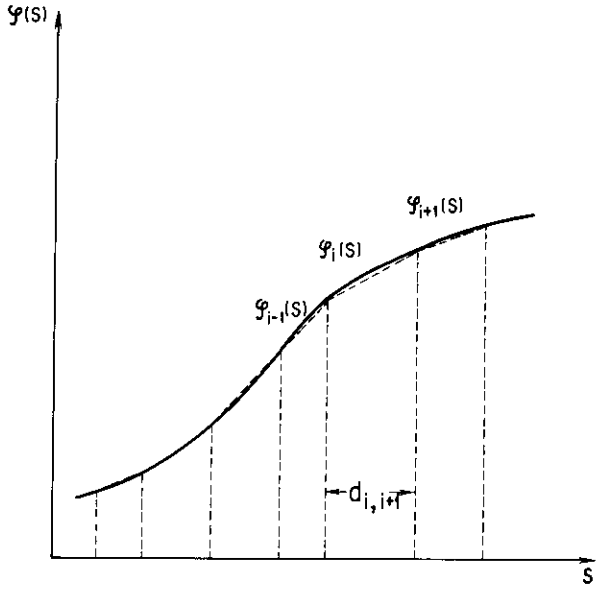

Fig. 6 Approximation of the axial potential curve in the electrostatic field. The actual potential is approximated by the straight broken lines.

The results of the integration have been utilized by Fert[6] and Timm[7] to the matrix notation of the double aperture lens. Timm[7] has expressed the matrix for the uniform field segment in the form of Eq.(2.3.4), as

$$M_{u.f.}=\begin{pmatrix} 1 & \dfrac{2d_{i,i+1}}{\sqrt{\varphi_i}+\sqrt{\varphi_{i+1}}}\sqrt{\varphi_i} \\ 0 & \dfrac{\sqrt{\varphi_i}}{\sqrt{\varphi_{i+1}}} \end{pmatrix}, \tag{4.1.2}$$

and that for the infinitesimal breaking point as

$$M_{b.p.}=\begin{pmatrix} 1 & 0 \\ \dfrac{(\varphi')_{i-1,i}-(\varphi')_{i,i+1}}{4\varphi_i} & 1 \end{pmatrix}. \tag{4.1.3}$$

Here, $\varphi'=d\varphi/ds$, d is the length of the field segment and the subscript '$i-1, i$' indicates the region between the i-1th and the ith breaking points. The matrix for the double aperture lens can be obtained, by making use of the matrices above, and regarding the effect of the breaking point region as same as that of the single aperture lens,

$$M_{double\ aperture}=M^{(2)}_{b.p.}\cdot M_{u.f.}\cdot M^{(1)}_{b.p.}, \tag{4.1.4}$$

where the superscript (1) and (2) indicate the respective breaking points at the entrance and the exit of the field segment. As seen in Eq.(4.1.3), $M_{b.p.}$ is equivalent to the matrix for the thin lens with the focal length of

$$f=-\frac{4\varphi_i}{(\varphi')_{i-1,i}-(\varphi')_{i,i+1}}, \tag{4.1.5}$$

which is consistent with that of the single aperture lens described later on (refer to section 4.2).

Since the ion energies before and after the double aperture lens are not equal, the determinant D of each matrix above obtained by Timm[7] is not unity. Fert[6], on the other hand, has expressed the transfer property in the form

$$\begin{pmatrix} r_2 \\ \sqrt{\varphi_2}\,r_2' \end{pmatrix}=\begin{pmatrix} a_f & b_f \\ c_f & d_f \end{pmatrix}\begin{pmatrix} r_1 \\ \sqrt{\varphi_1}\,r_1' \end{pmatrix}. \tag{4.1.6}$$

The matrix elements in Eq.(4.1.6) are related to those in the form of Eq.(2.3.4), on which Eqs.(4.1.2) and (4.1.3) are based, as

$$a_f=a,\ b_f=b/\sqrt{\varphi_1},\ c_f=c\cdot\sqrt{\varphi_2},\ d_f=d\cdot\sqrt{\varphi_2}/\sqrt{\varphi_1} \tag{4.1.7}$$

and its determinant is $a_fd_f-b_fc_f=1$.

Applying Eqs.(4.1.2) and (4.1.3) to the double aperture lens shown in **Fig. 5**, the resultant matrix is

$$\begin{aligned} M_{double\ aperture}&=\begin{pmatrix} 1 & 0 \\ \dfrac{V_2-V_1}{4d_\ell V_2} & 1 \end{pmatrix}\times\begin{pmatrix} 1 & \dfrac{2d_\ell\sqrt{V_1}}{\sqrt{V_1}+\sqrt{V_2}} \\ 0 & \dfrac{\sqrt{V_1}}{\sqrt{V_2}} \end{pmatrix}\times\begin{pmatrix} 1 & 0 \\ -\dfrac{V_2-V_1}{4d_\ell V_1} & 1 \end{pmatrix} \\ &=\begin{pmatrix} -\dfrac{\sqrt{V_2}-3\sqrt{V_1}}{2\sqrt{V_1}} & \dfrac{2d_\ell\sqrt{V_1}}{\sqrt{V_1}+\sqrt{V_2}} \\ -\dfrac{3}{8d_\ell}\cdot\dfrac{V_2-V_1}{V_2}\cdot\dfrac{\sqrt{V_2}-\sqrt{V_1}}{\sqrt{V_1}} & \dfrac{3\sqrt{V_2}-\sqrt{V_1}}{2\sqrt{V_2}}\cdot\dfrac{\sqrt{V_1}}{\sqrt{V_2}} \end{pmatrix}, \end{aligned} \tag{4.1.8}$$

replacing φ_i with V_i.

4.2 Focusing property of double aperture lens

The trajectory of an ion in the double aperture lens is typically shown in **Fig. 7**, where the ion moves from left to right. Between the apertures, the trajectory shows a parabola represented by

$$r=r_0+\frac{2}{k}\cdot\frac{v_{0r}}{v_{0s}}\left[\sqrt{1+k\cdot s}-1\right]. \tag{4.2.1}$$

Here, r_0, v_{0r} and v_{0s} are the transverse distance, the transverse and the axial velocity components of the ion, respectively, just behind the entrance aperture. The velocity components are positive when their respective directions coincide with the r and s axes shown in **Fig. 7**. The quantity k is

$$k=-\frac{E}{V_1-V_0}=\frac{1}{d}\cdot\frac{V_2-V_1}{V_1-V_0}, \tag{4.2.2}$$

V_0 being the potential where the ion has zero kinetic energy, so that k is positive for both cases of the negative and positive ions. The ion beam accelerated in the double aperture lens, therefore, is focussed, if the velocity component ratio v_{0r}/v_{0s} of each ion is negative.

As the criterion of the focusing strength of the double aperture lens, the focal length of the entrance single aperture lens is important quantity. It is defined, as shown in **Fig. 4(b)**, being associated with the incident beam parallel to the beam axis, namely, being analogous to that in the geometrical optics. In such a case, the velocity component ratio of each ion is obtained[5),8)] as

$$\frac{v_{0r}}{v_{0s}}=\frac{r_0(E_1-E_2)}{4|V_1-V_0|}\cdot\frac{q}{|q|}, \tag{4.2.3}$$

where, $|q|$ is the number of charges of the ions, E_1 and E_2 are the field strength before and after the aperture, respectively. Eq.(4.2.3) shows that v_{0r}/v_{0s} is negative irrespective of the charge states of ions, because $E_1=0$ and $E_2<0$ for the negative ions, while $E_1=0$ and $E_2>0$ for the positive ions. Hence, the beam is always focussed after the entrance aperture, and the focal length has been given[5),8),9)] approximately in the electron optics, by utilizing Eq.(4.2.3), as

$$f=\frac{4V}{E_1-E_2}, \tag{4.2.4}$$

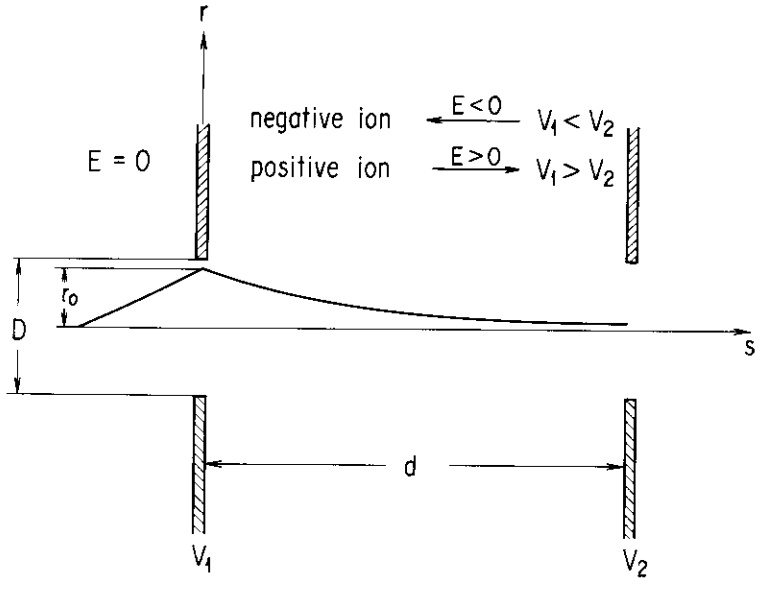

Fig. 7 The focusing trajectory of an ion in the double aperture lens.

if $E \lesssim V/D$. Here, E denotes the fields on either side of the aperture, D is the aperture diameter and V is the aperture potential relative to V_0. The fields E_1 and E_2 are the same as those in Eq. (4.2.3).

Eq.(4.2.4) holds also for positive ions. It should be noted, however, that the potential V is negative for positive ions, while positive for negative ions, because V originates from the relation

$$\frac{1}{2}mv^2 = e|V| = e|V_1 - V_0|, \tag{4.2.5}$$

where, m and v are the mass and the velocity of the ions at the aperture, respectively, V_1 is the potential at the aperture and V_0 is the same as in Eq.(4.2.2).

Since the shorter focal length indicates the stronger focusing strength, Eq.(4.2.4) shows that the larger field difference produces the stronger focusing effects on ions. This fact is applied to the acceleration tube system of the electrostatic accelerator, in case of low energy acceleration. The unfavorable focusing condition, due to the small field difference at the entrance of the tube system, is improved by short-circuiting some tubes to equi-potential, which causes the field difference to increase without changing the terminal potential.

4.3 Acceleration tube for the tandem accelerator

The acceleration tube of the tandem accelerator can be regarded as a series of double aperture lenses connected by the field free drift spaces. It has two parts for ion acceleration, those for the low energy (L.E.) and the high energy (H.E.) acceleration, preceeding and following the stripper, respectively. In the former part, the ions of the negative state of $q=-1$ are accelerated and the focal length of the aperture of the acceleration unit is given by Eq.(4.2.4) with

$$V = V_1 - V_0, \tag{4.3.1}$$

where V_0 and V_1 are the same as those for Eq.(4.2.5).

In the latter part, on the contrary, the ions of the positive charge state of $+q$ are accelerated. Furthermore, if the ions extracted from the ion source are of the form of the compound, and are broken up into the individual elements at the stripper, the masses of the ions in the H.E. acceleration part are different from those in L.E. acceleration part. Thus, the focal length in the H.E. acceleration part is given by Eq.(4.2.4), but V should be represented as

$$V = -\left\{(V_T - V_1) + \frac{1}{q}\left[(V_T - V_0)\frac{m'}{m} - \Delta E_{st}\right]\right\}, \tag{4.3.2}$$

where m and m' are the respective masses of the ions before and after the stripper, V_T is the terminal potential in MV and ΔE_{st} is the energy loss in the stripper in MeV.

The ion optics of the acceleration tubes has been studied by Elkind[6]. He has extended the first order focusing theory and has analyzed the focusing and defocusing properties at the transition region between the uniform field and the field free drift space. This transition region is a smoothly varying fringing field which depends on the tube diameter, and has a weaker effect on the focusing strength than that estimated from the abrupt breaking point. Because the kinetic energies of the ions at the entrance unit is relatively low, it is considered to be important that its focal length should be described accurately. Elkind[6] has modified Eq.(4.2.4) as

$$f^* = f\zeta = \frac{4\zeta V}{E_1 - E_2}, \tag{4.3.3}$$

where ζ is a function of $V/(E_1-E_2)$ and the aperture diameter D, and $\zeta \geqq 1$.

In the present calculation, the parameter ζ represented by[11]

$$\zeta = a + b \cdot \frac{D}{f^*} \tag{4.3.4}$$

with $a = 1.0$, $b = 0.57$ is adopted. The diameter D is in the same unit as that for f. From Eq. (4.3.4) the modified focal length f^* is given as

$$f^* = \frac{2V\{1+\sqrt{1+0.57D\cdot(E_1-E_2)/V}\}}{E_1-E_2} \tag{4.3.5}$$

with the respective values of $V's$ given by Eqs.(4.3.1) and (4.3.2) for L.E. and H.E. acceleration parts.

4.4 Transfer matrix for acceleration tube

The transfer matrix for the acceleration tube is represented as

$$M_{acc\ tube} = M_{drift}^{(n+1)} \cdot M_{acc\ unit}^{(n)} \cdot M_{drift}^{(n)} \cdots\cdots M_{drift}^{(2)} \cdot M_{acc\ unit}^{(1)} \cdot M_{drift}^{(1)}, \tag{4.4.1}$$

where, $M_{acc\ unit}$ is the transfer matrix for the acceleration unit which can be replaced with the transfer matrix for the double aperture lens, given by Eq.(4.1.8). It is modified by using the focal length expressed by Eq.(4.3.5) with the result of

$$M_{acc\ unit} = \begin{pmatrix} a & b \\ c & d \end{pmatrix}, \tag{4.4.2}$$

where

$$\begin{aligned}
a &= 1 - \frac{1}{f_1^*} \cdot \frac{2\,d\ell}{\sqrt{V_1}+\sqrt{V_2}} \sqrt{V_1} \\
b &= \frac{2\,d\ell}{\sqrt{V_1}+\sqrt{V_2}} \sqrt{V_1} \\
c &= -\frac{1}{f_1^*} \frac{\sqrt{V_1}}{\sqrt{V_2}} - \frac{1}{f_2^*} + \frac{1}{f_1^*} \cdot \frac{1}{f_2^*} \frac{2\,d\ell}{\sqrt{V_1}+\sqrt{V_2}} \sqrt{V_1} \\
d &= -\frac{1}{f_2^*} \cdot \frac{2\,d\ell}{\sqrt{V_1}+\sqrt{V_2}} \sqrt{V_1} - \frac{\sqrt{V_1}}{\sqrt{V_2}} \cdot
\end{aligned} \tag{4.4.3}$$

Here, f_1^* and f_2^* are the focal lengths of the entrance and exit single aperture lenses, respectively, given by Eq.(4.3.5).

5. Beam envelope optics

There are two ways of describing the ion transfer properties. One is the ray tracing that is used to study the behavior of individual ion trajectories. The other is the phase space ellipsoid method that treats the beam envelopes characterized by the boundaries of the phase space volume.

The latter is based on the following concept. Each ion contained in the ion beam can be specified at each location by the transverse momentum p and the transverse position r. A pair of the parameters p and r represents a point in a phase space, and the pairs of all of the ions at the respective locations constitute a closed volume in the phase space. From the surface of this volume, the beam envelope can be defined as is seen later.

In this report, the calculation is performed according to this method, the details of which are described below.

5.1 Liouville's theorem

At every point in the phase space volume, an ion density distribution τ is introduced as

$$\tau=\tau(r_1, r_2, \cdots\cdots r_{3N}, p_1, p_2 \cdots\cdots p_{3N}), \tag{5.1.1}$$

where r and p are the position coordinate and its canonical conjugate momentum of the ion, respectively, t is time and N denotes the number of ions. As the ions move from a certain point to another through some optical devices, the phase space volume is also transformed according to the ion transfer properties.

During this transfer, the density distribution in the phase space obeys Liouville's theorem. The theorem states[1),2)] that in the vicinity of an ion, the density distributions remains constant throughout the motion, if the ions move in an external magnetic field or in a general external field with forces which do not depend on the velocity. If interacting forces between ions are negligible, as is the case in this report, the problem can be reduced to the six-dimentional phase space[2)], and the number of ions in an infinitesimal phase space volume is given as

$$dN=\tau(z, x, s, p_z, p_x, p_s, t)dz\cdot dx\cdot ds\cdot dp_z\cdot dp_x\cdot dp_s\,. \tag{5.1.2}$$

As the consequence of Liouville's theorem, it can be said that the phase space volume encompassing all ions does not change its size, although it generally changes its shape. If the motions of the ions in each coordinate are independent of other coordinates, the theorem can be applied to each coordinate separately and the motions in z, x and s are specified independently.

5.2 Acceptance and emittance

In general, optical system consists of a number of devices, each of which has an effective aperture limiting the unrestricted expansion of the beam size. Therefore, it is an important problem to know what size and divergence are permissible for the beam to pass through all such effective apertures.

The problem is solved with the aid of the concepts of acceptance and emittance as described below. The acceptance is defined as the phase space volume, within which the ions must lie in order to be transferred through an optical system without losses. In the paraxial

ray optics, the phase space volume can be described by the separated phase space areas for the individual coordinates, and the acceptance area can be approximated by an ellipse[1),12)], which are represented generally as

$$\gamma_p r^2+2\alpha_p rp+\beta_p p^2=\varepsilon_p \tag{5.2.1}$$

with

$$\beta_p\gamma_p-\alpha_p^2=1, \tag{5.2.2}$$

where r denotes x or z coordinate of the ions and p is the corresponding transverse momentum. The area of the ellipse, S_p, is given by

$$S_p=\pi\varepsilon_p. \tag{5.2.3}$$

The phase space area of the ions can also be approximated by an ellipse[3)] and represented as Eq.(5.2.1). From the viewpoint of the divice system, the ellipse is called[1)] an 'acceptance ellipse' of 'acceptance ε_p', while from that of the ion beam, a 'beam ellipse' of 'emittance ε_p'. Under the transformation through any optical device, the ellipse is transferred into an ellipse, and since its size is unchanged, ε_p is constant throughout the traveling of the ion beam. If the beam ellipse coincides with or is included within the acceptance ellipse, all of the ions are transferred through the whole system, otherwise a fraction of the ions are lost.

Through Eq.(2.3.3), the Eqs.(5.2.1) and (5.2.2) are expressed as

$$\gamma r^2+2\alpha rr'^2+\beta r'^2=\varepsilon \tag{5.2.4}$$

with

$$\beta\gamma-\alpha^2=1 \tag{5.2.5}$$

where, $\gamma=\gamma_p/p_s$, $\alpha=\alpha_p$, $\beta=\beta_p\cdot p_s$ and $\varepsilon=\varepsilon/p_s$. If the beam energy is unchanged, p_s is constant in the paraxial beam optics, so that Eq.(5.2.4) represents the ellipse in $r-r'$ phase space with the constant area of $S=\pi\varepsilon$. On the contrary, if the beam undergoes the energy change, as is the case in the acceleration tubes, the area is reduced in inverse proportion to the increase of the axial momentum.

In the present code, the initial beam ellipse given by Eq.(5.2.4) at the starting point is transformed through the subsequent devices, and the beam envelope trajectory is calculated as described in the following sections. Its size is so controlled, by adjusting the parameters of the quadrupole lenses, that all of the ions can pass through the whole system, without being obstructed by the effective apertures caused by the devices. This procedure correponds to that controles the shape of the beam ellipse so as to be included within the acceptance ellipse.

5.3 Beam envelope

The beam envelope calculation is performed on the basis of the phase space ellipse represented by Eq.(5.2.4). The ellipse is shown in **Fig. 8**. The outermost ion of the beam is specified on the ellipse by the point at which r has the maximum value, $r_{max}=\sqrt{\beta\varepsilon}$, as shown in **Fig. 8**. Therefore, the beam envelope at the location s is given by

$$R(s)=\sqrt{\beta\varepsilon}. \tag{5.3.1}$$

In order to obtain the transformation of the ellipse through an optical device, the inverse transformation for the device

$$\begin{pmatrix} r_1 \\ r_1' \end{pmatrix}=\frac{1}{D}\begin{pmatrix} d & -b \\ -c & a \end{pmatrix}\begin{pmatrix} r_2 \\ r_2' \end{pmatrix} \tag{5.3.2}$$

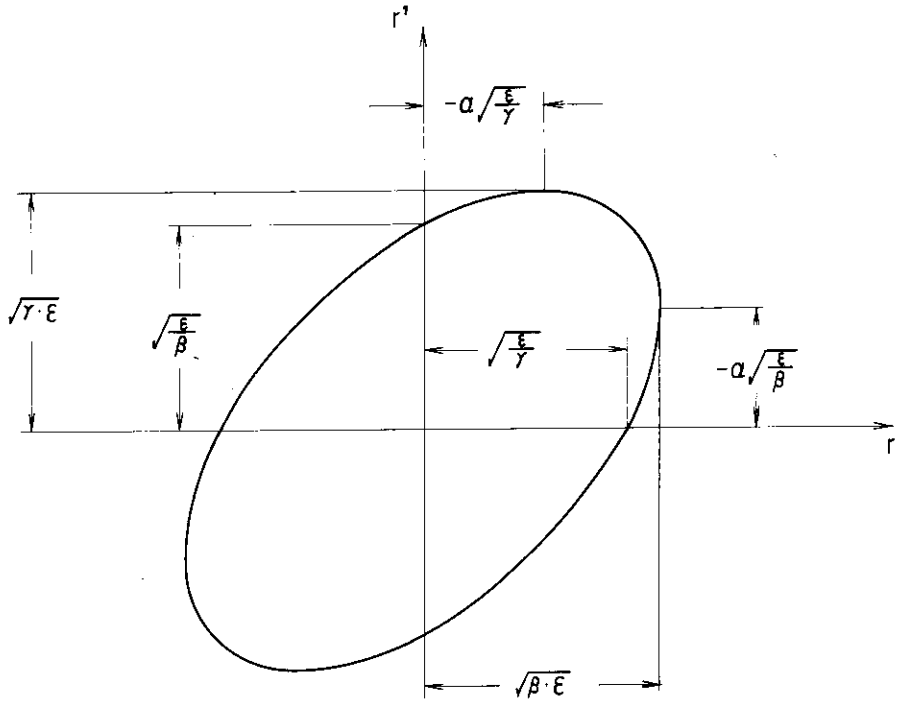

Fig. 8 The phase space ellipse. From Ref. 1.

with

$$D=ad-bc \tag{5.3.3}$$

is inserted into Eq.(5.2.4). The resultant matrix notation

$$\begin{pmatrix}\beta_2\\ \alpha_2\\ \gamma_2\end{pmatrix}=\frac{1}{D}\begin{pmatrix}a^2 & -2ab & b^2\\ -ac & ad+bc & -bd\\ c^2 & -2cd & d^2\end{pmatrix}\begin{pmatrix}\beta_1\\ \alpha_1\\ \gamma_1\end{pmatrix} \tag{5.3.4}$$

with

$$\varepsilon_2=D\varepsilon_1 \tag{5.3.5}$$

is obtained, showing the transformation property of the ellipse parameters β, α and γ. Here, ε_1 and ε_2 are the respective emittances before and after the transformation. The determinat D is equal to 1 if the ion energies are equal before and after the device, otherwise $D=p_{s1}/p_{s2}$ as is shown in Eq.(2.3.6).

In the field free drift space, β_2, α_2 and γ_2 at $s_2=s_1+\ell$ are obtained from β_1, α_1 and γ_1 at $s=s_1$ and the elements of the transfer matrix for the drift space, Eq.(3.1.1), as

$$\begin{pmatrix}\beta_2\\ \alpha_2\\ \gamma_2\end{pmatrix}=\begin{pmatrix}1 & -2\ell & \ell^2\\ 0 & 1 & -\ell\\ 0 & 0 & 1\end{pmatrix}\begin{pmatrix}\beta_1\\ \alpha_1\\ \gamma_1\end{pmatrix}. \tag{5.3.6}$$

The beam envelope $R(s)$ in the drift space is

$$R(s)=\sqrt{\varepsilon}(\beta_1-2(s-s_1)\alpha_1+(s-s_1)^2\gamma_1)^{1/2}. \tag{5.3.7}$$

The position of the extremum of $R(s)$ is obtained by equating $dR/ds=0$, which yields the position s_w

$$s_w=s_1+\frac{\alpha_1}{\gamma_1}. \tag{5.3.8}$$

From the condition that $R(s)$ should be real, it is obtained that γ_1 must be positive, so that $d^2R/ds^2\,(s=s_w)=\sqrt{\varepsilon}\cdot\gamma_1^{3/2}>0$, which indicates that the extremum at $s=s_w$ is the minimum, namely, the beam has a waist at s_w. The waist is ahead of s_1 if α_1 is positive and behind s_1 if α_1 is negative.

It is obtained from Eq.(5.3.6) that the parameters β, α and γ at the waist are

$$\beta_w=\frac{1}{\gamma_1},\quad \alpha_w=0,\quad \gamma_w=\gamma_1, \tag{5.3.9}$$

which shows that the ellipse at the waist is on the principal axes with its area of $s=\pi\varepsilon$.

The expansion of $R(s)$ around s_w

$$\begin{aligned} R(s_w+\Delta s)&=R(s_w)+R'(s_w)\cdot\Delta s+\frac{R''(s_w)}{2!}\cdot(\Delta s)^2+\cdots\cdots \\ &\fallingdotseq R(s_w)\left(1+\frac{1}{2}\gamma_w^2\cdot(\Delta s)^2\right) \end{aligned} \tag{5.3.10}$$

shows, together with Eqs.(5.3.1) and (5.3.9), the following characteristics of the beam envelope near the waist.

1. If $\gamma_w\gg 1$, the beam has a narrow size and a large divergence, and
2. if $\gamma_w\ll 1$, it has a large size and is nearly parallel to the beam axis.

6. Charge exchange

In the tandem accelerator, the charge exchange of negative ions is carried out by means of the stripper, which causes the beam transfer in the accelerator to be complicated. It produces a wide band of charge states and also gives rise to ion scattering processes in the ion beams. In this section, these two problems in the ion optics calculation are described.

6.1 Charge distribution

Some electrons in the atomic shells of the accelerated negative ions are stripped in the foil or gas stripper system at the end of the L.E. acceleration part. The positive ions thus obtained are accelerated moreover by the electric field of opposite direction, and gain the final energy of

$$E_f=\frac{m'}{m}(V_T-V_0)+q\cdot V_T-\Delta E_{st} \tag{6.1.1}$$

in MeV. Here, m and m' are the masses of ions before and after the stripper, respectively, q is the charge state of the positive ions, V_T is the terminal potential in MV, V_0 is negative potential in MV, where the negative ions have zero kinetic energy, and ΔE_{st} is the energy loss of the ions in the stripper system in MeV. If the terminal potential associated with the final energy E_f is required, Eq.(6.1.1) is represented as

$$V_T=\frac{E_f+\Delta E_{st}+(m'/m)V_0}{q+(m'/m)} . \tag{6.1.2}$$

In the present calculation, the charge state q used in Eq.(6.1.1) or (6.1.2) is chosen on the basis of the charage state distribution obtained through the semi-empirical formulae[13] for the average equilibrium charge states and the equilibrium charge fraction. Betz[13] has reported the detailed survey work for the charge exchange mechanism and the equilibrium charge states for heavy ions, penetrating through gaseous and solid media. An universal expression for average charge states produced in solid has been found by Nikolaev and Dmitriev[14],

$$\bar{q}=z\cdot[1+(z^{-\alpha}\cdot v/v')^{-\frac{1}{k}}]^{-k} \tag{6.1.3}$$

for $z\geq 16$, where z is the atomic number of the incident ion, $v'=3.6\times10^6$ m/sec, v is the ion velocity, $\alpha=0.45$ and $k=0.6$. For gas media, Dmitriev and Nikolaev[15] have obtained an expression

$$\bar{q}=z\cdot\log[v/(m\cdot z^{\alpha_1})]/\log(n\cdot z^{\alpha_2}) \tag{6.1.4}$$

for $0.3\leq\bar{q}/z\leq0.9$, where the ion velocity v is in units of 10^6 m/sec. The parameter values are $\alpha_1=0.4$, $\alpha_2=0.3$, $m=0.9$ and $n=7.0$ in argon and nitrogen. In the region $\bar{q}/z<0.3$, a different empirical relation has been given as[15]

$$\bar{q}=A\cdot v\cdot z^{1/2}, \tag{6.1.5}$$

where $A=0.18$ in argon and nitrogen.

The equilibrium charge fraction may be approximated by a Gaussian distribution

$$F(q)=\frac{1}{\sqrt{2\pi d^2}}\exp\left[-\frac{(q-\bar{q})^2}{2d^2}\right]. \tag{6.1.6}$$

The distribution width d has been found to be represented by[14]

$$d=d_2\sqrt{\bar{q}\cdot[1-(\bar{q}/z)^{1/k}]}, \tag{6.1.7}$$

where $d_2=0.5$ and $k=0.6$.

The energy loss ΔE_{st} used in Eqs.(6.1.1) and (6.1.2) is obtained from the calculation of Ziegler[16]. The numerical values of the total stopping for the stripper materials (MeV/(mg/cm^2)) *vs* ion energy (MeV/amu) are taken from the curves in Ref. 16 and tabulated. At the calculation of Eq.(6.1.1) or (6.1.2), the energy loss ΔE_{st} is obtained from these values by interpolation.

6.2 Effect of ion scattering

According to Joy[17], a mean square scattering angle of heavy ions in thin foils and in gases, is given by

$$\langle\phi_s^2\rangle=0.250\left[\frac{z_s(z_s+1)}{A_s}\right]\cdot\frac{Z_i^2}{E_i^2}\cdot T, \tag{6.2.1}$$

where, ϕ_s is in mrad, z_s and A_s are the atomic number and the mass number of the stripper material, respectively, Z_i is the atomic number of the incident ion, E_i is its energy in MeV, and T is the stripper thickness in $\mu g/cm^2$. Replacing T with $\rho\times L$, where ρ is the density in $\mu g/cm^3$ and L is the stripper length in cm, $\langle\phi_s^2\rangle$ can be written as

$$\langle\phi_s^2\rangle=\Theta_s^2\cdot L\,. \tag{6.2.2}$$

Joy[17] has considered first an ion beam running along the beam axis, namely, that of zero emittance. The effects of the scattering process caused by the ion beam may be described by means of the additional angular divergence and the displacement from the beam axis. Both effects are explained in **Figs. 9(a)** and **(b)** with the associated coordinates, where r denotes either of x or z. The discussions here can be restricted to r and θ_r in case of the paraxial beam.

Assuming the bivariate normal density distribution[18] for r and θ_r after the scattering, and referring, for example, to the discussions in Ref. 19, the mean square values and the covariance of r and θ_r are obtained as

$$\begin{aligned}\langle r^2\rangle&=M_{11}=\frac{1}{6}\Theta_s^2L^3\\ \langle\theta_r^2\rangle&=M_{22}=\frac{1}{2}\Theta_s^2L\\ \langle r,\theta_r\rangle&=M_{12}=M_{21}=\frac{1}{4}\Theta_s^2L^2,\end{aligned} \tag{6.2.3}$$

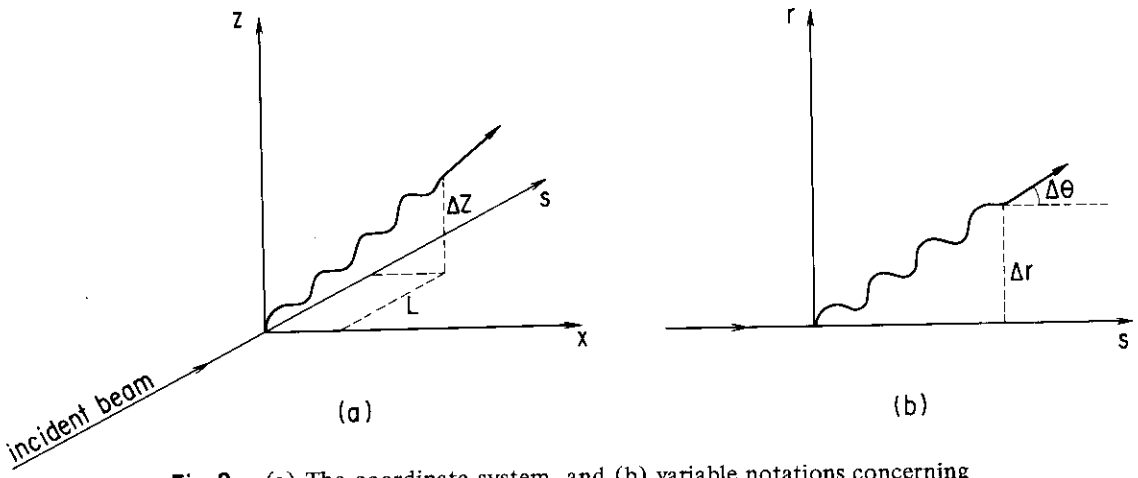

Fig. 9 (a) The coordinate system, and (b) variable notations concerning the scattering process of the ions in the stripper. Displacement r denotes either of x or z. From Ref. 17.

where M_{ij}'s are the elements of the variance/covariance matrix M,

$$M=\begin{pmatrix} M_{11} & M_{12} \\ M_{21} & M_{22} \end{pmatrix}. \tag{6.2.4}$$

The geometrical interpretation of the error matrix[18] shows that the standard deviations of the two correlated variables r and θ_r are represented as the half-length of the projections of the error ellipse on the two coordinate axes. This ellipse is called the ellipse of the standard deviations and is given[18] by

$$M_{22}r^2-2M_{12}r\theta_r+M_{11}\theta_r^2=\det(M), \tag{6.2.5}$$

where $\det(M)$ is the determinant of the matrix M. Putting

$$M_{11}=\beta\cdot\Delta\varepsilon,\quad M_{22}=\gamma\cdot\Delta\varepsilon,\quad M_{12}=M_{21}=-\alpha\cdot\Delta\varepsilon \tag{6.2.6}$$

with

$$\beta\gamma-\alpha^2=1, \tag{6.2.7}$$

Eq.(6.2.5) is

$$\gamma r^2+2\alpha r\theta_r+\beta\theta_r^2=\Delta\varepsilon. \tag{6.2.8}$$

Since $\theta_r\cong\tan\theta_r=r'$, it is found that the ellipse of standard deviations directly corresponds to the phase space ellipse for the new beam in the $r-r'$ plane, $\Delta\varepsilon$ being the increment of the emittance. Applying to the present problem, the ellipse is obtained as shown in **Fig. 10**.

In case that the incident beam has a finite emittance, Joy[17] has obtained the overall emittance as follows+. The effects of the stripper on the incident beam are attributed to the scattering processes in the drift space of length L, and are given through

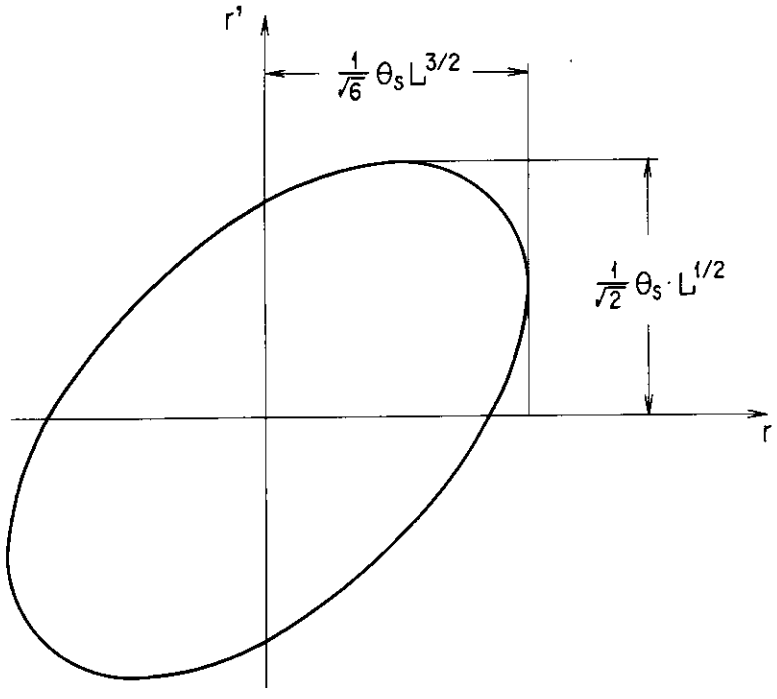

Fig. 10 The phase space ellipse of the beam after the stripper of length L. Incident beam with zero emittance is assumed. From Ref. 17.

+ The procedure is described here by using the ellipse parameters β, α and γ, while Joy[17] has discussed the problem through the variance/covariance matrices.

$$\begin{pmatrix}\beta_2\\ \alpha_2\\ \gamma_2\end{pmatrix}=\begin{pmatrix}1 & -2L & L^2\\ 0 & 1 & -L\\ 0 & 0 & 1\end{pmatrix}\begin{pmatrix}\beta_1\\ \alpha_1\\ \gamma_1\end{pmatrix}+\Delta, \tag{6.2.9}$$

where, β_2, α_2, γ_2 and β_1, α_1, γ_1 refer to the exit and entrance of the stripper, respectively. The second term Δ is caused by the scattering process and is represented as

$$\Delta=\frac{1}{\Delta\varepsilon}\begin{pmatrix}M_{11}\\ -M_{12}\\ M_{22}\end{pmatrix}=\frac{1}{\Delta\varepsilon}\begin{pmatrix}1/6\cdot\Theta_s^2L^3\\ -1/4\cdot\Theta_s^2L^2\\ 1/2\cdot\Theta_s^2L\end{pmatrix}. \tag{6.2.10}$$

Assuming that the scattering processes are concentrated at the center of the stripper, Eq. (6.2.9) is equivalent to

$$\begin{pmatrix}\beta_2\\ \alpha_2\\ \gamma_2\end{pmatrix}=\begin{pmatrix}1 & -L & L^2/4\\ 0 & 1 & -L/2\\ 0 & 1 & 1\end{pmatrix}\left[\begin{pmatrix}1 & -L & L^2/4\\ 0 & 1 & -L/2\\ 0 & 0 & 1\end{pmatrix}\begin{pmatrix}\beta_1\\ \alpha_1\\ \gamma_1\end{pmatrix}+\Delta'\right]. \tag{6.2.11}$$

From Eqs.(6.2.9), (6.2.10) and (6.2.11),

$$\Delta'=\begin{pmatrix}1 & -L & L^2/4\\ 0 & 1 & -L/2\\ 0 & 0 & 1\end{pmatrix}^{-1}\times\Delta=\frac{1}{\Delta\varepsilon}\begin{pmatrix}1/24\cdot\langle\phi_s^2\rangle L^2\\ 0\\ 1/2\cdot\langle\phi_s^2\rangle\end{pmatrix}. \tag{6.2.12}$$

The right hand side of Eq.(6.2.12) indicates that the effects of the scattering processes are represented as the phase space ellipse on the principal axes, with the half axes of $\sqrt{\frac{1}{24}\langle\phi_s^2\rangle L^2}$ and $\sqrt{\frac{1}{2}\langle\phi_s^2\rangle}$. Therefore, if the input beam makes a waist at the center of the stripper, it is considered that a new waist with a new emittance of

$$\varepsilon_s=\left[\left(r_{max}^2+\frac{1}{24}\langle\phi_s^2\rangle L^2\right)\left(r'^2_{max}+\frac{1}{2}\langle\phi_s^2\rangle\right)\right]^{1/2} \tag{6.2.13}$$

is formed there. Here, r_{max} and r'_{max} are half the major and minor axes of the incident beam phase space ellipse.

For foil strippers, the L^2-dependent term can be neglected and the emittance is reduced to

$$\varepsilon_s\cong r_{max}\cdot\left(r'^2_{max}+\frac{1}{2}\langle\phi_s^2\rangle\right)^{1/2}, \tag{6.2.14}$$

which indicates that the beam size is unchanged, while the beam divergence increases to $(r'^2_{max}+\frac{1}{2}\langle\phi_s^2\rangle)^{1/2}$.

The new ellipse parameters β_2, α_2 and γ_2 are given as

$$\begin{aligned}\beta_2&=\frac{1}{\varepsilon_s}\left(r_{max}^2+\frac{1}{24}\langle\phi_s^2\rangle L^2\right)\\ \alpha_2&=0\\ \gamma_2&=\frac{1}{\varepsilon_s}\left(r'^2_{max}+\frac{1}{2}\langle\phi_s^2\rangle\right).\end{aligned} \tag{6.2.15}$$

7. Parameter search of quadrupole lenses

For the purpose of the suitable ion transfer throughout the system, the electrostatic and magnetic quadrupole lenses (abbreviated as Q-lenses, hereafter) are used to form beam waists at some desired locations on the beam axis. In order to obtain the optimum parameters of the Q-lenses for such operations, it is necessary to carry out the parameter search calculation.

As described in section 3.2, the focusing strength of a quadrupole element is determined by a field parameter k. Therefore, that of a doublet Q-lens is determined by two parameters k_1 and k_2 and a triplet Q-lens by three parameters k_1, k_2 and k_3. Practically, however, the triplet Q-lens is usually used with $k_1=k_3$, so that its focusing strength is also characterized by two parameters k_1 and k_2[+].

The aim of the parameter search is to obtain the k_1 and k_2 values which form the waists at the same locations in $x-s$ and $z-s$ planes simultaneously.

7.1 Mathematical description

Let the locations of the waists formed by the Q-lens by

$$W_x=W_x(k_1, k_2; a_x, b_x \cdots\cdots) \tag{7.1.1}$$

and

$$W_z=W_z(k_1, k_2; a_z, b_z \cdots\cdots) \tag{7.1.2}$$

There may be some optical devices between the Q-lens and the waist, such as deflection magnets or acceleration tube units with the fixed parameters a_x, b_x, $\cdots\cdots$, a_z, b_z, $\cdots\cdots$. If there is no optical devices between the Q-lens and the waist, the locations W_x and W_z are measured from the exit of the last quadrupole element. If there are any devices, the locations are measured from the exit of the last device. The situations are illustrated in **Figs. 11(a)** and **(b)**.

The location of the waists, W_x and W_z, are given by

$$W_x=-\alpha_x/\gamma_x, \quad W_z=-\alpha_z/\gamma_z \tag{7.1.3}$$

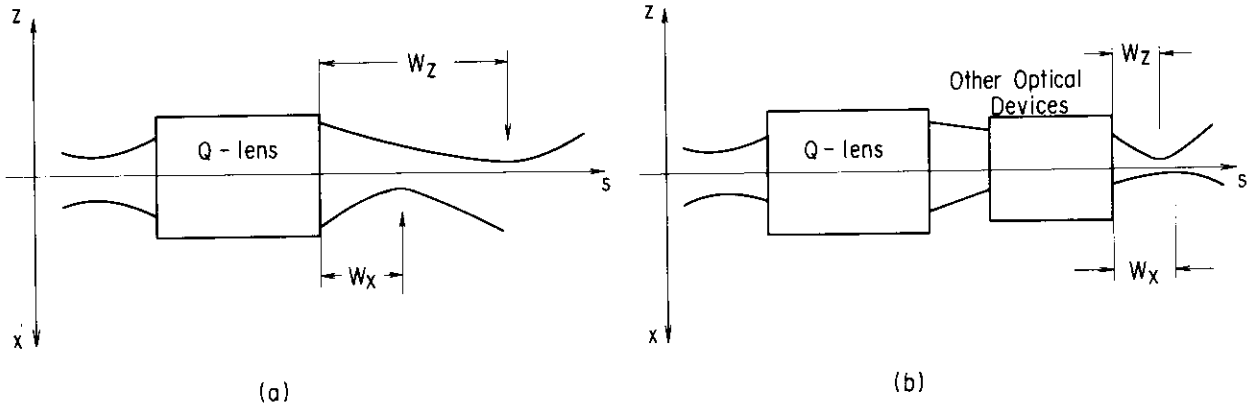

Fig. 11 Beam forcusing by means of Q-lens, (a) without and (b) with other devices between the Q-lens and the waist locations.

+ In the present report, the discussion is restricted to the triplet Q-lens.

as described in section 5.3. Here, α_x, γ_x, α_z and γ_z are the values at the exit of the last optical device, depending on k_1, k_2 and the parameters a_x, b_x, ····, a_z, b_z, ····. If one of the field parameters, for example k_2, is fixed, W_x and W_z vary with k_1 as typically shown in **Fig. 12**. The line $W=W_0$ indicates the desired waist location at W_0. The k_1 values that form the waist at W_0 in each plane are derived from the crossing points of W_x or W_z curve over the line $W=W_0$.

In order to obtain the k_1 and k_2 values which form the waists at the same location W_0 in both planes simultaneously, the successive approximation is used[20] in the present calculation as described below.

Consider a function

$$F(W_x, W_z)=(W_x-W_0)^2+(W_z-W_0)^2. \tag{7.1.4}$$

To make this function minimum with respect to k_1 and k_2,

$$\begin{aligned}\frac{\partial F}{\partial k_1}&=2(W_x-W_0)\frac{\partial W_x}{\partial k_1}+2(W_z-W_0)\frac{\partial W_z}{\partial k_1}=0\\ \frac{\partial F}{\partial k_2}&=2(W_x-W_0)\frac{\partial W_x}{\partial k_2}+2(W_z-W_0)\frac{\partial W_z}{\partial k_2}=0\end{aligned} \tag{7.1.5}$$

should be solved for k_1 and k_2. Expanding W_x and W_z around $k=\bar{k}_1^{(w)}$ and $k=\bar{k}_2^{(w)}$, which are taken as the first approximate values of $k_1^{(w)}$ and $k_2^{(w)}$,

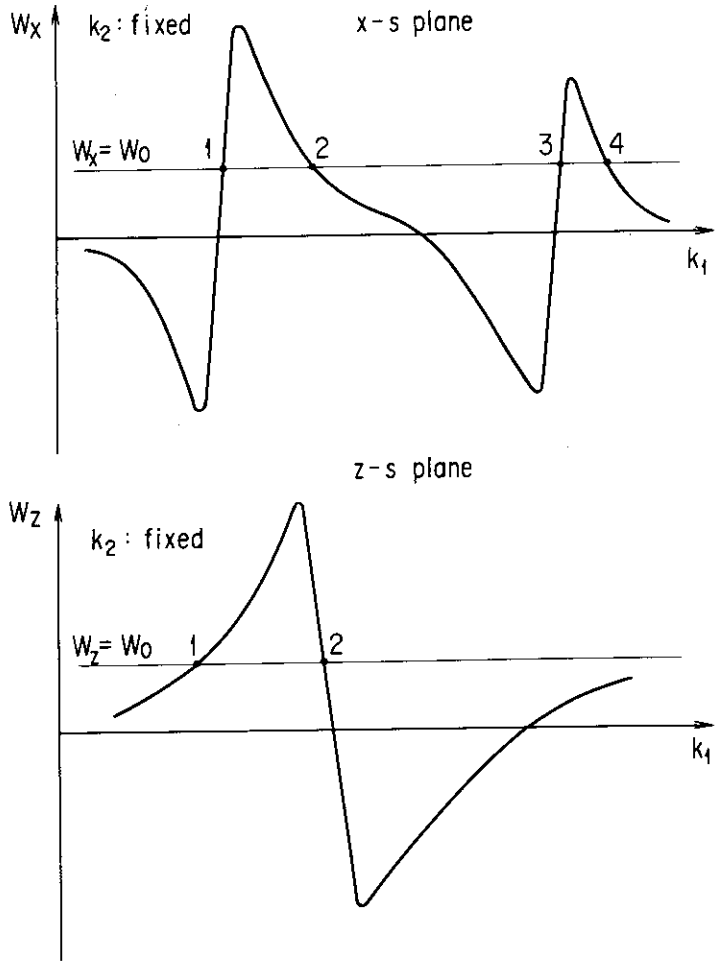

Fig. 12 Variations of the waists with one of the parameters, k_1. Another parameter, k_2, is fixed. Lines at $W=W_0$ indicate the locations of the desired waists at W_0. The numerals by the crossing points are for the notations IWX_SELECT and IWZ_SELECT. See text.

$$W_t(k_1, k_2; a_t, b_t \cdots\cdots) \cong \overline{W}_t(\bar{k}_1^{(w)}, \bar{k}_2^{(w)}; a_t, b_t \cdots\cdots) + \left(\frac{\partial W_t}{\partial k_1}\right)_{k_1=\bar{k}_1^{(w)}} \cdot \Delta k_1 + \left(\frac{\partial W_t}{\partial k_2}\right)_{k_2=\bar{k}_1^{(w)}} \cdot \Delta k_2, \tag{7.1.6}$$

here, $\Delta k_1 = k_1 - \bar{k}_1^{(w)}$, $\Delta k_2 = k_2 - \bar{k}_2^{(w)}$ and t denotes x or z. Substituting Eq.(7.1.6) for W_x and W_z in Eq.(7.1.5),

$$\sum_t \left[\sum_{i=1}^{2} \left(\frac{\partial W_t}{\partial k_i}\right) \cdot \left(\frac{\partial W_t}{\partial k_j}\right) \cdot \Delta k_i + (W_t - W_0)\frac{\partial W_t}{\partial k_j}\right] = 0 \tag{7.1.7}$$

$$j = 1, 2$$

here, $\partial W_t/\partial k_i = (\partial W_t/\partial k_i)_{k_i=\bar{k}_i^{(w)}}$. The quantities $\Delta k_i (i=1, 2)$ obtained by solving Eq.(7.1.7) give the second approximate values for k_i as $\bar{\bar{k}}_i^{(w)} = \bar{k}_i^{(w)} + \Delta k_i$. The second approximate value $\bar{\bar{W}}_t$ is also obtained, by replacing $\bar{k}_i^{(w)}$ with $\bar{\bar{k}}_i^{(w)}$. New $\bar{\bar{W}}_t$ may be substituted for $\bar{W}_t$ in the right hand side of Eq.(7.1.6) to get its higher approximate values.

Repeating the same procedures, the desired parameters $k_1^{(w)}$ and $k_2^{(w)}$ would be obtained with satisfactory accuracy.

7.2 Behavior of waists

It is found from **Fig. 12** that each curve W_x or W_z has two ways of crossing over the line $W=W_0$. One is that with a steep slope, while the other with a gentle slope. These can be distinguished from each other through the γ values near the crossing points, namely, the value for the steep slope is considerably smaller than that for the gentle slope.

The waist given on the steep slope, i.e. with the small γ value, looks undesirable for the beam transport operation, because it moves rapidly along the beam axis even with a slight change of k_1 value. As mentioned in section 5.3, however, the beam envelope with a small γ value at the waist is broad but has small divergence, so that the problem above hardly affects the actual operation. The waist given on the gentle slope, on the contrary, does not move with k_1 so strikingly. This tendency is favorable, beacause the beam envelope with the large γ value is narrow but has rather large divergence at the waist.

A number of pairs of the k_1 and k_2 parameters, which give the waist at W_0, are obtained by generating the waist location vs k_1 curves with the various k_2 values fixed. **Fig. 13** plots such k_1 and k_2 pairs as the k_2 vs k_1 representation. A series of the pairs obtained by tracing a crossing point at every k_2 values is represented as a curve. In **Fig. 13**, therefore, the same number of curves as that of the crossing points in each waist-k_1 curve are drawn for the respective planes, which are designated as $x-s$ and $z-s$. If any curves for different planes intersect with each other, the intersecting points give desired $k_1^{(w)}$ and $k_2^{(w)}$ values, while if no intersecting points, no parameters desired are given in the region of k_1 and k_2 values under consideration.

For each plane, two kinds of curves are obtained in the k_2-k_1 representation. They are related to the parameter pairs associated with the steep and gentle slopes in **Fig. 12**. Accordingly, four kinds of intersecting points are available in **Fig. 13**. The aspects of the beam envelopes near the waists based on such pairs are shown in **Fig. 14**. For the actual accelerator operation, the aspects shown as (b) and (c) in **Fig. 14** are undesirable for the suitable beam transport. Since such ill-shaped waist pairs originate from the large differences between γ_x and γ_z values, the condition

$$\frac{Max\ (\gamma_x, \gamma_z)}{Min\ (\gamma_x, \gamma_z)} < C_1 \tag{7.2.1}$$

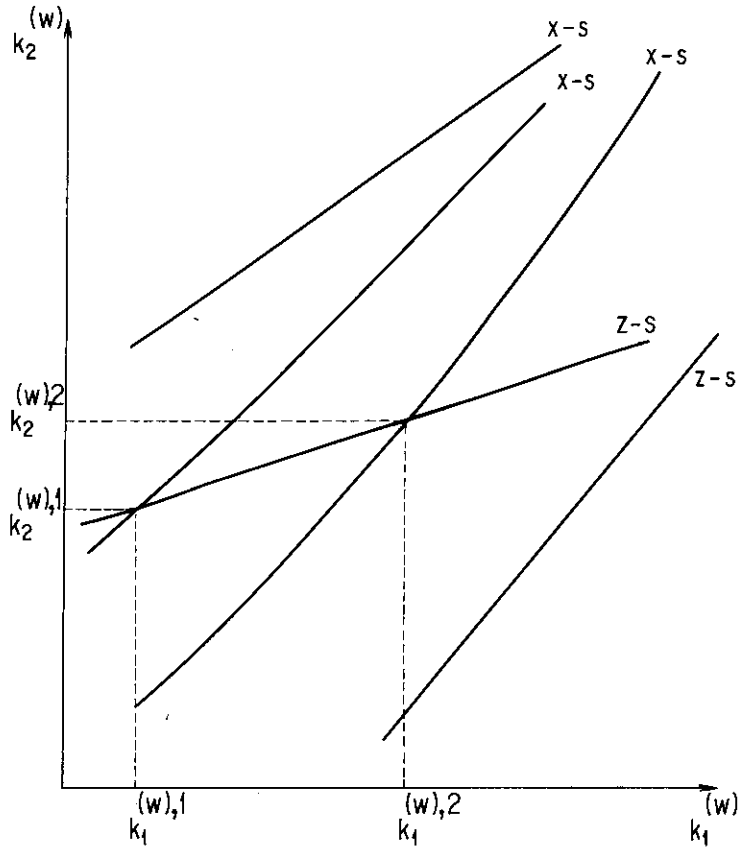

Fig. 13 Representation of the parameter pairs of k_1 and k_2, which give the waists at the desired locations in the $x-s$ and $z-s$ planes. The parameter pairs obtained from the intersecting points of the curves denoted as $x-s$ and $z-s$ give the waists at the same locations in both planes.

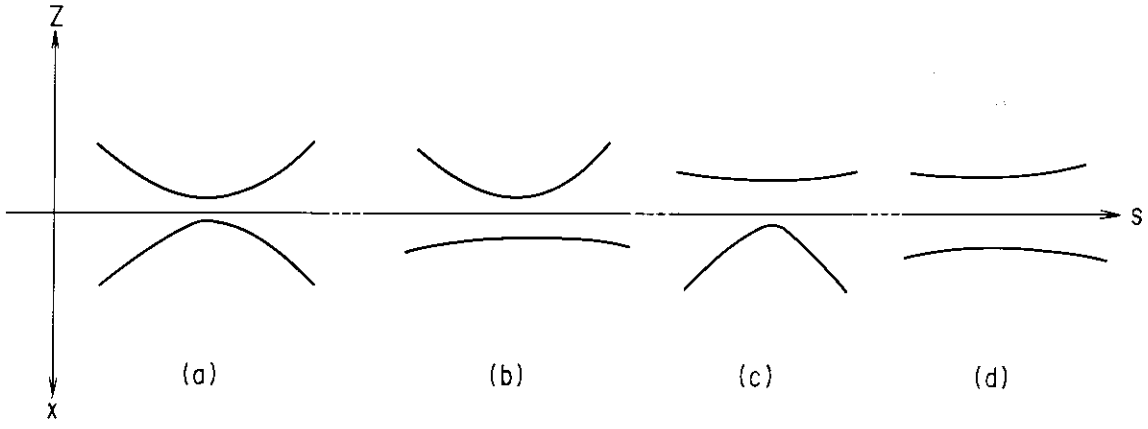

Fig. 14 Four kinds of the shapes of the beam envelopes near waist points.

should be satisfied with $k_1^{(w)}$ and $k_2^{(w)}$, in order to carry out the normal beam transport. The quantity C_1 is a constant of around 5.

Furthermore, to avoid the rather small or large magnification of the beam size,

$$\frac{Max(\sqrt{\beta_t^{(w)}\cdot\varepsilon_t^{(w)}},\ \sqrt{\beta_t^{(w-1)}\cdot\varepsilon_t^{(w-1)}})}{Min(\sqrt{\beta_t^{(w)}\cdot\varepsilon_t^{(w)}},\ \sqrt{\beta_t^{(w-1)}\cdot\varepsilon_t^{(w-1)}})}<C_2\,, \tag{7.2.2}$$

where (w) and $(w-1)$ indicate the waist under consideration and that precedes it by one, respectively, t denotes x or z, and C_2 is again a constant of around 5.

No optimum $k_1^{(w)}-k_2^{(w)}$ pairs may be obtained in the following three situations.

1. The waist-k_1 curves in **Fig. 12** have no crossing points over the $W=W_0$ lines in both planes. In this situation no waists are formed in both planes at the desired location W_0.
2. The curves for the k_2-k_1 representation in **Fig. 13** have no intersecting points. In this situation no k_1-k_2 pairs are found to form the waists at W_0 in both palnes simultaneously.
3. The k_1-k_2 pair that looks to be the desired one does not satisfy Eq.(7.2.1) and/or Eq.(7.2.2).

The ways of dealing with these situations are described in section 8.

7.3 First approximate values of $k_1^{(w)}$ and $k_2^{(w)}$

The essential problem in the successive approximation is to find the first approximate values of the resultant $k_1^{(w)}-k_2^{(w)}$ pairs. This problem is reduced to that of obtaining the approximate k_1 and k_2 values of the intersecting points in the k_2-k_1 representation. For this purpose, the curves in **Fig. 13** obtained for both planes are expressed as the quadrutic curves by means of the method of least squares,

$$k_2=A_t\cdot k_1^2+B_t\cdot k_1+C_t\,, \tag{7.3.1}$$

where the subscrit t denotes x or z. The first approximate values $\bar{k}_1^{(w)}$ and $\bar{k}_2^{(w)}$ are obtained by solving these simultaneous equations for x and z.

This process gives the fairly good approximate values for the $k_1^{(w)}-k_2^{(w)}$ pair desired. However, it takes a long computation time for obtaining the final results, and is inconvenient to get the optimum parameters of the Q-lenses at the accelerator operation time. Therefore, the code is provided with another method as descrived below.

The values $\bar{k}_1^{(w)}$ and $\bar{k}_2^{(w)}$ are searched under the assumption that they satisfy the relation

$$\left|\left(\frac{\partial w_t}{\partial k_i}\right)_{\substack{k_1=\bar{k}_1^{(w)}\\ k_2=\bar{k}_2^{(w)}}}\cdot\Delta k_i\right|>\left|W_0-W_t(\bar{k}_1^{(w)},\ \bar{k}_2^{(w)})\right| \tag{7.3.2}$$

$$t=x,\ z,\quad i=1,\ 2$$

which can be deduced to

$$|W_t(\bar{k}_1^{(w)}+\Delta k_1, k_2)-W_t(\bar{k}_1^{(w)},\ \bar{k}_2^{(w)})|>|W_0-W_t(\bar{k}_1^{(w)},\ \bar{k}_2^{(w)})|$$

and (7.3.3)

$$|W_t(\bar{k}_1^{(w)},\ \bar{k}_2^{(w)}+\Delta k_2)-W_t(\bar{k}_1^{(w)},\bar{k}_2^{(w)})|>|W_0-W_t(\bar{k}_1^{(w)},\ \bar{k}_2^{(w)})|\,.$$

To begin with, one of the parameters, k_2 for example, is fixed at its lower limit k_{min} given. The waists in one of the planes, $x-s$ plane for example, are calculated with k_1 from k_{min} to k_{max} in steps of Δk_1. When a certain k_1 value satisfies the relation Eq(7.3.3), namely,

$$|W_x(k_1+\Delta k_1, k_2)-W_x(k_1, k_2)|>|W_0-W_x(k_1, k_2)| \tag{7.3.4}$$

the same relation for W_z with this k_1-k_2 pair is examined. If it also satisfies Eq.(7.3.3) for W_z, this pair is taken as $\bar{k}_1^{(w)}-\bar{k}_2^{(w)}$ pair, while if not, the procedure is continued with k_2 increased by Δk_2. If k_1 value exceeds the upper limit k_{max}, it returns to k_{min} and k_2 is increased again by Δk_2. In such a way, $\bar{k}_1^{(w)}$ and $\bar{k}_2^{(w)}$ values are obtained in the region $k_{min} \leqq k_i \leqq k_{max}$, $i=1$ and 2. The behavior of the procedure is respresented in **Fig. 15.**

The implicit k_2-k_1 representation may be that as shown in **Fig. 13** or **15**, so that if the execution starts only from the point $n=0$ in **Fig. 15**, the $\bar{k}_1^{(w)}-\bar{k}_2^{(w)}$ pair would be missed. Therefore, the execution is repeated, shifting the starting points in turn until the $\bar{k}_1^{(w)}-\bar{k}_2^{(w)}$ pair is obtained or k_2 reaches k_{max}, as shown in the figure.

Each of two methods mentioned above has both merits and demerits. The method 1 takes long computation time, but can obtain $\bar{k}_1^{(w)}$ and $\bar{k}_2^{(w)}$ as good approximate values. Hence it gives surely the solution through the successive approximation, provided that there is an intersecting point of curves in the k_2-k_1 representation. The method 2, on the contrary, takes less time to get $\bar{k}_1^{(w)}$ and $\bar{k}_2^{(w)}$ values, but if Δk_i value is unsuitably chosen for Eq.(7.3.2), it may cause the divergence in the successive approximation process.

In the present code, both methods can be used complementarily.

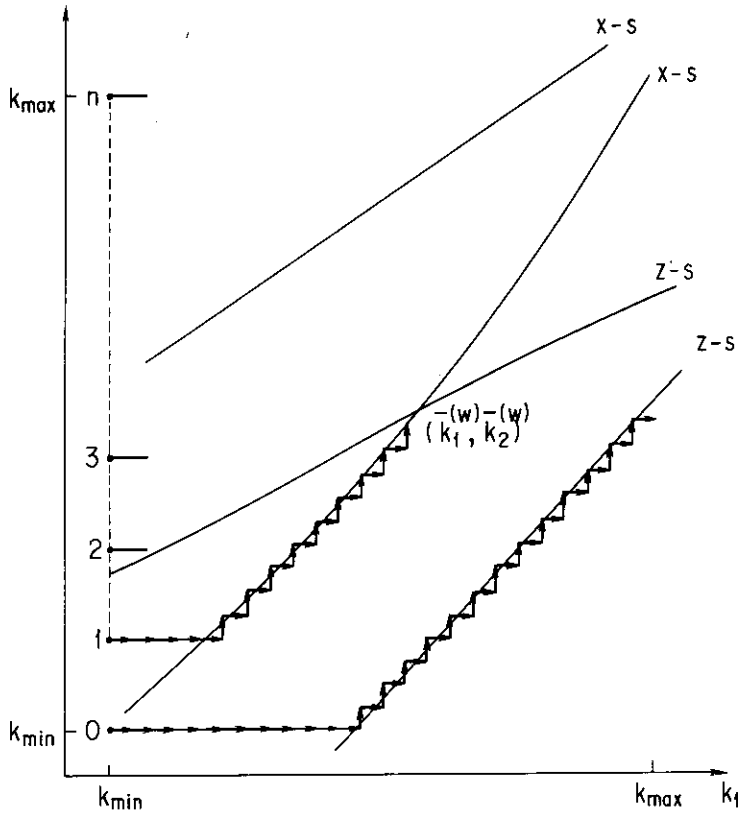

Fig. 15 The behavior of parameter search process.

8. Construction of the code

The beam trajectory calculation is performed by means of the VAX-11/780 computer equipped with a picture display system, MPS. This computer system has been installed as the data analyzing system associated with the JAERI tandem accelerator.

The computation proceeds in order of the optical devices arranged along the beam line of the accelerator system. The beam trajectory calculated can be displayed on a CRT of MPS, extending successively when every execution for each optical device is finished. The final results for the device parameters and so forth are provided with the output sheets of the line printer, and the resultant trajectory displayed on the CRT can be copied on a hard copy plotter.

The following two modes of calculation are possible. In the calculation mode 1, the terminal potential is derived from the final energy desired and the charge state selected. In the mode 2, the terminal potential is given and the final beam energy is obtained by selecting the charge state.

For each mode, two submodes can be selected. One is that calculates the trajectory, being given the Q-lens parameters as described in section 8.4. The other is that searches for the optimum Q-lens parameters to guide the beam from the starting point to the target.

The input data are read through a terminal keyboard and from the data files housed in the disk. There are seventeen data files. One of them, INITIAL.DAT, contains the initial values of the beam emittance parameters, the potential limit imposed on the acceleration tube units and the dimension of the stripper.

Other two files of E_LOSS_F.DAT and E_LOSS_G.DAT tabulate the numerical values concerned with the energy loss of ions in the foil and gas stripper materials, respectively.

The remaining fourteen files include the attributes and parameters of the optical devices in order along the accelerator beam line and the beam lines in the independent target rooms. The arrangement of these devices is shown in **Fig. 16**, which is the schematic view of the accelerator system.

In this section, the flow of the code is outlined first. The functions of the individual subroutines that constitute the code are described subsequently. Those subroutines which are important for the calculation are illustrated with the flow charts of the computation. The data files are also explained for the format with which the data are written. Finally, the process of calculating the beam trajectory, by utillizing those subroutines, is illustrated and summarized.

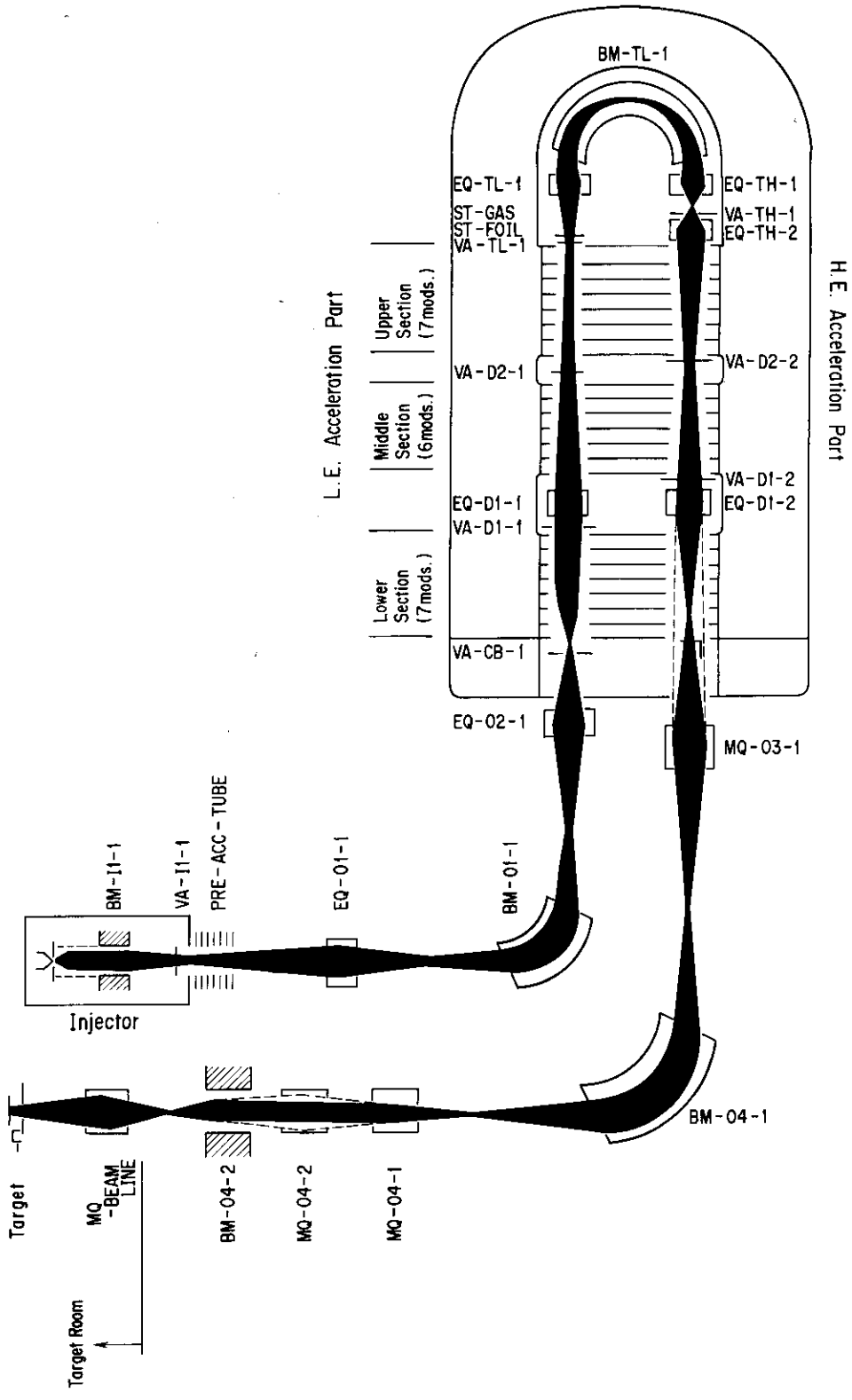

Fig. 16 Schematic view of the JAERI tandem accelerator system. The optical devices along the beam line are named conveniently as,

BM– : bending magnet
DS– : double slit
EQ– : electrostatic Q-lens
MQ– : magnetic Q-lens
ST– : stripper
VA– : variable aperture.

8.1 Outline of the code

The code is composed of the following six files; 1. BEAM, 2. MATRIX, 3. TRAJEC, 4. QLENS, 5. DISPLAY and 6. DISLENS. Each file consists of several subroutines as are listed in **Table 1.**

Table 1 List of files and subroutines

File Name	Subroutine Name	File Name	Subroutine Name
BEAM	MAIN	MATRIX	BAG_M
	CHARGE_EXCHANGE		DRIFT_M
	ENERGY_LOSS		THIN_LENS_M
	DEVICE_ARR		BENMAG_M
	DISPLAY_PREP		ACC_TUBE_M
	DEVICE_SRH		QLENS_M
	REPLACE_PARAM	QLENS	QLENS_TRAJ
	STORE_CALLBACK		QLENS_TRIPLET
	INPUT_OUTPUT		WAIST_CURVE
	SLT_APT_CONTROL		WAIST_K
TRAJEC	DRIFT_TRAJ		WAIST_LSF
	THIN_LENS_TRAJ		WAIST_CROSS
	BENMAG_TRAJ		SUC_APPROX
	ACC_TRAJ	DISPLAY	DISPLAY_TRAJ
	STRIPPER_TRAJ	DISLENS	DISPLAY_LENS

The outline of the flow of the code is shown in **Fig. 17**. The operations designated by the bold frames indicate the input of data through the terminal keyboard, while the double frames from the data files in the disk. The function at each step is as follows.

1° Reading of the initial beam parameters and others from the data file INITIAL.DAT.

2° Initialization of the picture display system through the subroutine DISPLAY_TRAJ. If the system is not to be used, this step is bypassed.

3° Selection of the calculation mode.

4° Input of the data to be used in the calculation.

5° Derivation of the terminal potential for the mode 1, or of the final ion energy for the mode 2. The charge state distribution for each mode is also calculated and is shown on the terminal. The calculation is made through the subroutine CHARGE_EXCHANGE.

6° Selection of the charge state to be used for the operation.

7° Reading of the sequence of the optical devices with their attributes and parameters, from the data file TANDEM.DAT and those for the respective beam lines. The sequence is stored in the buffer memory through the subroutine DEVICE_ARR. After some preparations through the subroutine DISPLAY_PREP, the device arrangement is displayed on the CRT through the subroutine DISPLAY_TRAJ.

8° Initialization of variables used in the calculation.

9° Calculation of the trajectory. Details are described in section 8.4.

10° Display of the resultant trajectory through the subroutine DISPLAY_TRAJ. Operation of a function switch box, a peripheral of MPS, to control the executional flow

is made. Details are described in sections 8.2.5 and 8.4.

11° Printing out of the results of the calculation on the line printer.

For the steps 9° and 10°, refer to **Figs. 34(a)-(d)** and **35**.

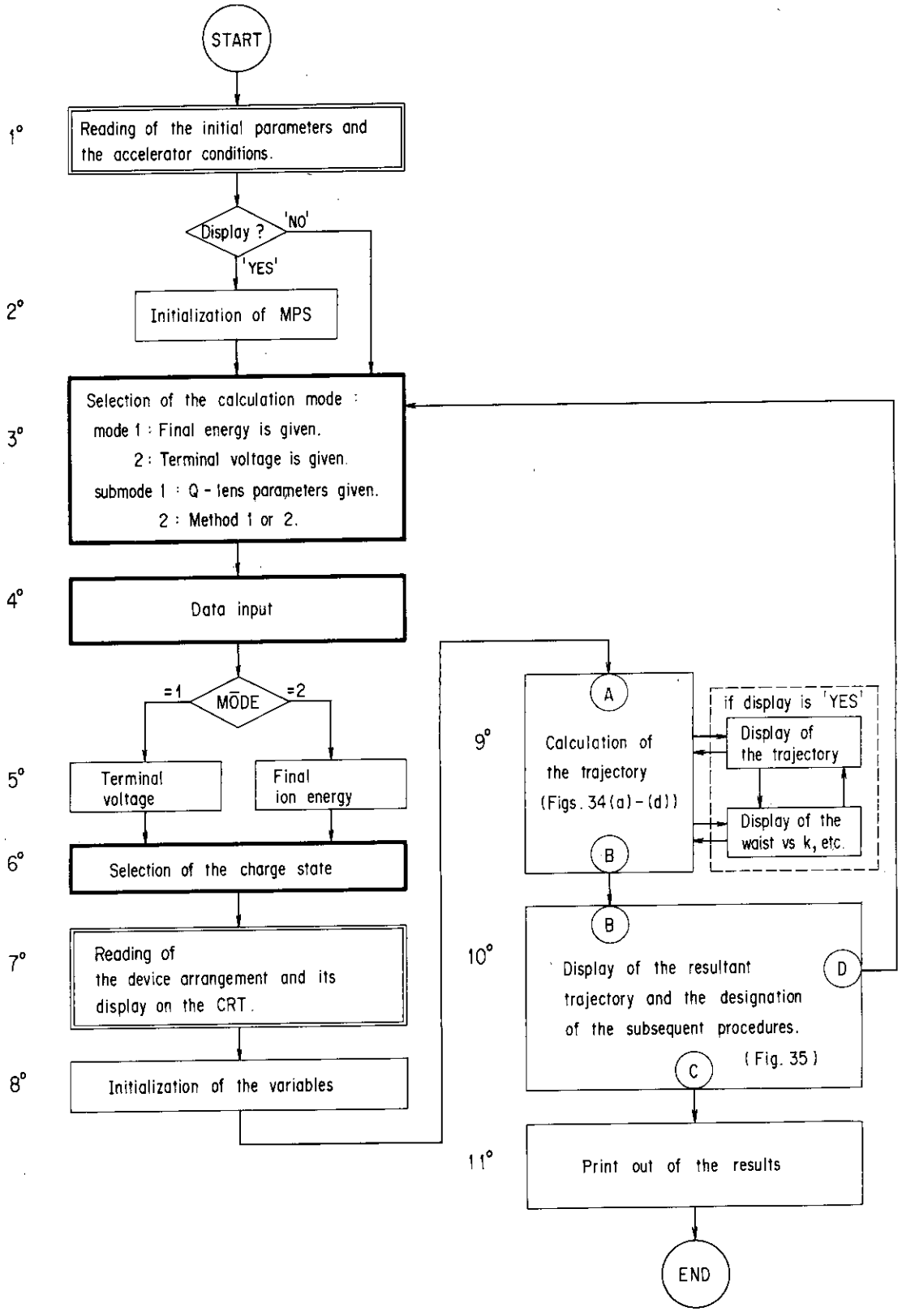

Fig. 17 Outline of the computational flow. Operations designated by the bold frames indicate the input of data through the terminal keyboard, while by the double frames from the data files in the disk.

8.2 Individual files

8.2.1 BEAM

The file BEAM is the main file of the code and contains a main routine and nine subroutines. Each of them is described below.

(I) MAIN:

The main routine MAIN governs the flow of the computation, the ontline of which is illustrated in section 8.1.

(II) CHARGE_EXCHANGE:

This subroutine calculates the charge state distribution produced by the stripper, and derives the terminal voltage or the final ion energy in accordance with the calculation mode selected.

Fig. 18 shows the flow of the computation. The meanings of the variables are as follows.

E_f : The final ion energy required in MeV.

ΔE_{st} : The energy loss of ions in MeV in the stripper materials.

m and m': The masses of ions before and after the stripper, respectively.

MODE : The calculation mode.

$\bar{q}$: The average equilibrium charge state which is obtained through Eq.(6.1.3) for the foil stripper, while through Eq.(6.1.4) or Eq.(6.1.5) for the gas stripper.

V_{limit} : The potential limit in MV imposed on the acceleration tube units.

V_T : The terminal potential in MV of the tandem accelerator.

V_0 : The negative potential in MV where the negative ions have zero kinetic energy.

(III) ENERGY_LOSS:

This subroutine estimates the energy loss of ions in the stripper materials. The energy loss is obtained on the basis of the calculation of Ziegler[16]. The numerical values of the total stopping for the stripper materials (MeV/(mg/cm^2)) *vs* ion energy (MeV/amu) are taken from the curves in Ref. 16 and are tabulated in the files of E_LOSS_F.DAT for the foil stripper and E_LOSS_G.DAT for the gas stripper. The energy loss ΔE_{st} in MeV is obtained from these values by interpolation, being multiplied by the stripper thickness.

(IV) DEVICE_ARR:

The function of this subroutine is illustrated in the description for the step 7° in section 8.1. It reads the sequence of the optical devices from the data file TANDEM.DAT and from the files for the individual beam lines. The attributes and the parameters of each device are also read and all of them are stored in the buffer memory.

In case that some Q-lenses in the accelerator system are not used in the actual operation, the space occupied by those Q-lenses are dealt with as the drift spaces. The device notation (refer to section 8.3.2) 'ELE' or 'MAG' is replaced with 'DRI' and the lengths of the corresponding drift spaces are calculated.

(V) DISPLAY_PREP:

This subroutine prepares variables necessary for displaying the arrangement of the optical devices on the CRT.

(VI) DEVICE_SRH:

The calculation of the trajectory proceeds in order of the optical devices one by one. However, if some devices are set between the Q-lens and the desired waist location, the calculation for those devices have to be made many times repeatedly until the optimum parameters of the Q-lens are decided. The subroutine DEVICE_SRH is used, for convenience, for sending the input parameters for those devices beforehand, together with those of the Q-lens, to the searching program routine.

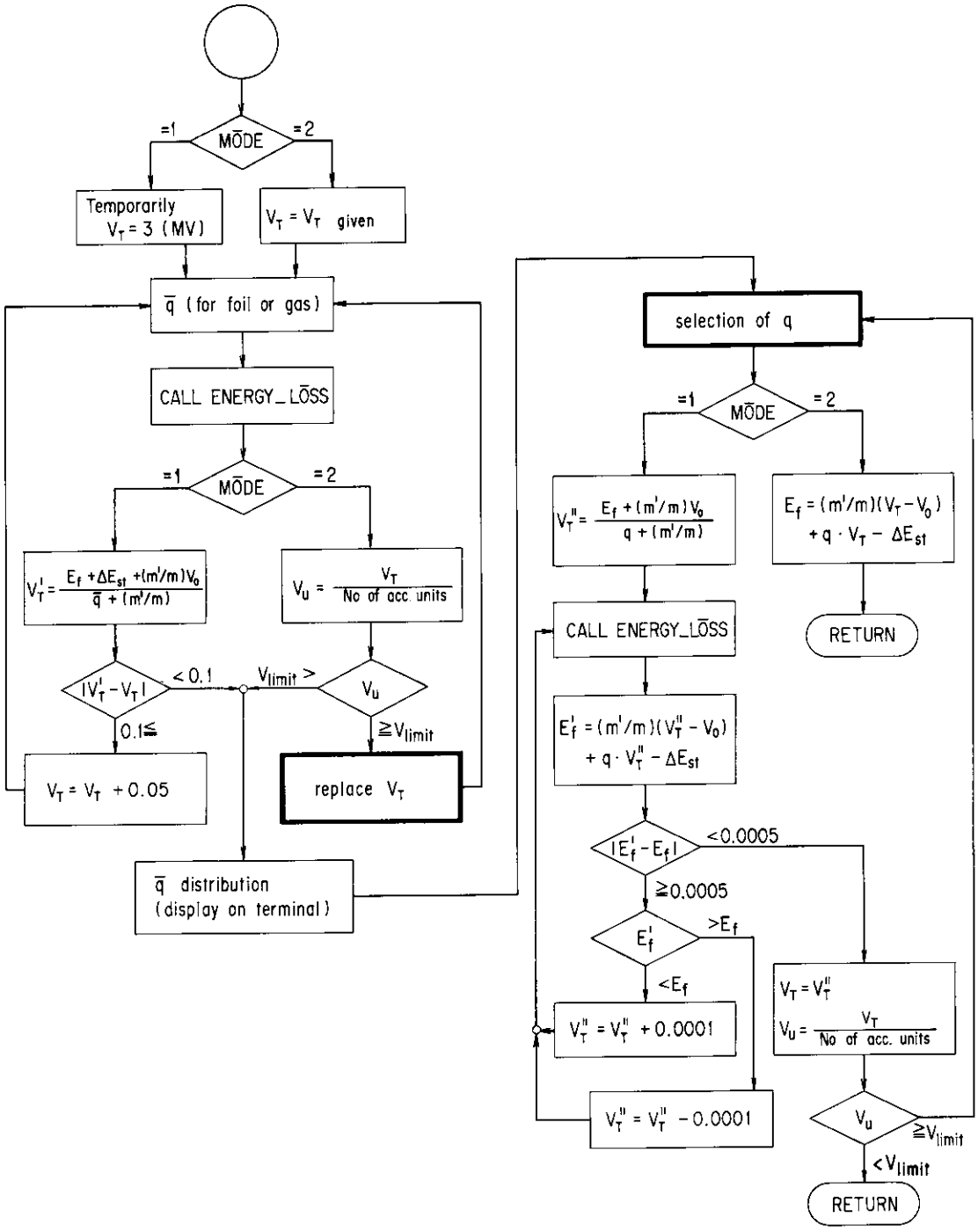

Fig. 18 Computational flow of the subroutine CHARGE_EXCHANGE. It calculates the charge state distribution in ion beam caused by the stripper. The terminal voltage in MV or the final ion energy in MeV is also calculated. Operations designated by the bold frames indicate the input of data through the terminal keyboard.

(VII) REPLACE_PARAM:

At the step 10° in section 8.1, if more trajectories are desired to be calculated, the input parameters currently used should be replaced with those necessary for the succeeding calculation. The new parameters are read through the terminal keyboard, and the replacement is performed through this subroutine.

(VIII) STORE_CALLBACK:

Prior to the next calculation at the step 10° in section 8.1, the results obtained and the trajectory displayed on the CRT can be stored temporarily in the disk. Later, they can be called back onto the memory and can be displayed again. This subroutine deals with such processes, according to the designations through the function switches of MPS (refer to section 8.2.5).

The subroutine is used also, at the final step 11° in section 8.1, to call back the results which have been stored in the disk and send them to the subroutine INPUT_OUTPUT to print them out.

(IX) INPUT_OUTPUT:

This subroutine creates a file OUTPUT.DAT, in which the results of the calculation together with the input parameters used are written. An example of the output list is shown in section 8.6.

(X) SLT_ATR_CONTROL:

This subroutine determines the minimum slit width or aperture radius, through which the beam can pass. The beam size at the slit or the aperture is compared with the half of the slit gap width, d_t, or the aperature radius, r_t, where t denotes x or z. If the beam size is larger than d_t or r_t, d_t or r_t is increased by 1.0 mm and compared with $\sqrt{\beta_t \cdot \varepsilon_t}$ repeatedly. When the inequality

$$\sqrt{\beta_t \cdot \varepsilon_t} < \begin{cases} d_t & \text{for the slit,} \\ r_t & \text{for the aperture,} \end{cases} \tag{8.2.1}$$

is satisfied, the value of d_t or r_t is decided as its minimum value.

The initial values of d_t and r_t are given to be zero, and the behavior of their gradual opening is seen on the CRT.

8.2.2 TRAJEC

The file TRAJEC is composed of five subroutines which are concerned with the beam envelope trajectories controlled by the optical devices other than Q-lens. The subroutine that calculates the effects of the ion scattering on the trajectory due to the stripper, is also included.

The beam envelope trajectories are represented by Eq.(5.3.1) and are calculated by taking s along the beam axis in steps of a small distance Δs. The initial value of β is given in the data file INITIAL.DAT and is read at the beginning of the computation.

The subroutines included are described below.

(I) DRIFT_TRAJ:

This subroutine calculates the trajectories in the field free drift space. The flow of the computation is shown in **Fig. 19**. The meanings of the variables and notations in the figure are as follows.

ℓ : The length of the drift space in m.

Δs : The small distance taken along the beam axis, in steps of which the trajectory is calculated. Its numerical value is typically given to be 0.1 m.

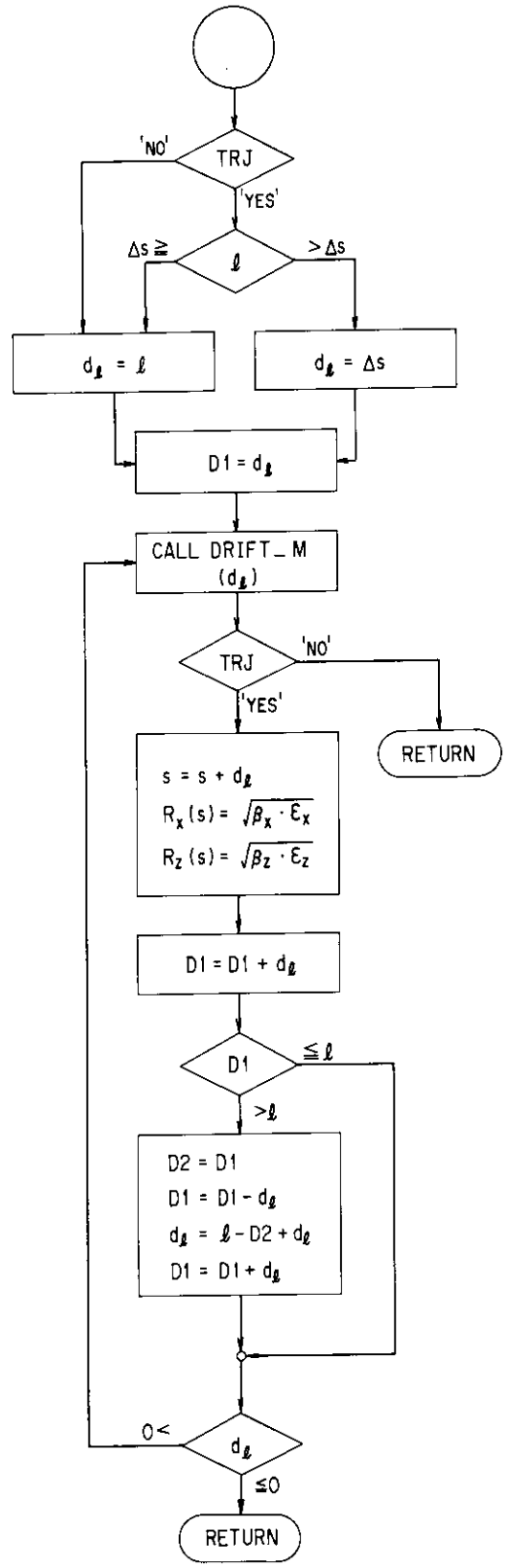

Fig. 19 Computational flow of the subroutine DRIFT_TRAJ, for obtaining the beam envelope trajectory in the field free drift space.

TRJ : During the searching process, the detailed calculation of the trajectory within the devices is not necessary. The repetition of the calculation only at the both ends of the devices is sufficient to get the optimum Q-lens parameters. After their decision, the trajectory is calculated with them in steps of the small distance Δs in order to be displayed on the CRT. The notation TRJ indicates whether the current flow is for the calculation of the detailed trajectory (YES), or for that of the parameter search (NO).

D1, D2 and d_ℓ : These variables are used to partition the length of the drift space. The last small distance supposed in the original drift space, given by $\ell - n \cdot \Delta s < \Delta s$ with an integer n, is obtained in the process shown in the last frame in the figure.

(II) THIN_LENS_TRAJ

This subroutine calculates the effect of thin lens on the beam envelope trajectory. The flow is shown in **Fig. 20**. The variable f is the focal length.

(III) BENMAG_TRAJ:

This subroutine calculates the deflection of the trajectory due to the bending magnet. The flow is shown in **Fig. 21**. The meanings of the variables and notations in the figure are as follows.

ρ : The curvature, in m, of the beam axis in the magnet.

φ : The bending angle.

BEN_PLANE : The notation that designates the bending plane of the magnet. If the bending plane is $x-s$ plane, BEN_PLANE is 'X', if $z-s$ plane, BEN_PLANE is 'Z'.

TRJ : Same as that described at (I) in the present section.

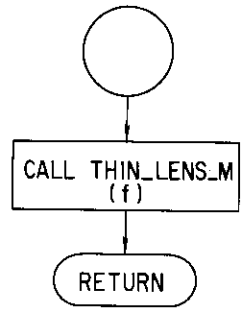

Fig. 20 Computational flow of the subroutine THIN_LENS_TRAJ, for obtaining the effect of the thin lens on the beam envelope trajectory.

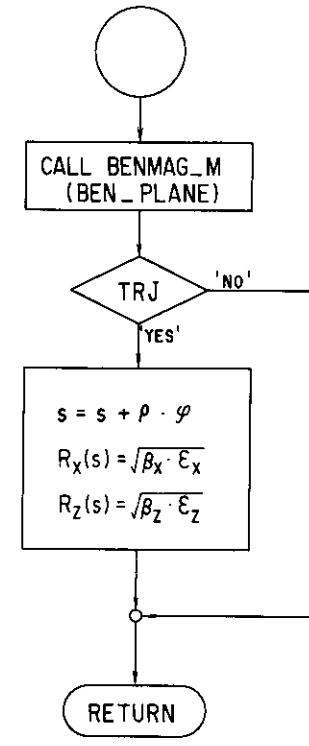

Fig. 21 Computational flow of the subroutine BENMAG_TRAJ, for obtaining the effects of the bending magnet on the beam envelope trajectory.

(IV) ACC_TRAJ:

This subroutine calculates the trajectories in the acceleration tubes. The JAERI tandem accelerator has two acceleration tube systems, that for the pre-acceleration after the injector and that for the main acceleration. Their schematic structures are shown in **Fig. 22**. Both of them are considered to be the connected tube units, each of which is composed of the uniform field with the drift spaces at both ends, as mentioned in sections 4.3 and 4.4.

The pre-acceleration tube system consists of four tube units, as is shown in **Fig. 22(a)**. The main acceleration tube system is in a pile of twenty column modules with a high voltage terminal on the top, as is seen in **Fig. 16**. As the accelerator is of the folded type, both of the L.E. and H.E. acceleration parts are in the same pile.

The whole system is divided into three sections named the lower, middle and upper sections, containing seven, six and seven column modules, respectively. **Fig. 22(b)** indicates one of such sections, showing that one column module has three acceleration tube units. If some modules are short-circuited to the same potential, a series of the tube units included is regarded as a drift space with the sum length of the linked units.

Figs. 23(a) and **(b)** illustrate the flow of the computation. The former is that for the pre-acceleration and the latter for the main acceleration. The meanings of the variables and notations are as follows.

U_FIELD : The execution is repeated by turns for the drift spaces and the uniform fields. This notation controls the process, by taking 'YES' after the execution for the latter and 'NO' for the former.

N_UNIT : The number of the acceleration tube units. For the pre-acceleration system, N_UNIT = 4. For the main system, it takes 21, 18 or 21 for the lower, middle or upper section, respectively.

SHORT_CIRCUIT: This notation indicates whether the tube unit under consideration is short-circuited to others or not.

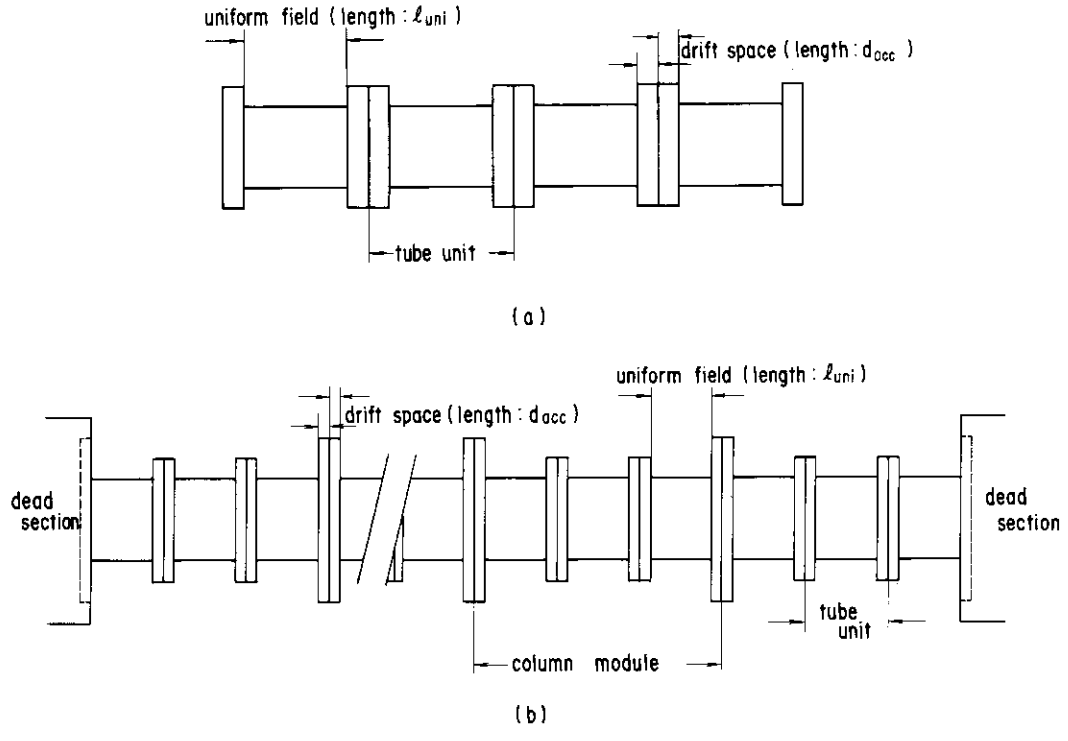

Fig. 22 Schematic views of the acceleration tubes in the JAERI tandem accelerator system. (a) Those for the pre-acceleration and (b) for the main acceleration.

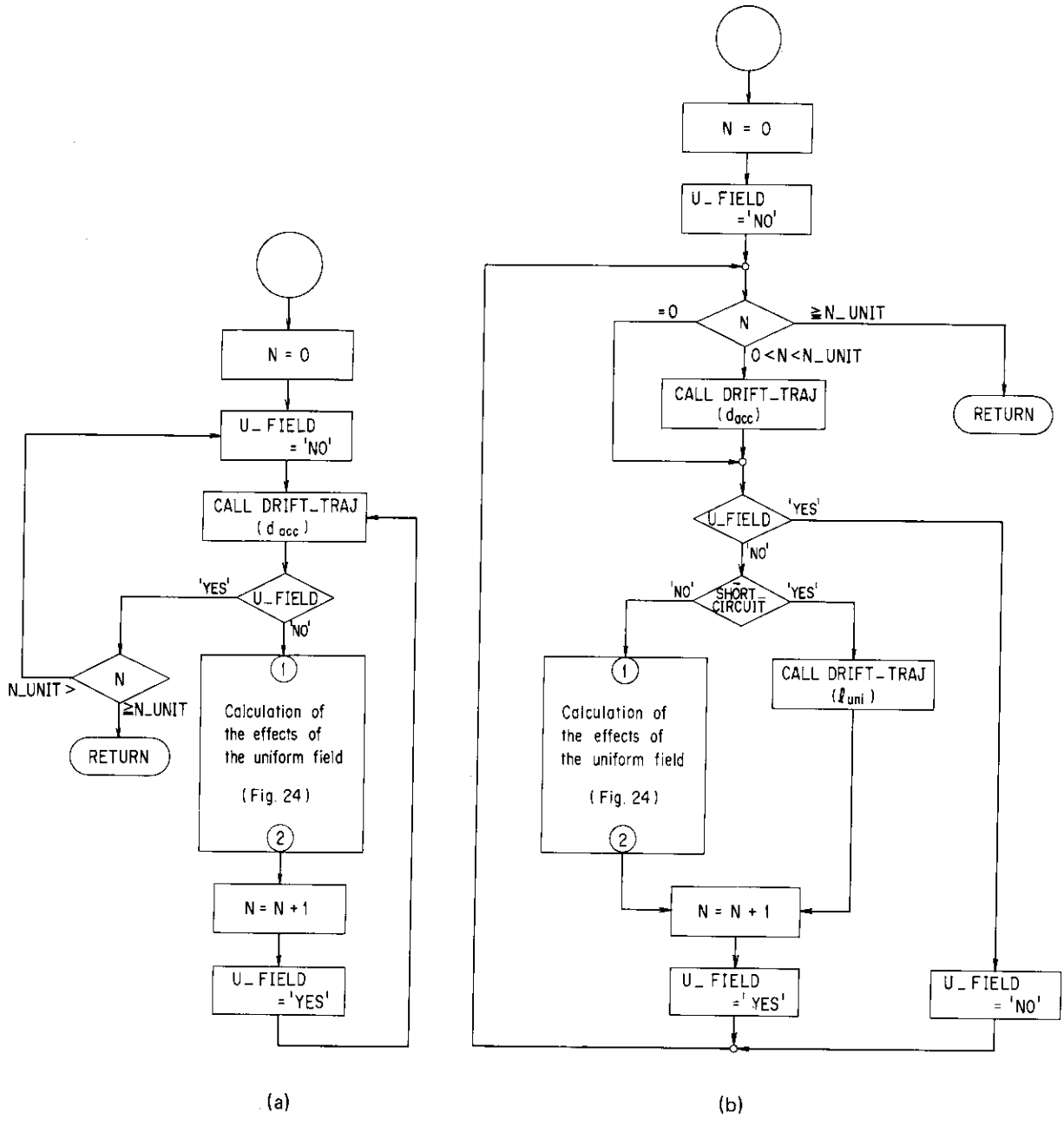

Fig. 23 Computational flows of the subroutine ACC_TRAJ. They calculate the beam envelope trajectories in (a) the pre-acceleration tube units and (b) the main acceleration tube units.

Fig. 24 shows the flow of the computation for the effect of the uniform field on the trajectory, which should be included in **Figs. 23(a)** and **(b)**.

This flow illustrates the calculation for the ion beam with the energy E_1, entering the uniform field whose potential at the entrance is V_1. The suffixes 1 and 2 to the variables denote the respective values at the entrance and the exit of the field, ΔV is the absolute value of the potential difference between both ends of the field. The reduced potentials V_{ent} and V_{exit} are given through Eq.(4.3.1) or Eq.(4.3.2). Other notations are as follows.

λ : The variable that takes -1 in tha L.E. acceleration part and +1 in the H.E. acceleration part.

d_{acc} : The length of the drift space in m.

ℓ_{uni} : The length of the uniform field in m.

TRJ : Same as that illustrated at (I) in this section.

q : The charge state of the ions.

ε : The beam emittance. Subscrits x and z denote the $x-s$ and $z-s$ planes, respectively.

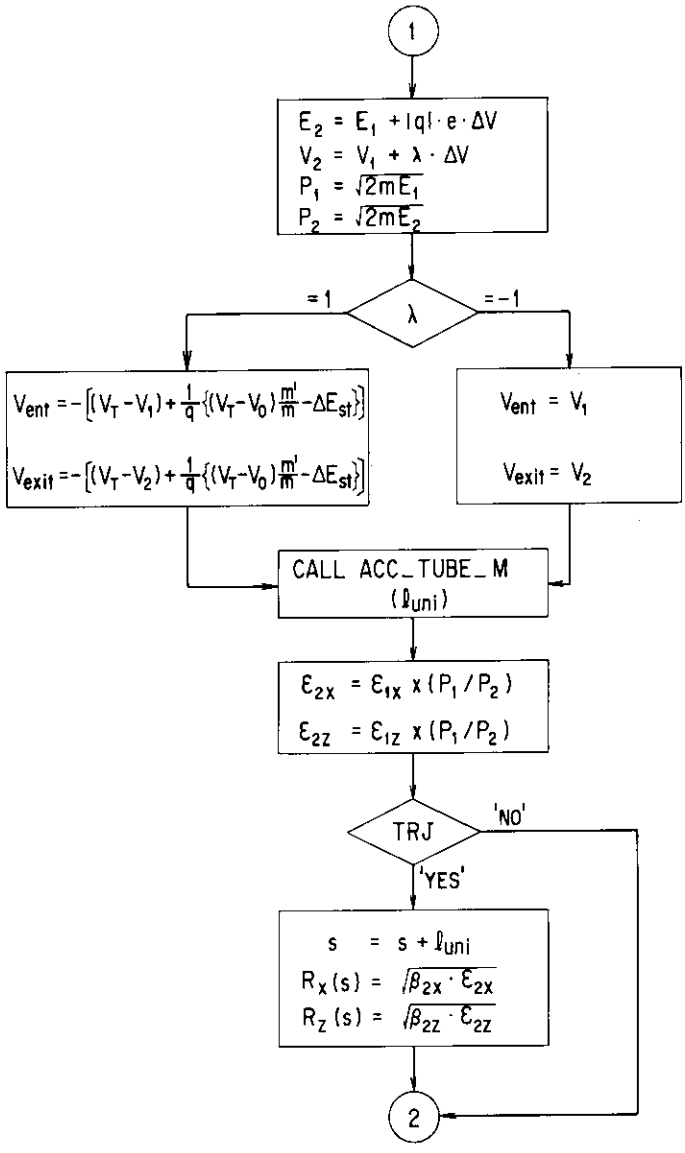

Fig. 24 Computational flow of the subroutine ACC_TRAJ, for calculating the effects of the uniform field in the acceleration tube units. This flow should be inserted in Figs. 23(a) and (b).

(V) STRIPPER_TRAJ:

This subroutine calculates the effects of the ion scattering due to the stripper. The calculation is based on the equations described in section 6.2, and the flow of the computation is shown in **Fig. 25**. The meanings of the variable ℓ and notation STRIPPER are as follows.

ℓ : The length, in m, of the gas stripper canal.

STRIPPER : If the foil stripper is used, this notation is 'F', if the gas stripper, it is 'G'. Others indicate the same meanings as in the text.

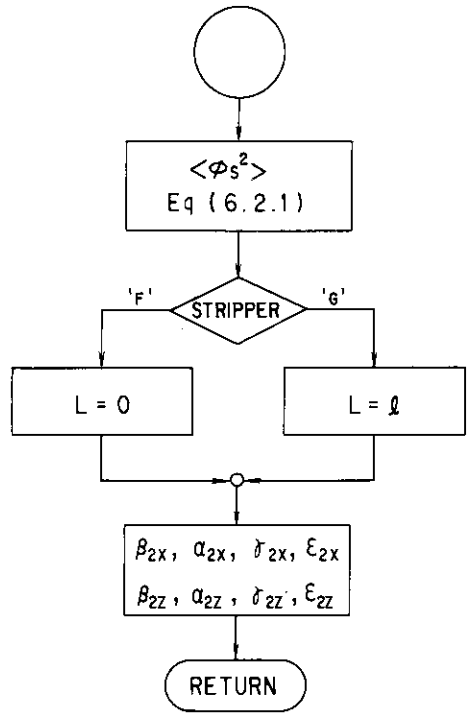

Fig. 25 Computational flow of the subroutine STRIPPER_TRAJ, for obtaining the effects of the ion scattering due to the stripper system.

8.2.3 MATRIX

The file MATRIX includes six subroutines. One of them, BAG_M, transforms the ellipse parameters β, α and γ. Other five calculate the elements of the transfer matrices for the individual optical devices, and call the subroutine BAG_M twice at the end of them to transform the ellipse parameters for the $x-s$ and $z-s$ planes.

(I) BAG_M:

This subroutine transforms the ellipse parameters β, α and γ through Eq.(5.3.4) with $D=1$. The elements of the transfer matrix in Eq.(5.3.4) are calculated with those for the individual optical devices.

(II) DRIFT_M:

This subroutine obtains the ellipse parameters transformed by the field free drift space.

(III) THIN_LENS_M:

This subroutine obtains the ellipse parameters transformed by the thin lens.

(IV) BENMAG_M:

This subroutine calculates the matrix elements for the bending magnet through Eqs. (3.4.5) and (3.4.6), and transforms the corresponding ellipse parameters. Since $\Delta p/p$ is negligibly small for the beam in the present case, the dispersion vector Eq.(3.4.7) is not taken into

account.

(V) ACC_TUBE_M:

This subroutine calculates the matrix elements for the acceleration tube unit through Eq.(4.4.3), with the focal length of the aperture lens given by Eq.(4.3.5). Since, for the acceleration unit, the ion energies at the entrance and the exit are not equal, D is not unity in Eq.(5.3.4). Therefore, the ellipse parameters calculated in the subroutine BAG_M should be multiplied by p_{s2}/p_{s1}, where p_{s1} and p_{s2} are the axial momenta of ions at the entrance and the exit of the tube unit, respectively. The corrections for the emittances are also made here, the current emittances being divided by p_{s2}/p_{s1}.

(VI) QLENS_M:

This subroutine calculates the matrix elements for the single quadrupole element through Eq.(3.2.1) or Eq.(3.2.2), and obtain the corresponding transformed ellipse parameters. For multiplet quadrupole lenses, the resultant parameters are calculated by using the present subroutine and the subroutine DRIFT_M by turns.

8.2.4 QLENS

The file QLENS contains seven subroutines, each of which plays a role in the searching process for the optimum parameters of Q-lenses.

The process continues until the resultant parameters $k_1^{(w)}$ and $k_2^{(w)}$ are obtained, satisfying the following numerical criterion. That is, the waists in both planes should be formed at the desired locations within the limits of ±0.005 m, namely,

$$|W_0-W_x|\leqq 0.005 \text{ and } |W_0-W_z|\leqq 0.005 \qquad (8.2.4.1)$$

where, W_0 indicates the desired waist location, W_x and W_z are the waist locations in the $x-s$ and $z-s$ planes, respectively.

The functions of the seven subroutines are described below.

(I) QLENS_TRAJ:

This subroutine controls the flow of computation for the searching process. As mentioned in section 7.3, the searching process can be performed through either of two ways. They are different from each other concerning the methods of obtaining the first approximate values of $k_1^{(w)}$ and $k_2^{(w)}$. One is rather minute method and the other is the convenient one, designated hereafter as method 1 and method 2, respectively. The method to be used is chosen at the beginning of the execution. It can be altered in the course of the execution, through the operation of the function switches related to the subroutine DISPLAY_TRAJ or DISPLAY_LENS selectively, as described in section 8.2.5 or 8.2.6.

There are three situations that can find no desired $k_1^{(w)}$ and $k_2^{(w)}$ values, as described in section 7.2. In order to surmount these situations, the following ways are used in the present calculation. For the situations 1 and 2 designated in section 7.2, the desired waist location W_0 is modified. For the situation 3, the constant value C_2 in Eq.(7.2.2) is changed to infinity, that is, the restriction for the magnification on the trajectory is released. The condition of Eq.(7.2.1) should be unchanged so as to avoid the ill-shaped waist pairs, but the large or small magnification may sometimes be tolerated for the suitable beam transport. After that, the searching process is carried out again. Details are illustrated below in the respective descriptions of the methods 1 and 2.

(I)-1 : Method 1.

The flow of the method 1 is illustrated in **Fig. 26**. The first step is to make the waist-k_1 curve with $k_2=k_{min}$. This is carried out by calling the subroutines QLENS_TRIPLET and WAIST_CURVE repeatedly in the region of k_1 values from k_{min} to k_{max} in steps of Δk_1. The

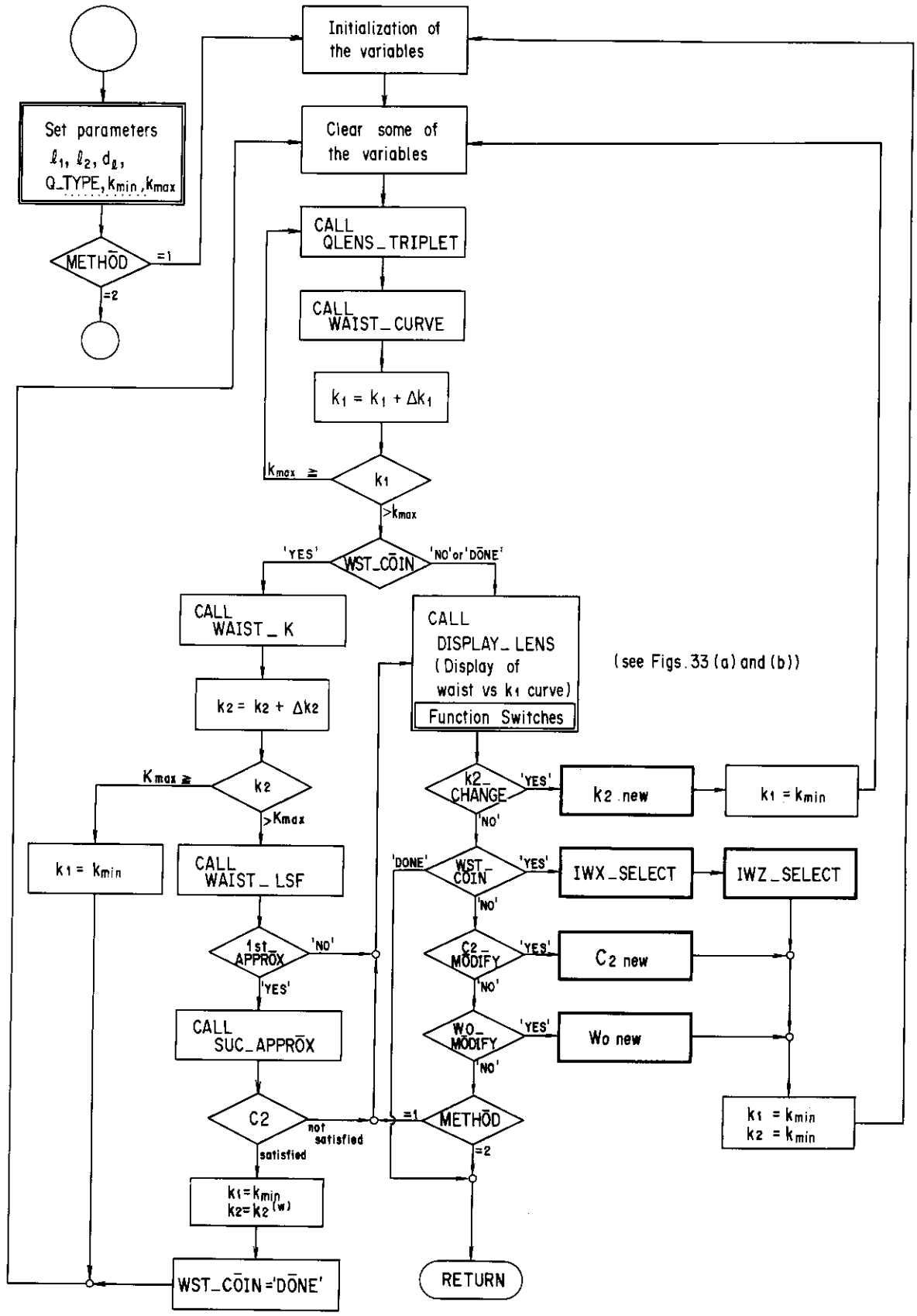

Fig. 26 Computational flow of the subroutine QLENS_TRAJ, for searching for the field parameters of Q-lenses, by means of the method 1. Operations designated by the bold frames indicate the input of data through the terminal keyboard. The variables in the double frame are data from the data files in the disk.

notation WST_COIN is initialized to be 'NO', and the waist-k_1 curve so produced is displayed on the CRT of the picture display system, MPS, by the subroutine DISPLAY_LENS.

By means of the function switches connected to MPS, several kinds of the processes to be made subsequently are selected. The most impotant one is to perform the searching process for the Q-lens parameters. If the switch assigned to this process is ON (refer to section 8.2.6 and **Table 3**), the notation WAIST_COIN is changed to 'YES'. At the same time, it is requested to input two numbers, IWX_SELECT and IWZ_SELECT, from the terminal keyboard, which designate the crossing points of the waist-k_1 curves over the $W=W_0$ lines in both planes, as shown in **Fig. 12**. After that, the Q-lens parameters are searched and determined, so as to make the crossing points designated by these numbers coincide at the same location on the k_1 axis.

As an example, if the waists shown in **Fig. 14(a)** are desired, the crossing points 2 or 4 for $x-s$ plane and 1 for $z-s$ plane in **Fig. 12** should be selected. This selection leads to the k_2-k_1 representation, where the γ values for both curves are large. Thus, the $k_1^{(w)}-k_2^{(w)}$ pair determined from the intersecting point gives the well-shaped narrow waists pair.

In this way, the k_1-k_2 pair satisfying the condition Eq.(7.2.1) can be obtained. If it also satisfies the condition Eq.(7.2.2), it can be taken as the desired $k_1^{(w)}-k_2^{(w)}$ pair. In such a case, the execution proceeds to make the waist-k_1 curves with $k_2=k_2^{(w)}$ determined above, and displays them on the CRT, as are shown in **Fig. 27**. It is seen that the k_1 value at one of the crossing points in one plane coincides with that in another plane. An example of the k_2-k_1 representation related to **Fig. 27** is shown in **Fig. 28**.

After the determination of the optimum $k_1^{(w)}-k_2^{(w)}$ pair, the execution returns to the MAIN routine through the designation of the function switch, and continue to calculate the subsequent beam trajectory.

If the first approximate values $\bar{k}_1^{(w)}$ and $\bar{k}_2^{(w)}$ are not obtained, the execution returns to display the previous waist-k_1 curves. This case corresponds to the situation 1 or 2 mentioned above, and the alternative $\bar{k}_1^{(w)}-\bar{k}_2^{(w)}$ pair can be found by using the modified value of W_0 in the calculation. The modified W_0 value is decided by examining the relative positions of the $W=W_0$ lines to the waist-k_1 curves displayed on the CRT.

If the condition of Eq.(7.2.2) is not satisfied after the successive approximation, the situation 3, the C_2 value is changed to infinity as mentioned above. For both cases, the execution proceeds through the designation of the function switches.

The meanings of the notations and variables are described below.

ℓ_1, ℓ_2	:	The lengths of the first and the second quadrupole elements of the triplet Q-lens, respectively. The length of the third elements is equal to that of the first one.
k_1, k_2	:	The field parameters of the first and the second elements of the triplet Q-lens, respectively. The parameter of the third element is taken to be equal to that of the first element.
k_{min}, k_{max}	:	The lower and upper limits, respectively, of the field parameter range, within which the optimum values are searched.
d_ℓ	:	The distance, in m, between the quadrupole elements.
Q_TYPE	:	This notation denotes the function of the Q-lens. If the Q-lens is of 'cdc' type, Q_TYPE = 'C', and if 'dcd' type, Q_TYPE = 'D'. Here the type 'cdc' designates the Q-lens whose transfer property for the $x-s$ plane is characterized as converging–diverging–converging, while the type 'dcd' as diverging–converging–diverging.
1st_APPROX	:	This notation indicates whether the intersecting point in the k_2-k_1

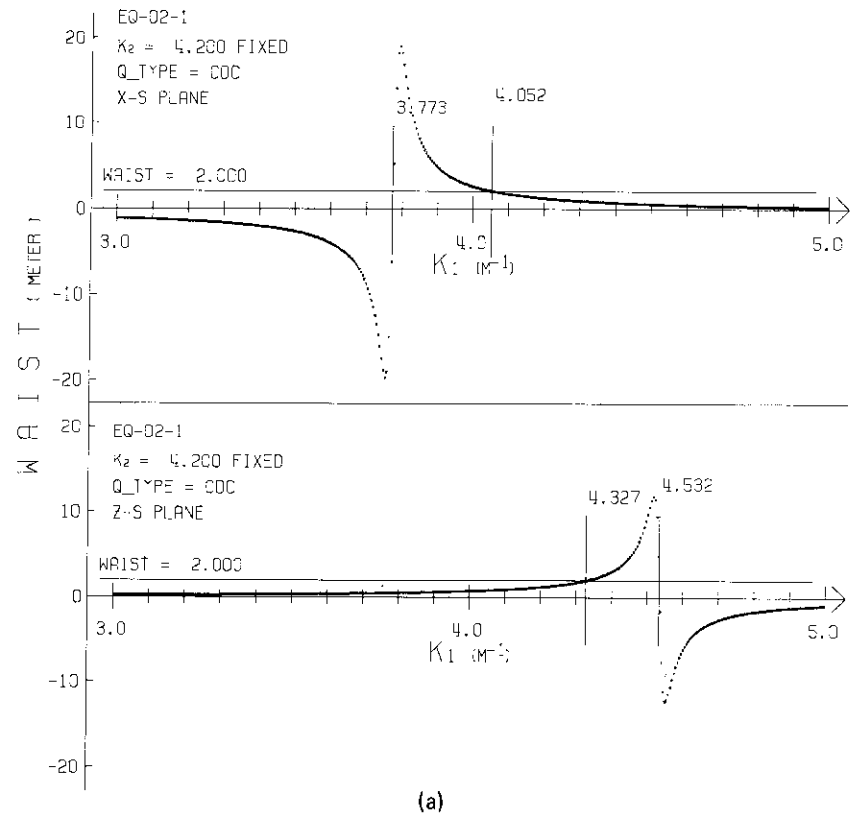

Fig. 27 Examples of waist-k_1 curves displayed on the CRT of MPS. (a) Calculated with a fixed k_2 value arbitrarily chosen, and (b) calculated with the k_2 value that gives the desired waists in both planes at the specific k_1 value. The parameters k_1 and k_2 are represented in unit of m^{-1} for convenience. The interval between every k_1 values, Δk_1, is taken to be 0.005 m^{-1}.

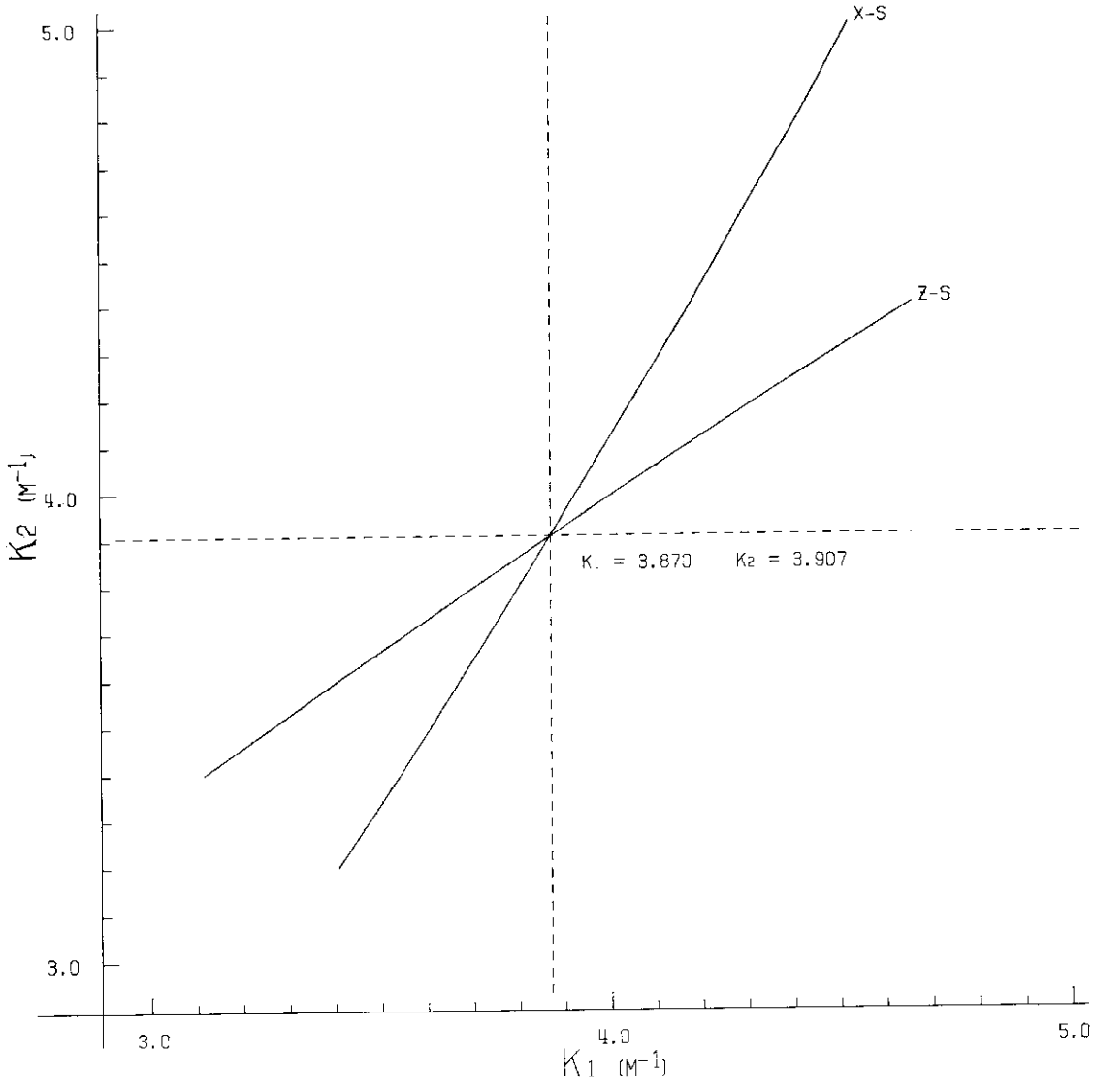

Fig. 28 The k_2-k_1 representation displayed on the CRT of MPS, related to the waist-k_1 curves shown in Fig. 27. The k_1 and k_2 values are represented in unit of m^{-1}.

representation exists or not.

WST_COIN,
K2_CHANGE,
C2_CHANGE
and W0_MODIFY : All of these notations are initialized to be 'NO'. They are turned to 'YES' through the function switches associated with the subroutine DISPLAY_LENS as described in section 8.2.6.

IWX_SELECT
and IWZ_SELECT : Two numbers to designate the crossing points of the waist-k_1 curves over the $W=W_0$ lines. See text.

(I)-2 : Method 2.

Fig. 29 shows the flow of the method 2. The execution starts with $k_1=k_2=k_{min}$ to obtain the first approximate values in the way described in section 7.3. The process of the calculation is illustrated in **Fig. 15**. When the $\bar{k}_1^{(w)}$ and $\bar{k}_2^{(w)}$ are found, both of APPR1 and APPR2 are 'YES' as shown in **Fig. 29**, and the execution proceeds to the successive approximation. The solution of the successive approximation is checked whether it satisfies the Eqs.(7.2.1) and (7.2.2). If both are satisfied, the execution returns to the MAIN routine. If not, the execution continues to obtain other $\bar{k}_1^{(w)}-\bar{k}_2^{(w)}$ pair.

Three situations, in which no $k_1^{(w)}$ and $k_2^{(w)}$ values are obtained, are distinguished through the notation APPR1 after the searching process over the whole region of k_1 and k_2 values under consideration. If APPR1 is 'NO', the situation is designated as 1, because it indicates that there are no crossing points for all of the waist-k_1 curves in both planes. If APPR1 is 'YES', the situation is designated as 2 or 3, because there are some crossing points at least in one plane, possibly in both planes simultaneously, as is seen in **Fig. 29**. In this case, the execution proceeds, assuming tentatively that the situation is designated as 3. If still no $k_1^{(w)}$ and $k_2^{(w)}$ values are obtained in spite of the release of the condition Eq.(7.2.2), the situation is concluded as 2.

The W_0 value is modified in the situations 1 and 2 as follows.

In the situation 1, the waist values are always larger than or always smaller than W_0 in both planes. The quantity ΔW_1 or ΔW_2 is calculated as

$$\Delta W_1 = Max\,(W_{min,x}-W_0,\ W_{min,z}-W_0) \tag{8.2.4.2}$$

in the former case, or

$$\Delta W_2 = Max\,(W_0-W_{max,x},\ W_0-W_{max,z}) \tag{8.2.4.3}$$

in the latter case. Here, $W_{min,x}$ and $W_{min,z}$ are the minimum values of the waist locations in the respective planes formed by all of the k_1-k_2 pairs in the whole region, while $W_{max,x}$ and $W_{max,z}$ are the maximum values. They are prepared in the subroutine WAIST_CROSS. The new W_0 value is given by

$$W_{0,new}^{(1)} = \begin{cases} W_0+(\Delta W_1+\delta W) & \text{for the former case} \\ W_0-(\Delta W_2+\delta W) & \text{for the latter case,} \end{cases} \tag{8.2.4.4}$$

where δW is taken to be 0.1 (m) in the present calculation.

In the situation 2, the $k_1^{(w)}$ and $k_2^{(w)}$ values can not be obtained on account of being no intersecting points in the k_2-k_1 representation. If the Q-lens is of the type 'cdc', the step of k_1 in the course of the searching process, as is shown in **Fig. 15**, encounters first the curve for the $x-s$ plane in the k_2-k_1 representation, and if the Q-lens is of the type 'dcd', it encounters first the curve for the $z-s$ plane[21]. After that, the k_1 step follows the curve, by crossing it rightward and upward, calculating also the waist locations, $W_t(k_1, k_2)$, on another plane

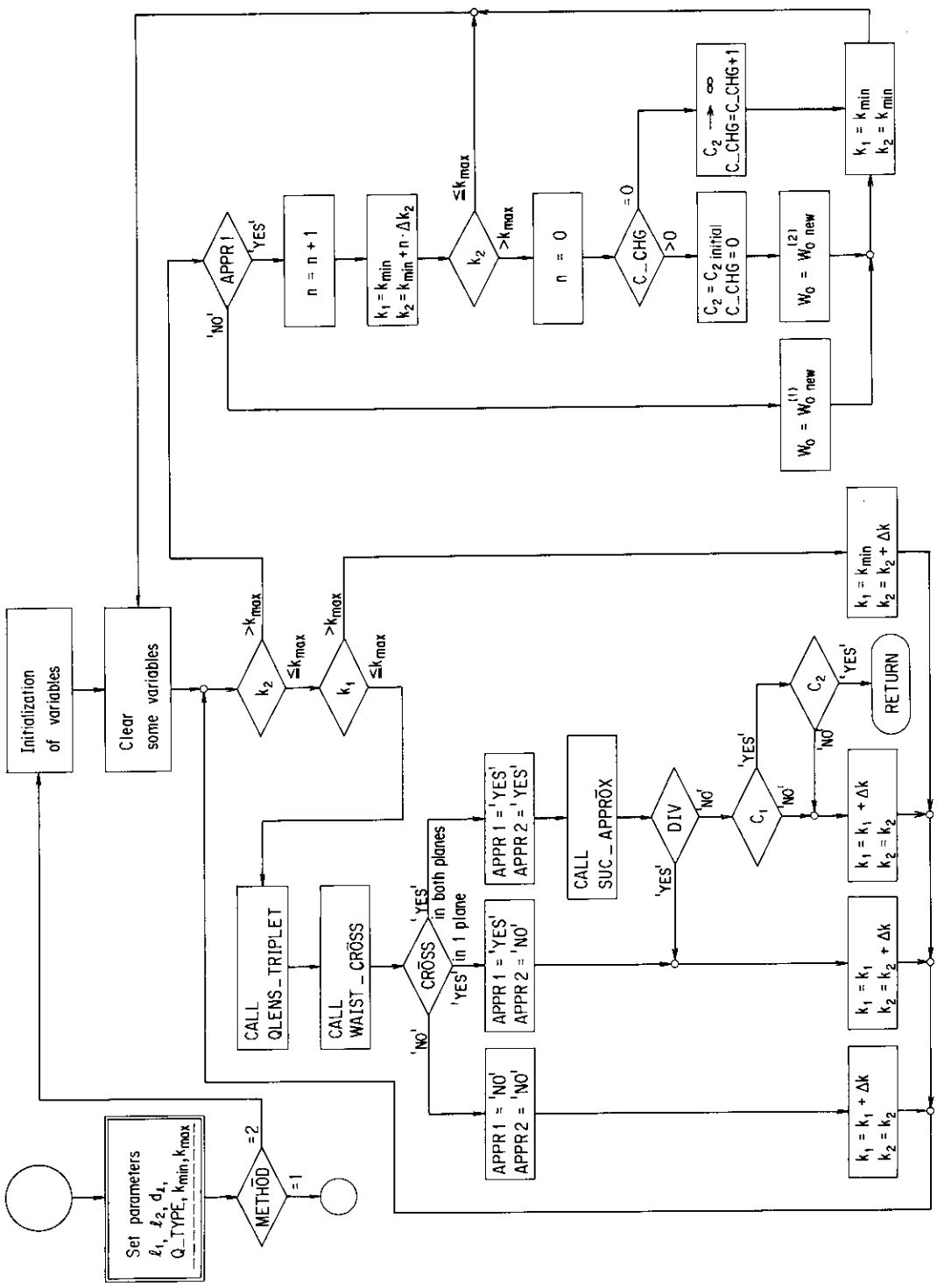

Fig. 29 Computational flow of the subroutine QLENS_TRAJ, for searching for the field parameters of Q-lenses, by means of the method 2.

at every k_1 steps. Here, t denotes z in case of 'cdc' type, while x in case of 'dcd' type. If the quantity

$$\Delta W=|W_0-W_t(k_1, k_2)| \tag{8.2.4.5}$$

is minimized at $W_t=\overline{W}_t$ with a k_1-k_2 pair, $\overline{W}_t$ is regarded as the nearest waist location to that of the desired waist on the plane t. The W_0 value in the present situation is modified to

$$W_{0,new}^{(w)}=\overline{W}_t. \tag{8.2.4.6}$$

For the situation 3, C_2 is changed to infinity in the same manner as in the method 1. The notations and variables in **Fig. 29** are explained below.

$\ell_1, \ell_2, d_\ell, k_1$

k_2, k_{min}, k_{max}

and

Q_TYPE : Same as those described for the method 1.

CROSS : This notation indicates whether the $\bar{k}_1^{(w)}$--$\bar{k}_2^{(w)}$ pair, that satisfies Eq.(7.3.1) in each plane, is found or not. If it satisfies Eq.(7.3.2) in both planes, APPR1 and APPR2 are set to be 'YES' and the executions proceeds to the successive approximation. If it satisfies in one plane but not in another, only APPR1 is set to be 'YES'. If no pairs in both planes, both of APPR1 and APPR2 remain 'NO' as they have been initialized.

DIV : This notation is set to be 'YES', if the successive approximation diverges, while 'NO' if not.

C_1 and C_2 : These indicate whether the respective conditions of Eqs.(7,2.1) and (7.2.2) are satisfied or not. If 'YES', satisfied, if 'NO', not satisfied.

n : This variable determines the starting points of the k_1 and k_2 values in the searching process, as is shown in **Fig. 15**. Initially, it is 0.

(II) QLENS_TRIPLET:

This subroutine transforms the β, α and γ values in the triplet Q-lens for both planes, being given those values at its entrance. The flow of the execution is shown in **Fig. 30**.

It is composed of two executional branches. One is used in the searching process, in which the notation TRJ is 'NO'. The other is used after the decision of the optimum parameters $k_1^{(w)}$ and $k_2^{(w)}$, in which TRJ is 'YES'. In the former branch, if the other optical devices are included between the Q-lens and the desired waist, the transformation of the β, α and γ values is extended to the exit of the last optical device. In the latter branch, however, it is carried out for the individual device separately, that is, the execution here is only for the Q-lens under consideration.

The notations and variables in the figure are explained as follows.

ℓ_i, k_i : The length, in m, and the field parameter, in m^{-1}, respectively, of the i th quadrupole element.

Q_TYPE : Same as described in section 8.2.4 (I).

Trajectory : The calculation of the beam envelope trajectory in the quadrupole element.

d_ℓ : The distance, in m, between the quadrupole elements.

OTHER_ELMT : This notation indicates whether some optical devices are between the Q-lens and the waist.

D1, D2 and δ : These variables are used to partition the length of the quadrupole element, in the same manner as that illustrated in section 8.2.2 (I) for the length of the field free drift space.

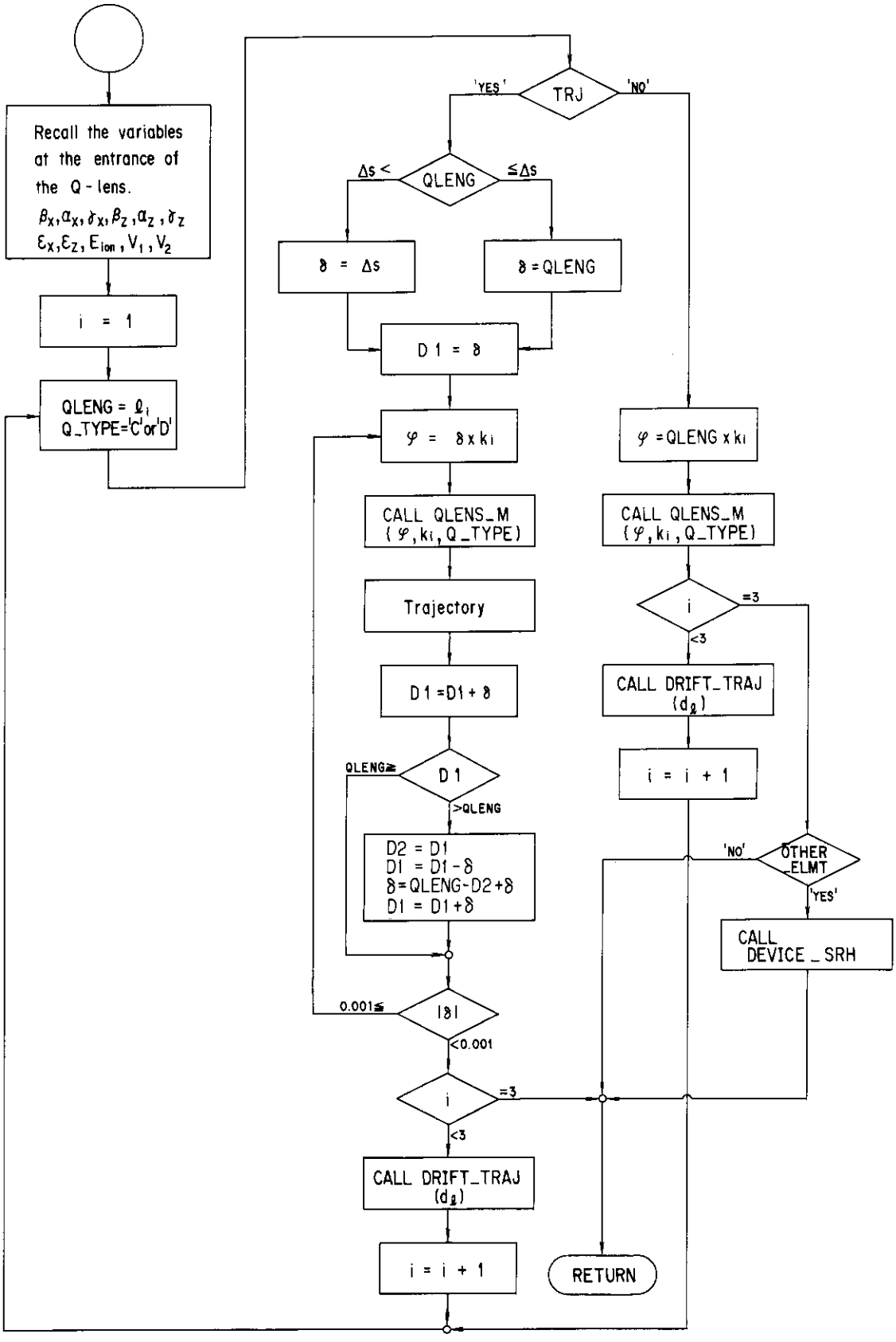

Fig. 30 Computational flow of the subroutine QLENS_TRIPLET, for calculating the beam envelope trajectory in the triplet Q-lens. The quantities concerning the lengths of the Q-lens elements and the drift spaces are represented in unit of m.

(III) WAIST_CURVE:

This subroutine is utilized in the flow of the method 1, in order to yeild the waist-k_1 curves. As is shown in **Fig. 26**, the β, α and γ values calculated in the subroutine QLENS_TRIPLET are used in this subroutine. Its executional flow is shown in **Fig. 31**.

The waist location W_t and a variable W_CROSS_t are calculated, where subcript t indicates x or z. A series of W_t values calculated with the successive k_1 under a fixed k_2 forms the waist-k_1 curve. A variable WW_t is the waist value calculated with the preceding k_1, so that W_CROSS_t is negative when the waist-k_1 curve crosses over the desired waist line $W=W_0$. The k_1 values at the crossing points are approximated as $AK1\_W(IW_t) = (2k_1-\Delta k_1)/2$. When WST_COIN is 'DONE' (refer to section 8.2.6 (I)), $AK1\_W(IW_t) = k_1^{(w)}$, which has been obtained through the successive approximation described in section 7.

At the end of the subroutine, the numerical values of W_x and W_z are modified to those suitable for being displayed on the CRT.

The meanings of the notations and variables are as follows.

IK : The W_x and W_z values are numbered in order of this number and constitute the waist-k_1 curves, ranging from IK = 1 to $((k_{max}-k_{min})/\Delta k_1)+1$.

IW_t : The crossing points of the waist-k_1 curves are numbered in order of this number.

WST_COIN : Same as described in section 8.2.6.

K2_CHANGE : Same as described in sections 8.2.4 (I)-1 and 8.2.6.

$AK1\_W(IW_t)$: The k_1 value at the IW_tth crossing point of the waist-k_1 curve.

IW_t_SELECT : This notation represents IWX_SELECT or IWZ_SELECT, according to $t=x$ or z, respectively.

(IV) WAIST_K:

This subroutine arranges the k_1-k_2 pairs, which give the crossing points of the waist-k_1 curves, in order of IW_t mentioned above. The k_2-k_1 representation as shown in **Fig. 13** is made on the basis of this arrangement.

(V) WAIST_LSF:

This subroutine obtains the k_2-k_1 representation Eq.(7.3.1), by means of the method of least squares. The intersecting point of the curves is also derived in this subroutine, which indicates the first approximate values $\bar{k}_1^{(w)}$ and $\bar{k}_2^{(w)}$ in the method 1.

(VI) WAIST_CROSS:

The first approximate values $\bar{k}_1^{(w)}$ and $\bar{k}_2^{(w)}$ in the method 2 are obtained through this subroutine. They are derived on the basis of the relation Eq.(7.3.2), and the procedure described in section 7.3

(VII) SUC_APPROX:

This subroutine performs the successive approximation described in section 7.1, by using the $\bar{k}_1^{(w)}$ and $\bar{k}_2^{(w)}$ obtained as the first approximate values. The examination of the resultant $k_1^{(w)}$ and $k_2^{(w)}$ values, whether they satisfy the conditions Eqs.(7.2.1) and (7.2.2), is also made in this subroutine.

Among seven subroutines mentioned above, QLENS_TRAJ is the main subroutine in the file QLENS and controls the executions in which the Q-lenses take parts. Those of WAIST_CURVE, WAIST_K and WAIST_ LSF are used for the method 1, WAIST_CROSS is for the method 2 and QLENS_TRIPLET and SUC_APPROX are for both.

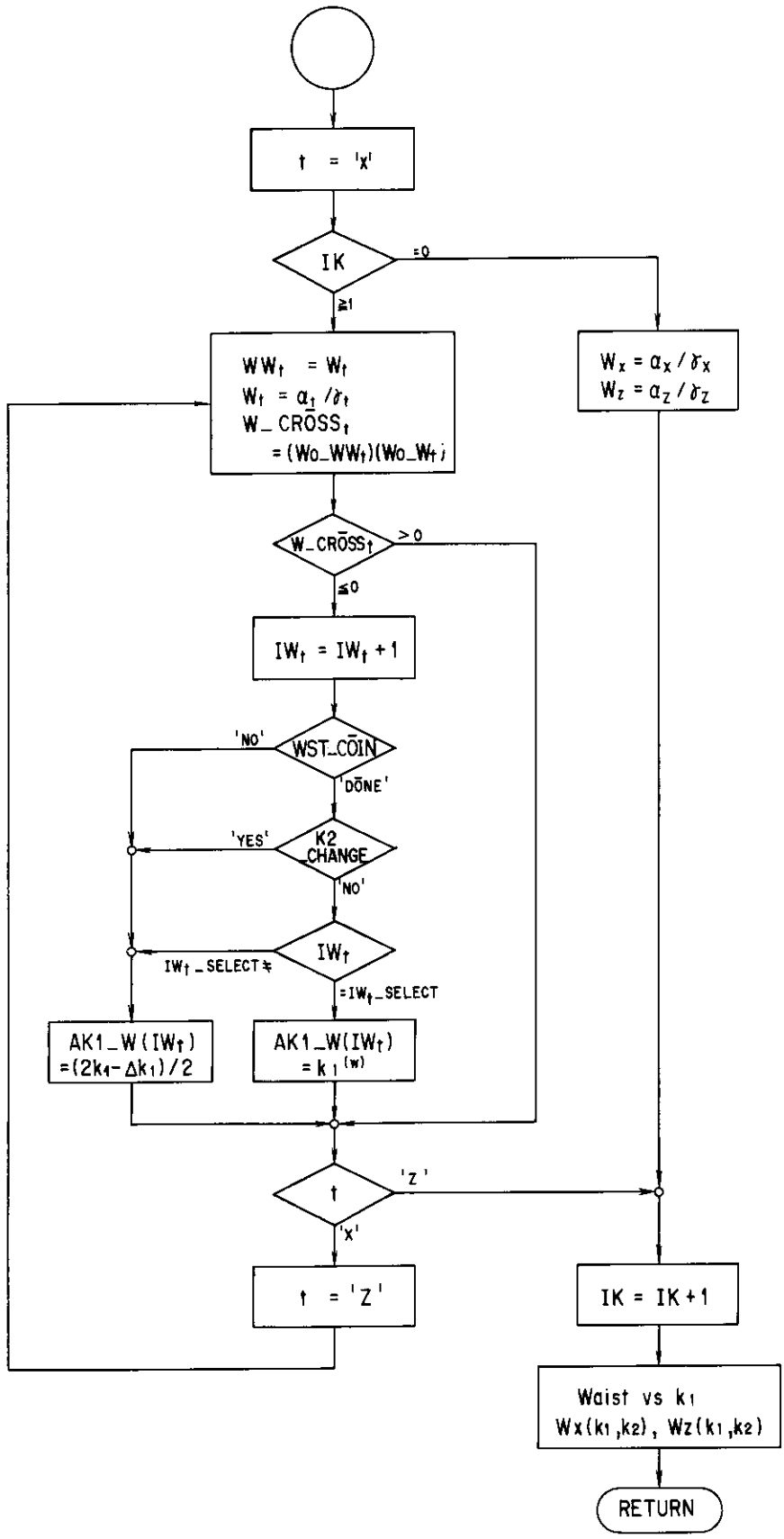

Fig. 31 Computational flow of the subroutine WAIST_CURVE, for calculating the waist-k_1 curves.

8.2.5 DISPLAY

The file DISPLAY is used for displaying on the CRT the beam envelope trajectory and the arrangement of the various optical devices provided in the accelerator system. The main input data, based on which the calculation is performed, are also displayed in the same picture.

(I) DISPLAY_TRAJ:

This is the only subroutine that constitutes the file DISPLAY. Its computational flow is shown in **Figs. 32(a)** and **(b)**. It is composed of three parts, as seen in **Fig. 32(a)**. One is that for the initialization of MPS, which is made at the beginning of the computation as mentioned in the step 2° in section 8.1. This part is used only once throughout the computation process. The second is that depicts on the CRT the arrangement of the optical devices, as well as the input data used in the calculation. The last is that displays the beam envelope trajectory which is renewed when the execution of each optical device is finished. On account of the execution in this part, the aspect of the trajectory is observed from the starting point to the target, just as extending through one device after another.

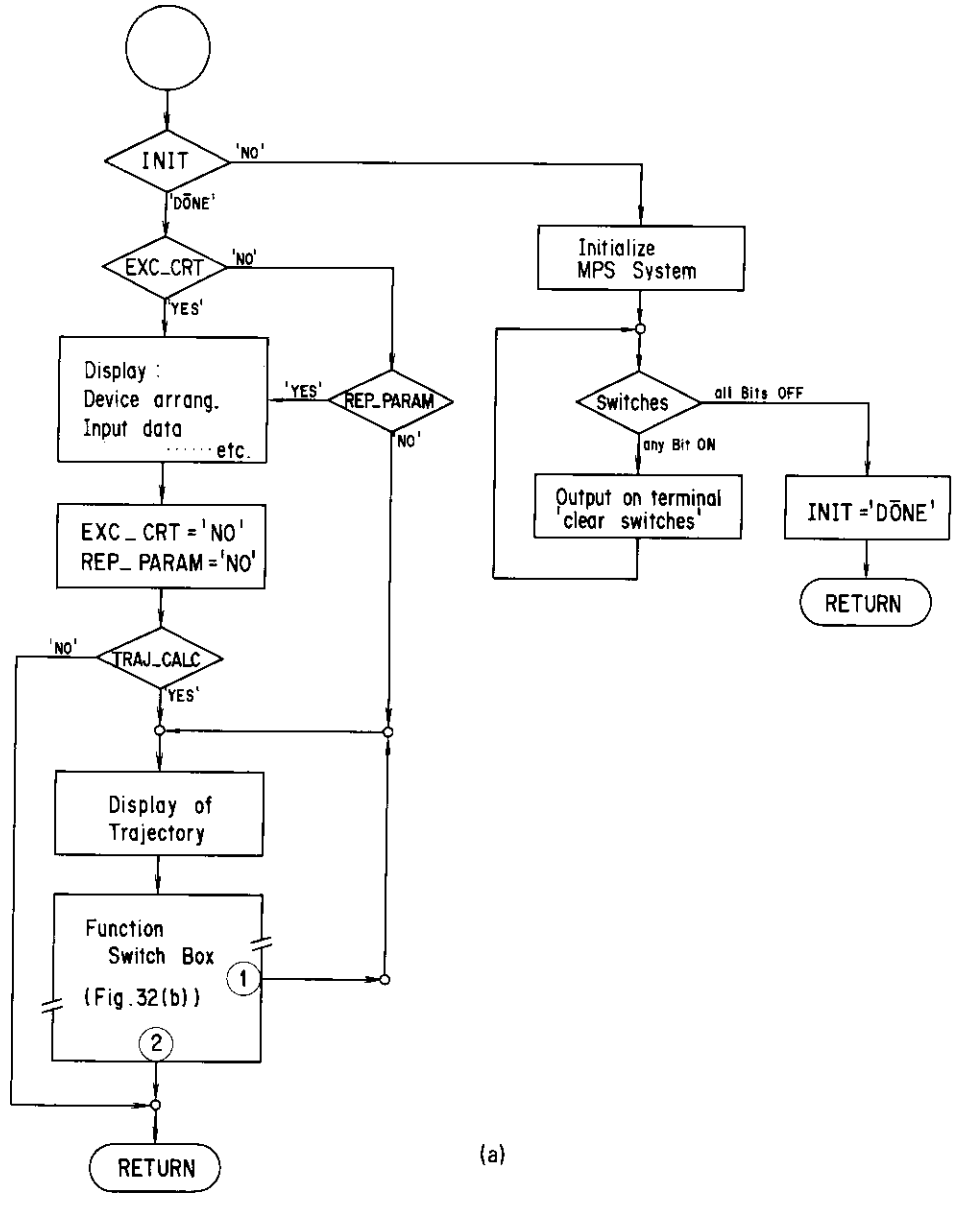

Fig. 32(a) Computational flow of the subroutine DISPLAY_TRAJ, for displaying the beam envelope trajectory.

Another important feature in the last part is the application of the function switch box connected to MPS. It has sixteen switches on a board and can represent 16 bits numbers by setting the switches ON or OFF. Each switch, therefore, may be called as 'bit'. To each bit-ON state, the specific function can be assigned under the program control. In the present code, one-bit-ON states are utilized, namely, the states of more than one bit ON simultaneously are excluded. The nine of the sixteen bit-ON states are used to direct the flow to the subsequent execution, which are described in **Table 2**.

When the searching process for the optimum Q-lens parameters is performed by means of the method 1, the advance of the trajectory on the CRT pauses at the entrances of every Q-lenses. At that time, the computational flow enters the present subroutine *before* QLENS_TRAJ and goes round within the last part, waiting for the indication through the bit 4. When this bit is ON, the flow exits the subroutine and enters QLENS_TRAJ, in order to execute the calculation illustrated in **Fig. 26**. During the execution thereafter, the display process is controlled by the subroutine DISPLAY_LENS. After the optimum Q-lens parameters are obtained, the flow returns to this subroutine and the execution proceeds to display the beam trajectory again.

If the searching process is carried out by means of the method 2, the flow enters the present subroutine *after* QLENS_TRAJ, where the calculation illustrated in **Fig. 29** is performed. It passes through the last part of the present subroutine only displaying the trajectory in the Q-lens under consideration, calculated with the optimum parameters obtained in QLENS_TRAJ.

After the calculation for all of the optical devices is finished, the execution continues to display the whole trajectory on the CRT with the present subroutine, until the bit 15 is set to be ON so as to terminate the computation. This state corresponds to the step 10° in section 8.1.

Table 2 Functions of individual function switches in the subroutine DISPLAY_TRAJ

Bit	Octal number	Functions
0	1	The menu of the switch box is shown on the terminal, where the indication of whole bit-ON states are described.
1	2	The picture displayed on the CRT is hardcopied.
3	10	Two methods of searching for the Q-lens parameters, described in section 7.3 and 8.2.4, can be exchanged with each other during the execution.
4	20	The picture of the trajectory on the CRT is exchanged to that of the waist-k_1 curves.
12	10000	The trajectory being displayed is stored numerically in the file SPC_N.DAT in the disk. The number N is given according to the order of the storage. This file is deleted at the end of the current computation.
13	20000	The trajectory stored formerly in the disk is replayed on the CRT. The number N that specifies the data file is required to be given through the terminal keyboard.
14	40000	When the next calculation is required with the input data different from those used in the current calculation, this bit should be ON. After receiving new input data through the terminal keyboard, the new calculation starts.
15	100000	If this bit ON after the calculation has been completed, the computation is brought to the end and the trajectory displayed on the CRT disappears.

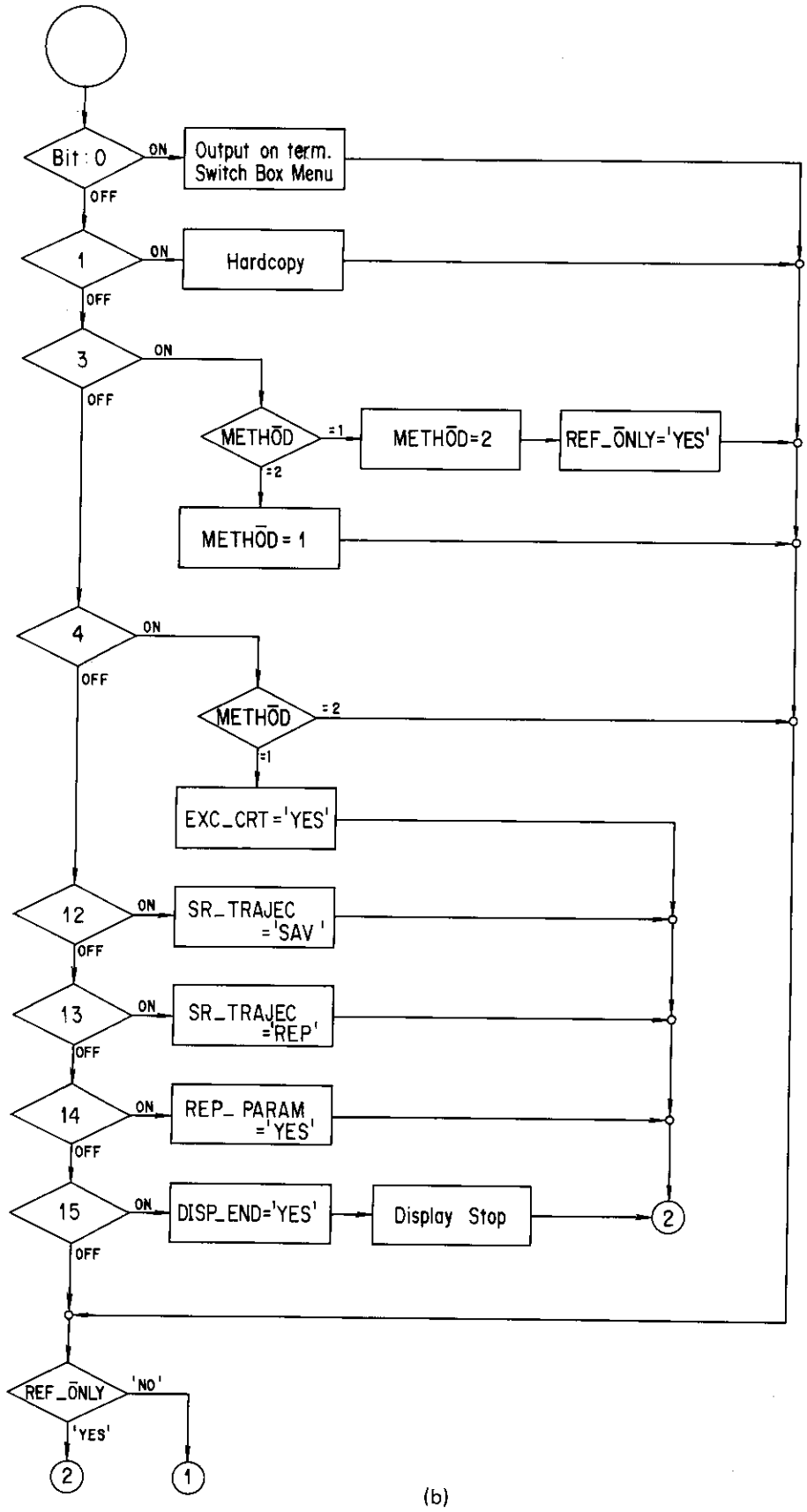

(b)

Fig. 32(b) Schematic diagram of the flow in the function switch box associated with the subroutine DISPLAY_TRAJ. This flow should be inserted in Fig.32(a).

The program is written utilizing many subroutines peculiar to and housed in MPS. The meanings of the notation and variables in **Figs. 32(a)** and **(b)** are as follows.

INIT : This notation indicates whether the initialization of MPS has been done or not yet.

EXC_CRT : This notation indicates whether the flow should pass through the second part of the subroutine or not. It is initialized to be 'YES', and turned to 'NO' when the flow has once passed through that part. It is turned to 'YES' again, if the flow exits and moves to the subroutine DISPLAY_LENS in order to display the waist-k_1 curves. When returns to this subroutine, the flow enters the second part and restore the previous picture on the CRT.

TRAJ_CALC : The arrangement of the optical devices is displayed through the second part of this subroutine, prior to the start of the trajectory calculation. The notation TRAJ_CALC is 'YES', if the calculation of the trajectory has already begun, while 'NO' if not yet. In case that the next calculation is required with the different input data, this notation is turned again to 'NO' in the MAIN routine.

REF_ONLY : This notation indicates whether the flow should pass through the subroutine directly (YES), or should go round within it (NO), waiting for the indication through any bit. Initially, it is set to be 'YES'.

SR_TRAJEC, REP_PARAM and DISP_END : To these notations, the characteristic values shown are given according to the respective bit ON states described in **Table 2**. They control the direction of the flow after its returning to the MAIN routine. Their meanings are illustrated in section 8.4.

8.2.6 DISLENS

The file DISLENS consists of the subroutine DISPLAY_LENS which controls the displays of the waist-k_1 curves and their related matters.

(I) DISPLAY_LENS:

This subroutine is called only from the subroutine QLENS_TRAJ. When the searching process for the Q-lens parameters is carried out by means of the method 1, the advance of the trajectory on the CRT pauses at the entrance of the Q-lenses. By turning on the function switch, the flow enters QLENS_TRAJ and calls the present subroutine DISPLAY_LENS.

Its flow is shown in **Figs. 33(a)** and **(b)**. As is seen in **Fig. 33(a)**, it displays four kinds of pictures, namely, the waist-k_1 curve for the $x-s$ plane, the waist-k_1 curve for the $z-s$ plane, those for both planes at the same time, and the k_2-k_1 representation. The function switch box is associated with this subroutine anew, and the pictures mentioned above are replaced by turns through the indication of these switches. The assignment of the execution to the individual switch-ON states are described in **Table 3**.

The meanings of the notations and variables in **Figs. 33(a)** and **(b)** are as follows.

K2_VS_K1 : This notation indicates whether the k_2-k_1 representation should be displayed or not. Initialized to be 'NO'.

PLANE : This notation indicates the kind of the picture that should be displayed. If it is 'X', the waist-k_1 curve for the $x-s$ plane, and if 'Z', that for the $z-s$ plane is displayed. If 'XZ', the curves for both

planes at the same time. **Figs. 27(a)** and **(b)** are the pictures designated by PLANE = 'XZ'.

WST_COIN : This notation is initialized to be 'NO', and is turned to 'YES' when the searching process starts. It is changed to 'DONE' in QLENS_TRAJ when the desired $k_1^{(w)}-k_2^{(w)}$ pair is obtained.

C2_MODIFY, W0_MODIFY and K2_CHANGE : To these notations, the characteristic values shown are given through the respective bits ON. They control the direction of the flow after its returning to the subroutine QLENS_TRAJ.

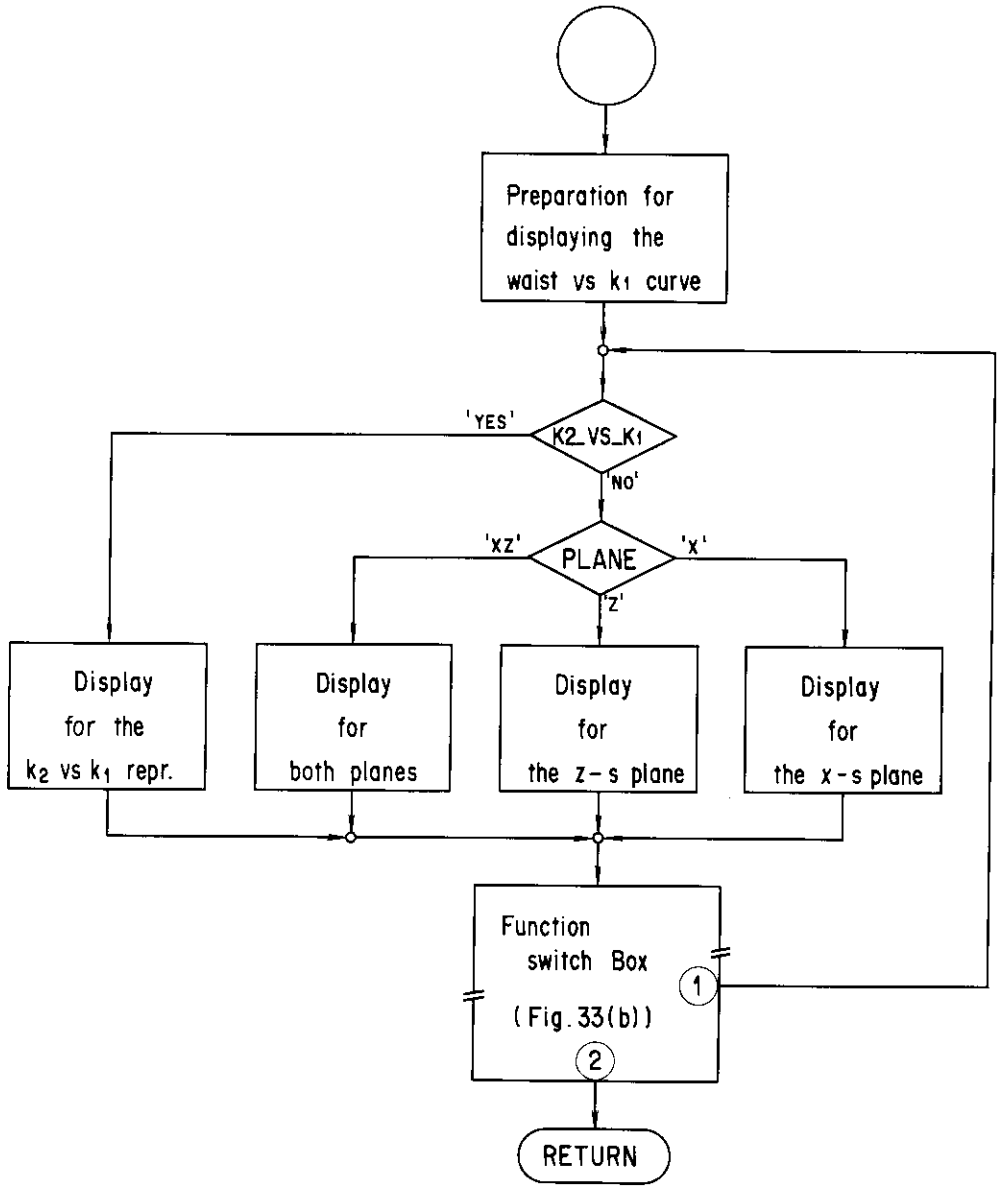

(a)

Fig. 33(a) Computational flow of the subroutine DISPLAY_LENS, for displaying the waist-k_1 curve and its relatives.

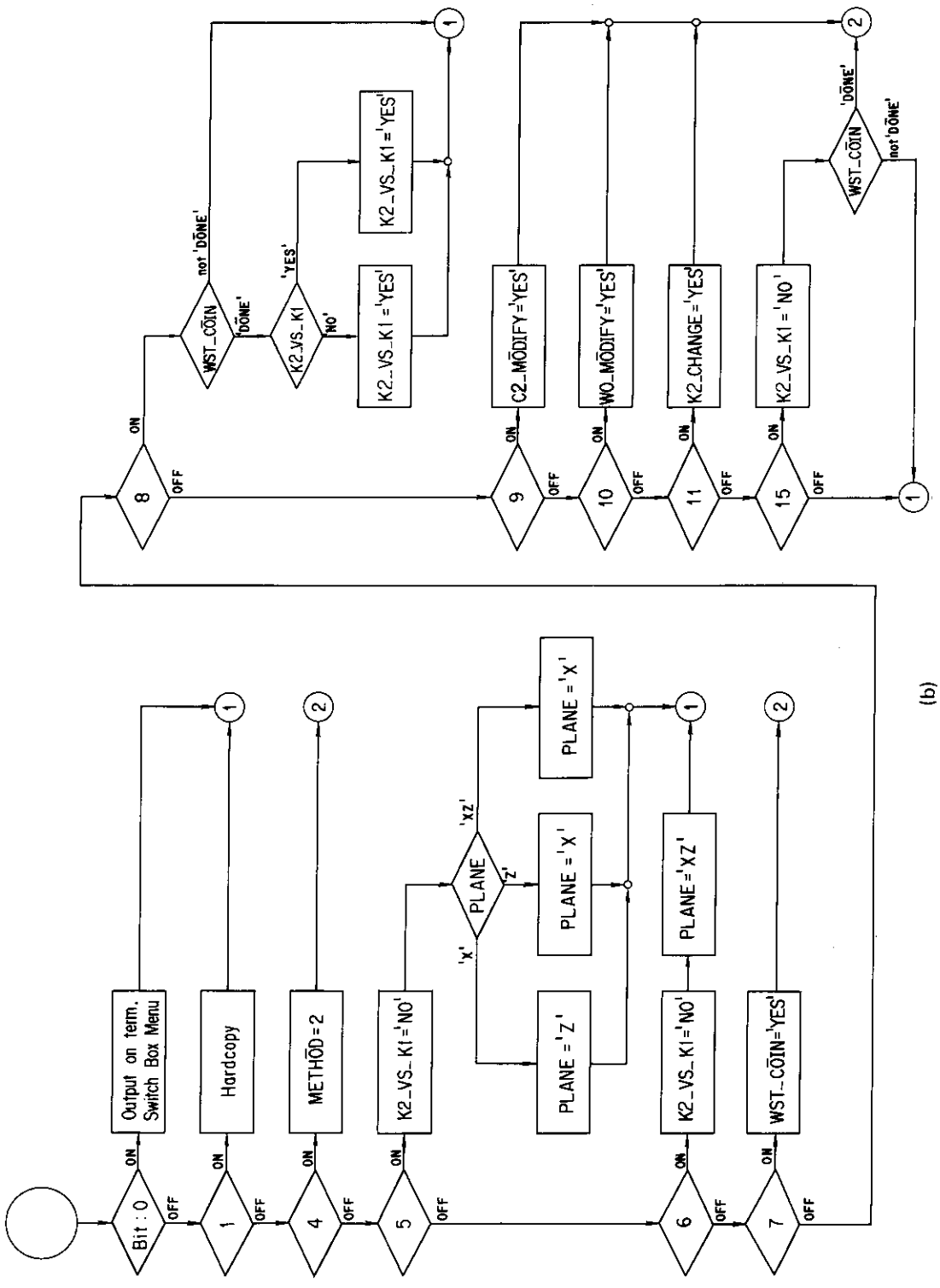

Fig. 33(b) Schematic diagram of the flow in the function switch box associated with the subroutine DISPLAY_LENS. This flow should be inserted in Fig. 33(a).

Table 3 Functions of individual function switches in the subroutine DISPLAY_LENS

Bit	Octal number	Functions
0	1	The menu of the switch box is shown on the terminal, where the indication of whole bit-ON states are described.
1	2	The picture displayed on the CRT is hardcopied.
4	20	The method of searching for the Q-lens parameters is exchanged from the method 1 to the method 2. The picture of the waist-k_1 curve or k_1-k_2 representation is replaced with that of the beam trajectory and the calculation proceeds.
5	40	The picture being displayed is exchanged with that of the waist-k_1 curve for the $x-s$ or $z-s$ plane, according to the current status of the notation PLANE.
6	100	The picture being displayed is exchanged with that of the waist-k_1 curves for both planes.
7	200	The searching process for the Q-lens parameters starts. After the process, the waist-k_1 curves with the optimum k_2 value obtained are displayed.
8	400	If the optimum parameters have been determined, the picture is replaced with the k_2-k_1 representation.
9	1000	The constant C_2 for Eq.(7.2.2) is exchanged. The new C_2 value is given through the terminal keyboard.
10	2000	The desired waist location W_0 is exchanged. The new W_0 value is given through the terminal keyboard.
11	4000	The calculation of the waist-k_1 curve is performed with different k_2 value. The new k_2 value is given through the terminal keyboard.
15	100000	After the calculation and examination of the waist-k_1 curves, the flow returns to the calculation of the beam trajectory.

8.3 Data files

8.3.1 INITIAL.DAT:

The data file INITIAL.DAT containes the following values;

1) the initial values of the beam emittance ellipse parameters, β_x, α_x, γ_x, β_z, α_z and γ_z, and corresponding beam emittance, ε_x and ε_z,
2) the initial energy of ions, E_INI in MV, at which ions have the initial parameter values described above,
3) the voltage limit imposed on the acceleration tube units, V_{limit} in MV, at the accelerator operation time, and
4) the mass and atomic numbers of the foil and gas stripper materials, A_f, Z_f, A_g and Z_g, respectively, and the length of the gas stripper canal, L_g, through which the gas flows.

These are written with the format as follows.

'(4E12.5)' BETA_X, ALPHA_X, GAMMA_X, EMITTANCE_X
'(4E12.5)' BETA_Z, ALPHA_Z, GAMMA_Z, EMITTANCE_Z
'(2F6.3)' E_INI, V_LIMIT

'(5F6.3)' STR_F_A, STR_F_Z, STR_G_A, STR_G_Z, STR_G_L

The notations indicate the respective variables described above+.

8.3.2 TANDEM.DAT:

In the data file TANDEM.DAT, the attributes and parameters of the optical devices are written, in order along the beam line from the starting point of ions to the energy analyzing magnet after the exit of the H.E. acceleration part. The eight kinds of devices can be contained in this file. They are acceleration tubes, bending magnets, drift spaces, electrostatic and magnetic Q-lenses, stripper systems, variable aperture systems and double slit system.

These are written in the file in a series of the following form for the individual devices,

```
'(A3, 2A1, A20)' DEVICE, A(NDEV), B(NDEV), DEV_NAME(NDEV)
'(7F10.5)'       C(NDEV), D(NDEV), E(NDEV), F(NDEV), G(NDEV), H(NDEV),
                 P(NDEV)
```

They are read in the subroutine DEVICE_ARR, being given the number NDEV to each of them as the serial number. Here, DEVICE represents one of the devices mentioned above, to which the device notation described below is assigned, DEV_NAME is its name given conveniently in the JAERI tandem accelerator system. The notations A and B are its attributes and C through P are its parameters. They are read as such symbolic notations in the subroutine DEVICE_ARR, and are related to the specific meanings and quantities for the individual devices in the MAIN routine, at the calculation of the beam trajectory (refer to section 8.4).

The device notations are explained below, together with the notations of the attributes and parameters related to them.

1) DEVICE = 'ACC' : Accelerator tube
   - A : It is read as a notation TUBE. If it is 'M', the acceleration tube is the main tube, and if 'P', the pre-acceleration tube.
   - D : The length of the acceleration tube unit.
   - E : The aperture radius of the tube unit.
   - F : The number of the acceleration tube units included in a section.
   - G : The length of the field free drift spaces between the tube units.
2) DEVICE = 'BEN' : Bending magnet
   - A : It is read as a notation BEN_PLANE. If it is 'X', the bending plane is the $x-s$ plane. If 'Z' it is the $z-s$ plane.
   - C : The curvature of the beam axis in the magnet.
   - D : The bending angle.
   - E : The entry angle to the magnet.
   - F : The exit angle from the magnet.
   - G : The gap distance between the pole pieces.
3) DEVICE = 'DRI' : Drift space
   - C : The length of the field free drift space.
4) DEVICE = 'ELE' : Electrostatic Q-lens
   - A : The function of the Q-lens, read as a notation Q_TYPE. If it is denoted as 'C', the Q-lens is of 'cdc' type, while 'D', 'dcd' type.
   - B : It is read as a notation OTHER_ELMT. If it is 'Y', there are some optical

+ Ordinarily, their numerical values are STR_F_A = 12, STR_F_Z = 6, STR_G_A = 14, STR_G_Z = 7 and STR_G_L = 0.91 (m), for the JAERI tandem accelerator system.

devices between the Q-lens and the waist location. If 'N', there are no devices.

C : The length of the first quadrupole element.

D : The length of the second quadrupole element.

E : The length of the drift space between the quadrupole elements.

F : The aperture diameter of the quadrupole element.

G : The waist location measured from the exit of the last devices preceding the desired waist. It is represented as W_0 in sections 7 and 8.

H : The lower limit of the field parameter range, within which the optimum k_1 and k_2 values are searched. It corresponds to k_{min} in section 8.2.4.

P : The upper limit of the field parameter range. It corresponds to k_{max} in section 8.2.4.

5) DEVICE = 'MAG' : Magnetic Q-lens

The same as for 'ELE'.

6) DEVICE = 'STR' : Stripper system

The attributes and parameters of the stripper system are given in INITIAL. DAT. The notation that indicates the stripper type used in the current operation is given at the step 4° in section 8.1. It is 'F' for the foil stripper and 'G' for the gas stripper. The foil thickness or the gas pressure is given at the same time at the step 4°.

7) DEVICE = 'APT' : Variable aperture system

C : The radius of the variable aperture. The JAERI tandem accelerator system has six kinds of apertures whose radii are 2.4, 3.2, 4.75, 6.5, 9.5 and 12.5 mm.

8) DEVICE = 'SLT' : Slit system

C : The slit gap in the $x-s$ plane.

D : The slit gap in the $z-s$ plane.

Additional two device notations are used for DEVICE, although they do not represent any actual devices. One is the indication of the waist location, and the other is that of the end of the file.

9) DEVICE = 'WST' : The waist location

This notation indicates that the waist should be formed here.

10) DEVICE = '***' : The end of the file

Since no attributes and parameters are necessary for the last two DEVICE notations, the data A, B and so on that follow them are dummy.

8.3.3 The data files for the individual beam lines

The JAERI tandem accelerator system has five target rooms in which thirteen beam lines, in total, are extended. The ion beam is deflected by means of a bending magnet after the beam energy analyzing magnet, and enters one of the beam lines in the target rooms, according to the intent of the experimenters.

The devices along each beam line, after the analyzing magnet, are registered in the individual data files, in the same way as described for TANDEM.DAT. The files are named L1. DAT, H3.DAT and so on, after the names of the beam lines. Thus, if the experiment is made by using the beam through the beam line L1, for example, all of the devices which participate in the beam transport are described in the two files of TANDEM.DAT and L1.DAT.

The names of thirteen files for the individual beam lines are as follows.

L1.DAT, L2.DAT, L3.DAT, L4.DAT, H1.DAT, H2.DAT, H3.DAT, H4.DAT, H5.DAT, R1.DAT, R2.DAT, N1.DAT and N2.DAT.

8.3.4 E_LOSS_F.DAT and E_LOSS_G.DAT

In these files, the numerical values of the total stopping (MeV/(mg/cm^2)) of carbon foil and nitrogen gas are tabulated for the various ions in a wide range of energy (MeV/amu). The values are taken from the curves in Ref. 16, and the energy loss of the ions in the foil or gas stripper is estimated on the basis of these values by interpolation.

8.4 Calculation of the beam envelope trajectory

The calculation of the beam envelope trajectory is positioned as indicated in **Fig. 17**, and its own computational flow is shown in **Figs. 34(a)-(d)**.

Fig. 34(a) is a block diagram of the flow. According to the kind of the device, the direction of the flow branches off. The serial number, NDEV, and the total number, NDEV_TOTAL, of the devices are given in the subroutine DEVICE_ARR.

Fig. 34(b) shows the flow for the acceleration tube, the bending magnet and the drift space.

Fig. 34(c) is the flow for the electrostatic or magnetic Q-lens. There are three flows in accordance with the submodes assigned at the step 3° in section 8.1, namely, the submodes (1) that uses the Q-lens parameters given as the input data, (2) that searches for the Q-lens parameters by means of the method 1, and (3) that by means of the method 2.

In the case of (1), the Q-lens parameters are required when the trajectory, being displayed on the CRT, reaches the entrances of every Q-lenses. The potential on the poles or the number of ampare-turns per pole of each element is given for the electrostatic or the magnetic Q-lens, respectively, through the terminal keyboard. The Q-lens parameters, k_1 and k_2, are derived from these values, using Eq.(3.2.3) or Eq.(3.2.4). An example of the input process is shown in section 8.6.

In the flow of the method 1, it is characteristic that the execution is controlled by the designation of the function switches.

Fig. 34(d) shows the flow for the stripper system, the aperture system and the double slit system. The variables ISLT and IAPT are the numbers that specify the individual double slit and the variable aperture systems, respectively. The device notation 'WST' leads to yield the beam sizes, R_W_X(NW) and R_W_Z(NW), at the position where this notation is set. These values are given as

$$\text{R\_W\_X(NW)} = (\sqrt{\beta_x \cdot \varepsilon_x})_{\text{NWth waist}} \qquad (8.4.1)$$
$$\text{R\_W\_Z(NW)} = (\sqrt{\beta_z \cdot \varepsilon_z})_{\text{NWth waist}}.$$

They represent the beam size at the NWth waist, and are used to estimate the magnification, by comparing it with the beam size at the next waist. It corresponds to the left hand side of Eq.(7.2.2).

The notations in **Figs. 34(a)-(d)** are described below.

BETW_QW : This notation denotes whether the NDEVth device is between some Q-lens and a waist or not. If 'YES', the device parameters have already been read in the subroutine DEVICE_SRH, together with those of other devices in the same Q-lens–waist region.

GIVEN_Q_PARAM : This notation designates which submode is chosen in the execution. If it is 'YES', the calculation is carried out with the Q-lens parameters given as the input data for the individual Q-lenses. If 'NO', the optimum parameters are searched.

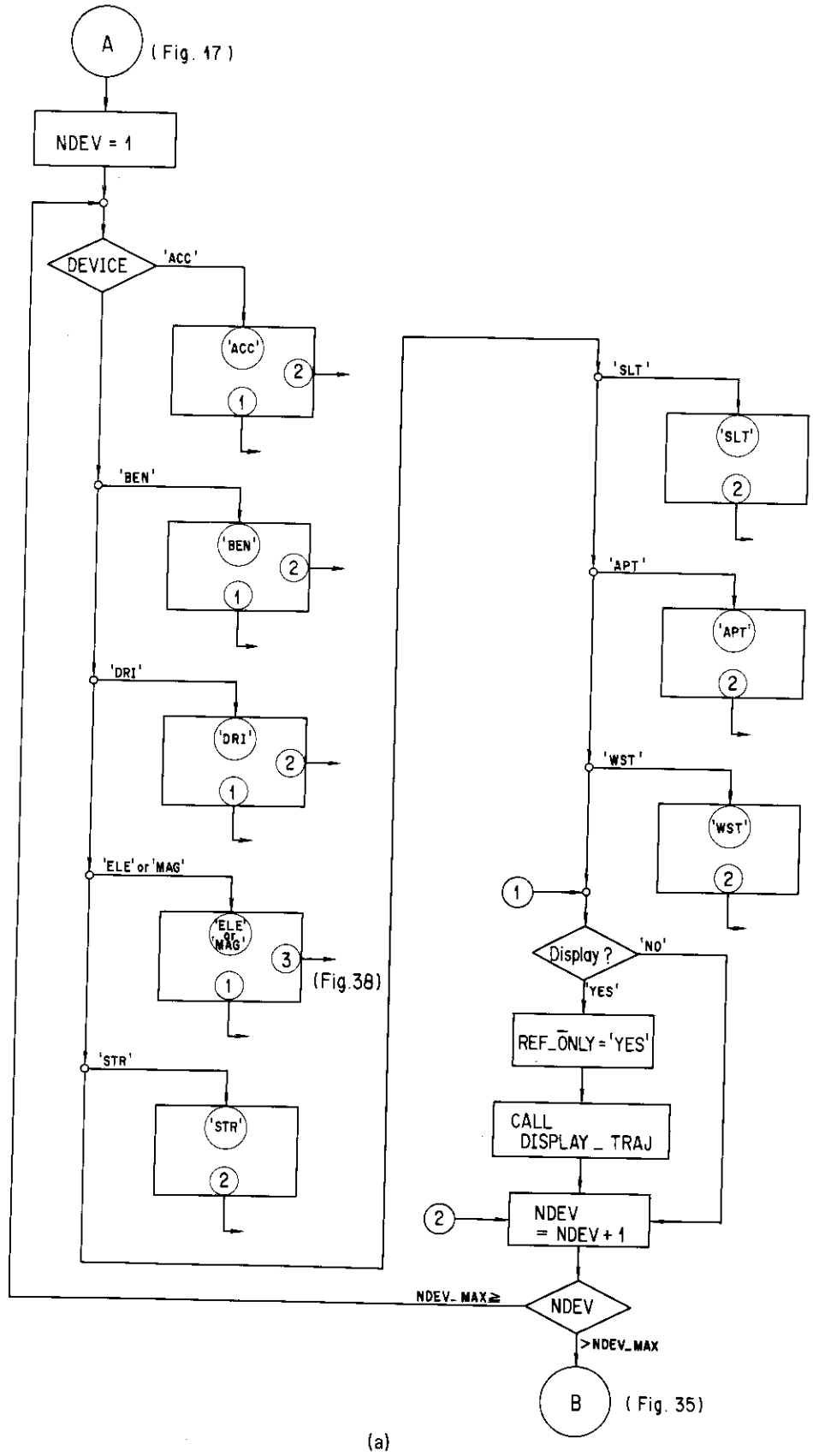

Fig. 34(a) Block diagram of the flow for calculating and displaying the trajectories, obtained in the individual devices. All of the flows in Figs. 34(a), (b), (c) and (d) should be inserted in the step 9° in Fig. 17.

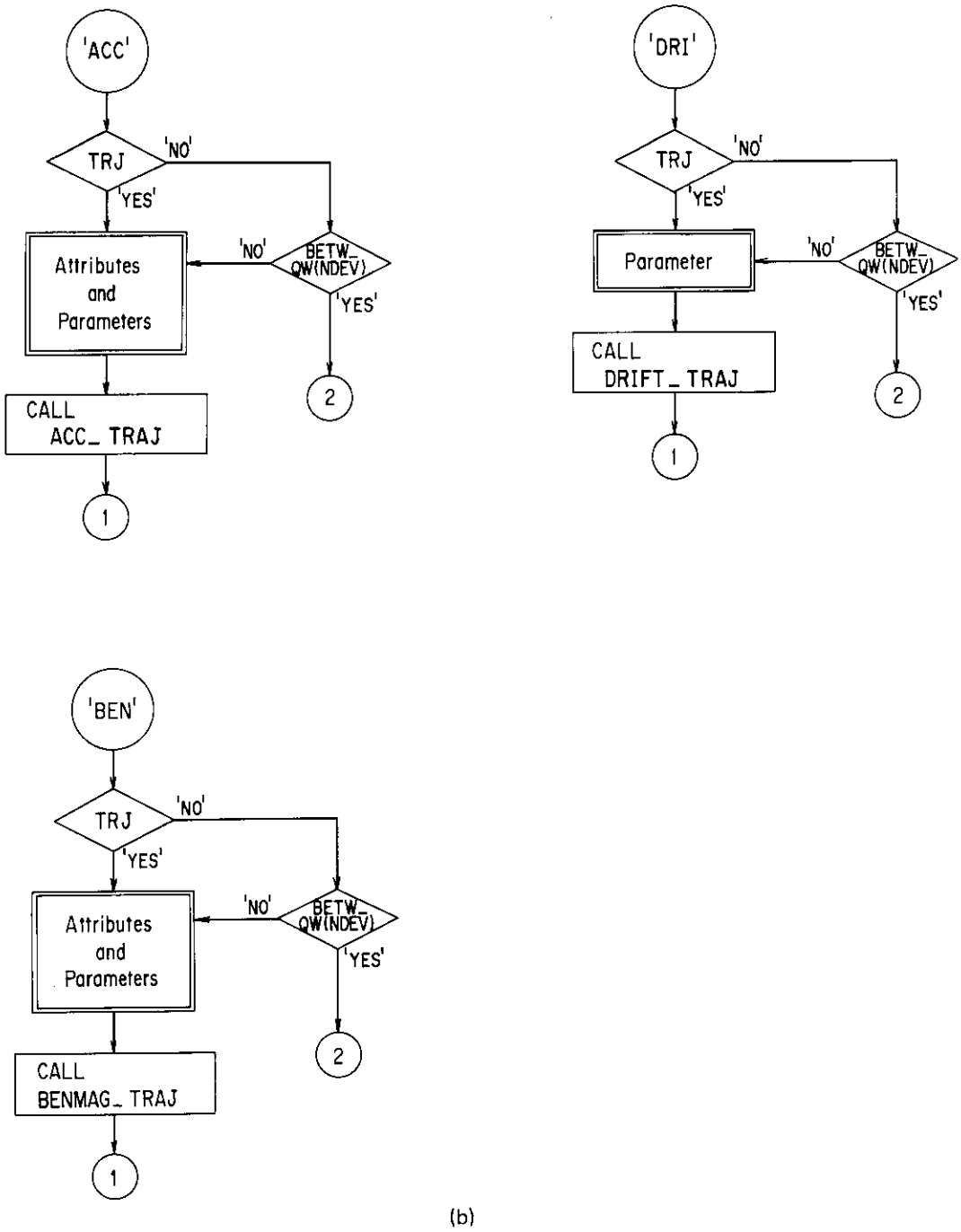

(b)

Fig. 34(b) The flows for calculating the trajectories in the acceleration tube units, the field free drift spaces, and the bending magnets. The attributes and parameters designated in the double frames indicate the data from the data files in the disk.

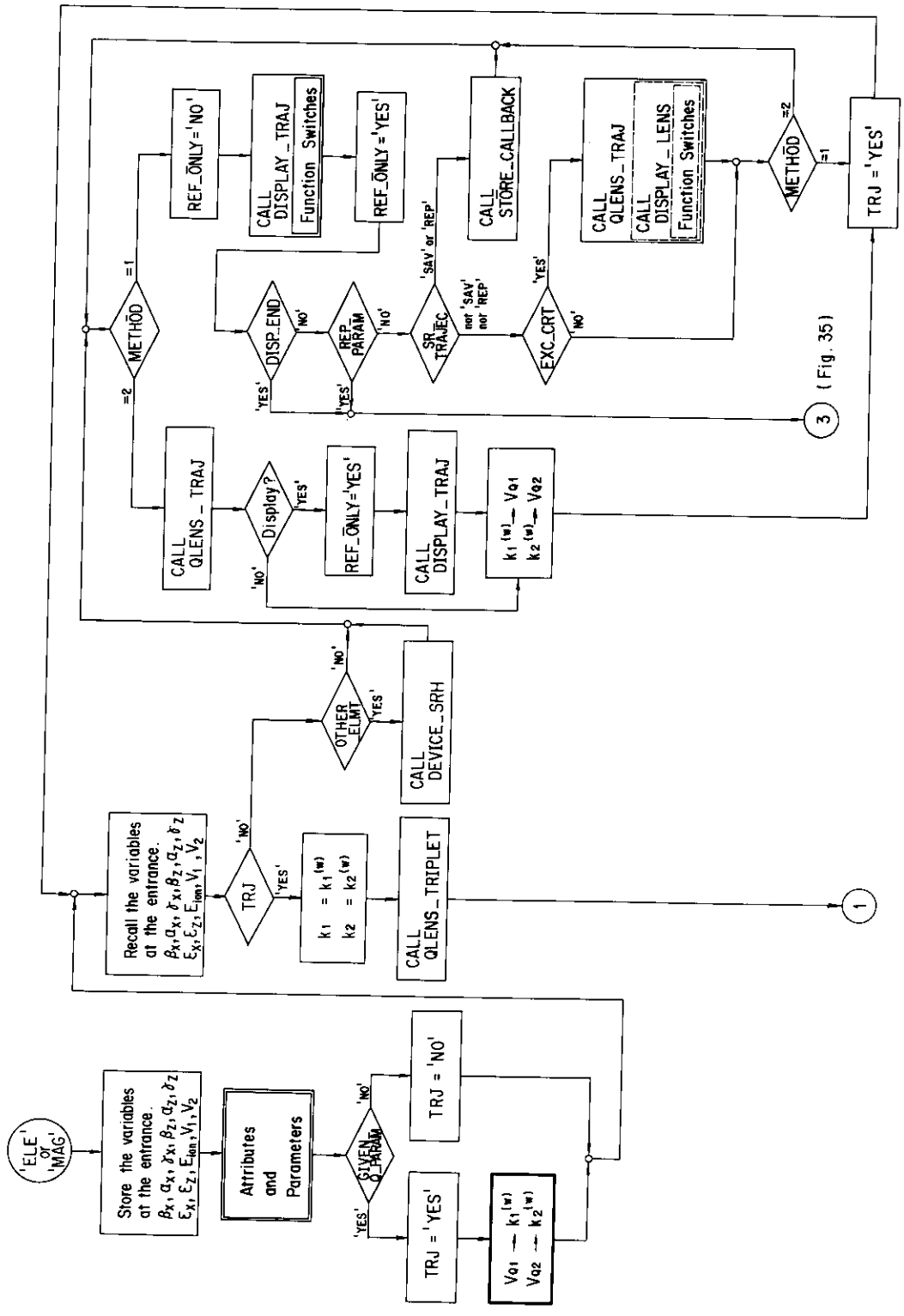

(c)

Fig. 34(c) The flow for calculating the trajectories in the electrostatic or magnetic Q-lenses. The attributes and parameters designated in the double frames indicate the data from the data files in the disk.

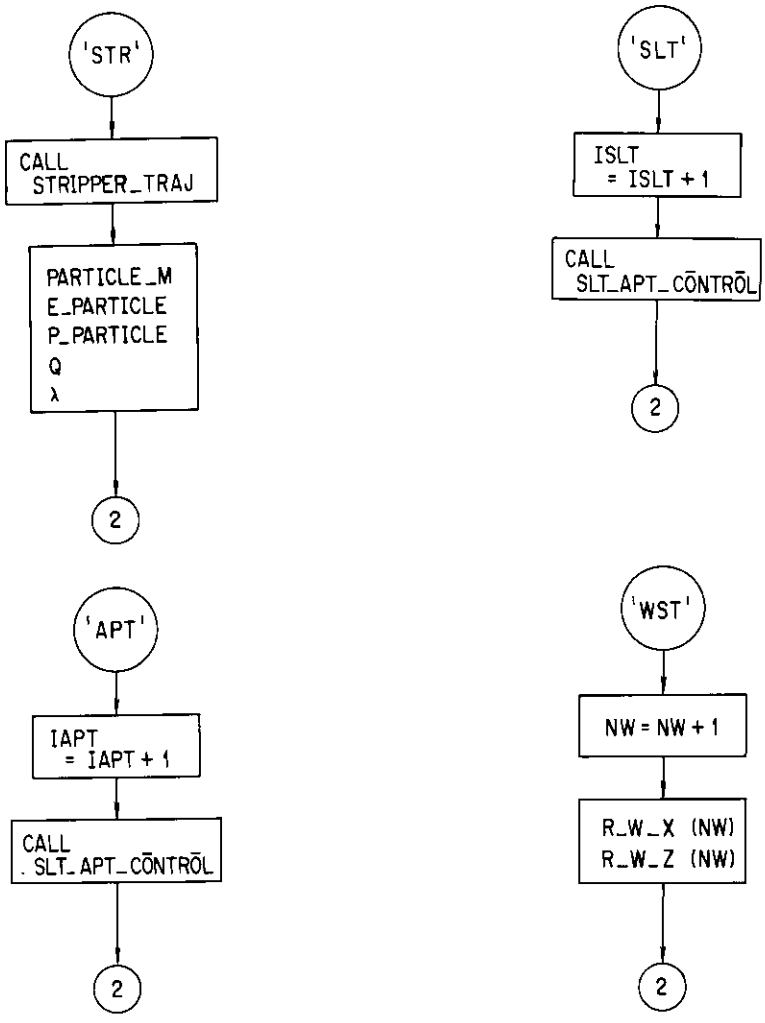

(d)

Fig. 34(d) The flows for calculating the trajectories in the stripper systems, the double slit systems, and the variable aperture systems. The waist is regarded here as a 'device' WST for convenience.

V_{Q1} and V_{Q2} : The electric potential on the poles for 'ELE' or the number of ampere-turns per pole for 'MAG' of each quadrupole element. The subscripts Q1 and Q2 denote the first and second elements, respectively. The values that should be denoted by Q3 is equal to that of the first.

DISP_END, REP_PARAM and SR_TRAJEC : These notations are explained in section 8.2.5.

PARTICLE_M : The mass of the ion.

E_PARTICLE : The energy of the ion.

P_PARTICLE : The momentum of the ion.

λ : This parameter is the same as that in section 8.2.2 (IV). It is +1 for the positive ions and is −1 for the negative ions. It changes from −1 to +1, due to the charge exchange through the stripper.

Others are same as those in sections 8.2.4, 8.2.5 and 8.2.6. The attributes and parameters shown in the double frames are those which have been read from the data files.

8.5 Final results

The final stage of the execution is illustrated in **Fig. 35**. The complete beam trajectory continues to be displayed on the CRT through the subroutine DISPLAY_TRAJ, until the function switches command the execution to proceed to the subsequent step.

There are three branches as shown in **Fig. 35**. One is led by the notation SR_TRAJEC. When it is 'SAV', the trajectory displayed on the CRT is stored in the disk. When it is 'REP', the trajectory stored in the disk, if any, is replayed on the CRT. The execution to store or to replay the trajectory is performed through the subroutine STORE_CALLBACK.

The second is decided by the notation REP_PARAM. If it is 'YES', the calculation with the input data different from those used in the current calculation starts. The replacement of the input data is made by the subroutine REPLACE_PARAM.

The last is caused by the notation DISP_END. If it is 'YES', the execution finishes. In this branch, the file OUTPUT.DAT, in which the results of the calculation are to be listed, is prepared by the subroutine INPUT_OUTPUT. According to the number of the trajectories stored in the disk, N_SPCFIL, the flow branches further. If no trajectories are stored, the results of the trajectory currently displayed are written in the file. In case of some trajectories are stored, the trajectories whose results are desired to be listed should be designated through the terminal keyboard. Finally, the contents of OUTPUT.DAT is printed out by the line printer. An example is shown in section 8.6.

8.6 Examples of the calculation

The designation and data required to be given through the terminal keyboard are as follows.

(I) The choice of the calculation mode, that is, the calculation with the given (1) final ion energy or (2) terminal voltage.

(II) The choice of the submode, that is, the calculation (1) that is carried out with the Q-lens parameters given as the input data or (2) that searches for the optimum Q-lens parameters.

(III)-1. The negative ion mass in amu, namely, the mass of the ions between the ion source and the stripper.

2. The positive ion mass in amu, namely, the mass of the ions after the stripper. This should be the mass of the atomic element to be required at the target as the projectile.
3. The atomic number of the element.
4. The final ion energy in MeV or the terminal voltage in MV, according to the calculation mode.
5. The beam line in the target room.
6. The initial ion energy in keV at the injecter.
7. The pre-acceleration voltage in kV after the injector.
8. Selection of the stripper, foil or gas.
9. Short-circuited column modules, if any.
10. The unnecessary devices, if any.
11. Selection of the charge state of ion.

For all of the examples shown below, the initial values for the beam sizes and the emittances are assumed to be

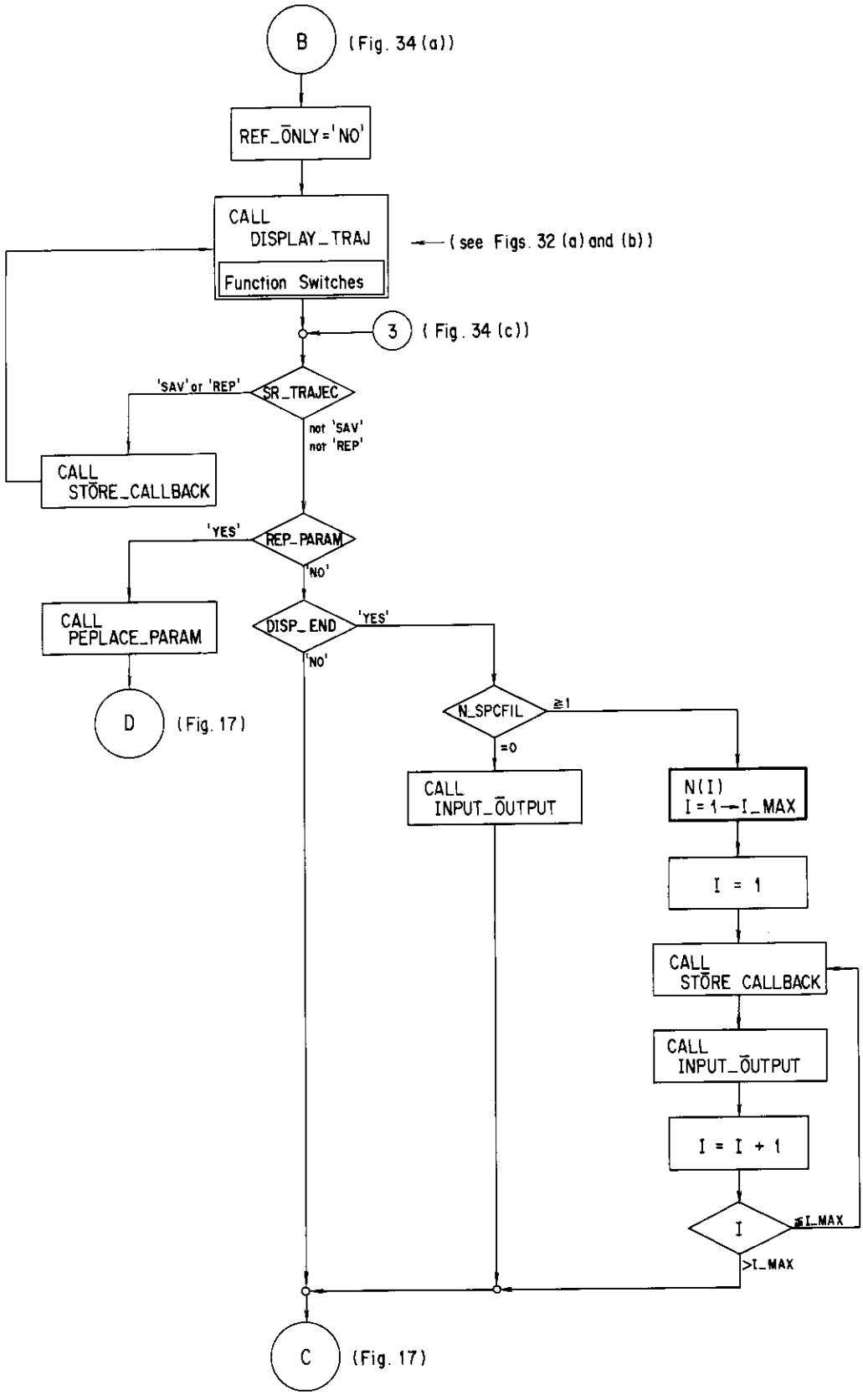

Fig. 35 Computational flow at the last step of the execution. Operation designated by the bold frame indicates the input through the terminal keyboard. This flow should be inserted in the step 10° in Fig. 17.

$$r_x = 6.5 \text{ mm}, \quad r'_x = 6.0 \text{ mrad}, \quad \varepsilon_x = 30 \text{ mm-mrad}$$
$$r_z = 5.0 \text{ mm}, \quad r'_z = 6.0 \text{ mrad}, \quad \varepsilon_z = 30 \text{ mm-mrad} \qquad (8.6.1)$$

with the ion energy of 25 keV, just behind the bending magnet BM-I1-1 on the injector (see **Fig. 16**). The related beam ellipse parameters are taken to be

$$\beta_x = 1.408, \quad \alpha_x = 0.8304 \quad r_x = 1.200$$
$$\beta_z = 0.8333, \quad \alpha_z = 0.0 \quad r_z = 1.200. \qquad (8.6.2)$$

Those for the $z-s$ plane show a waist at this location, but for the $x-s$ plane do not.

Example 1.

This example is to obtain the parameters for the acceleration of ^{10}B ions with the energy of 40 MeV at the target.

Fig. 36 shows the data input process from the terminal keyboard. The characters and numerals underlined are the input data. The negative ions are of the form of boron oxide, BO. Since the terminal voltage is relatively low, the eighth through fifteenth column modules are short-circuited, so as to increase the field gradient in the remaining acceleration tube units. The designation concerning the ion sources is that only for the calculation of the field strength of BM-I1-1 on the injector (see **Fig. 16**).

The resultant trajectory displayed on the CRT is shown in **Fig. 37**, and the optimum parameters obtained are listed and printed out as **Table 4**. The table contains the input data, based on which the calculation has been performed, and the output data obtained as the results. For the input data, the initial beam parameters of rx_max, drx_max and ex indicate the initial values of r_{max}, r'_{max} and ε for the $x-s$ plane, and rz_max, drz_max and ez for those of the $z-s$ plane. The numerals for short-circuited column modules show the individuals of those modules. A number i denotes the i th module from the lowest.

For the output, the double slit gaps, Gap_X and Gap_Z, are represented by the full width in mm in the x and z directions, respectively. Each value for the variable aperture radius, Apt_rad, indicates that the suitable aperture, whose radius is larger than that value, should be used. (For the aperture sizes, refer to section 8.3.2). For the Q-lenses, the potentials on the pole or the numbers of ampere-turns per pole of individual elements are deduced for the electrostatic or the magnetic Q-lenses, respectively, by using Eq.(3.2.3) or Eq.(3.2.4) with the optimum parameters k_1 and k_2 used for the beam transport. The field strengths for the bending magnets are calculated by taking the relativistic corrections into account.

Example 2.

This example is for the acceleration of ^{127}I ions with the final energy of 120 MeV. The resultant trajectory is shown in **Fig. 38**.

Example 3.

The calculation of the trajectory of ^{58}Ni ions, made through the mode 2 and the submode 1, i.e., giving the terminal voltage, 16 MV, and the Q-lens parameters as the input data. The way of giving the data is shown in **Fig. 39**.

```
$ RUN BEAM
      Do you display trajectory ?      [Y/N]   :  Y
      Given final energy ?             [Y/N]   :  Y
      Given Q_lens parameters ?        [Y/N]   :  N
      Which method ?                   [1/2]   :  2

      Which ion-source do you use ?
            Enter  1. for Heinicke Penning,
                   2. for Duoplasmatron,
                   3. for Lithium Exchange or
                   4. for Sputter Cone.       :  4

 1.   Enter negative_particle_mass (amu).     :  26
 2.   Enter positive_particle_mass (amu).     :  10
 3.   Enter atomic number of the particle.    :  5
 4.   Enter final particle energy (in MEV).   :  40
 5.   Which beam line ?
          L1,L2,L3,L4,H1,H2,H3,H4,H5,
                        R1,R2,N1, or N2       :  L4
 6.   Enter initial energy (in KEV).          :  25
 7.   Enter pre-acceleration voltage (in KV).:  200
 8.   Foil stripper or Gas stripper ?  [F/G] :  F
        Enter foil thickness (micro-gr/cm**2):  10
 9.   Any short-circuited units ?  [Y/N]     :  Y
                  Enter shorting unit number:
        8,9,10,11,12,13,14,15
10.   Any devices unnecessary ?          [Y/N] :  Y
                  How many devices ?            :  1
                  Enter device name.            :  EQ-TH-2


      Any correction for these input ? [Y/N] :  N


 CHARGE STATE INFORMATION (for Foil stripper)
 --------------------------------------------

                          Charge state        Fraction
 ------------------------------------------------------------
                              2               0.0236
                              3               0.4314
   Most probable =====>       4               0.5065
                              5               0.0383
                              6               0.0002

 Which charge state do you choose ?    4

 Now calculation begins.
```

Fig. 36 An example of the data input process from the terminal keyboard. Characters and numerals underlined are the input data. The calculation for the acceleration of ^{10}B ions with the final energy of 40 MeV are to be made.

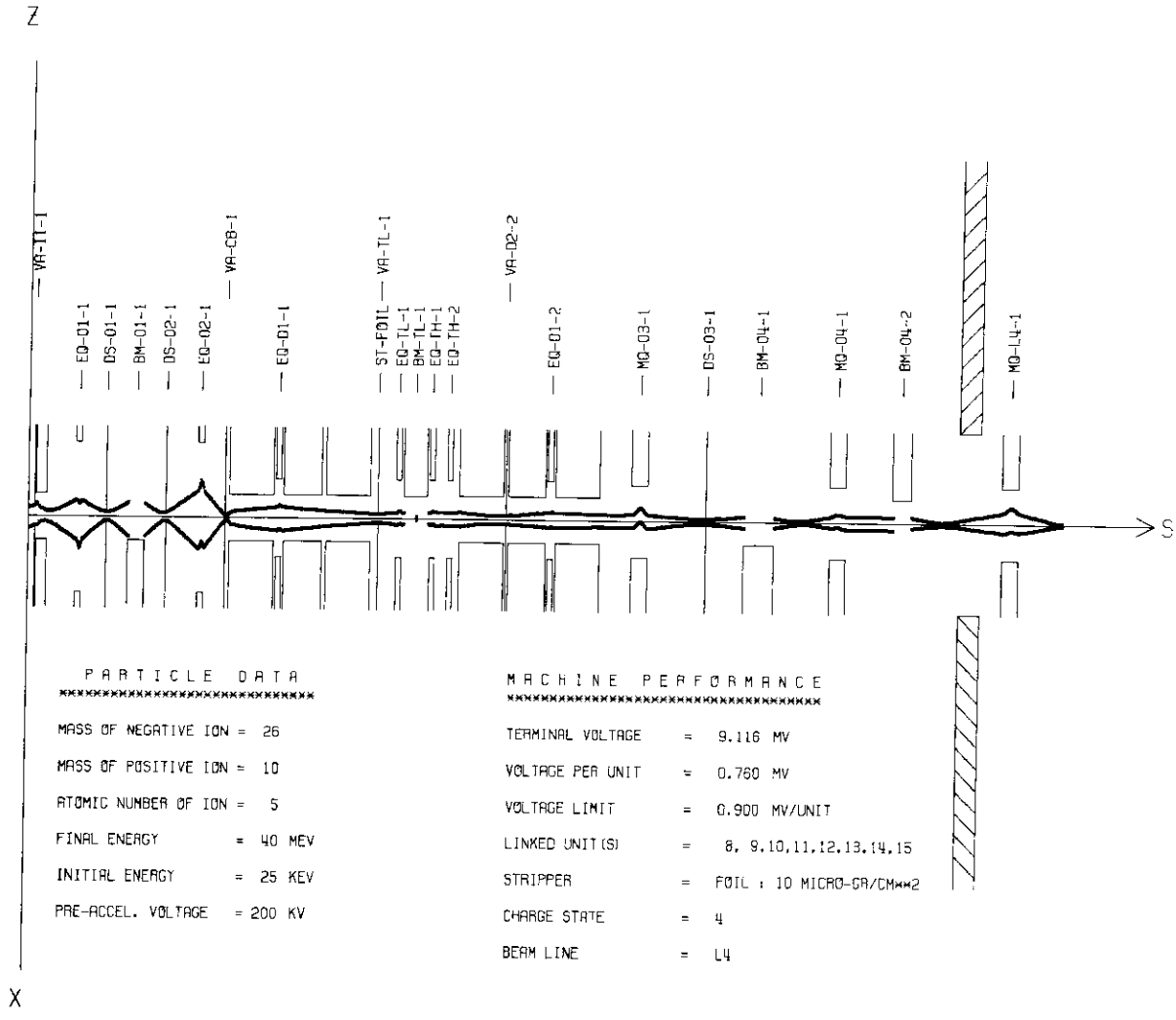

Fig. 37 The resultant trajectory obtained through the calculation designated by the input data shown in Fig. 36.

Table 4 Input and output parameters, used in and obtained by the calculation of Example 1. Output of the line printer.

```
****************************** INPUT ******************************

 Negative particle-mass (in amu)        =   26
 Positive particle-mass (in amu)        =   10
 Atomic number of the particle          =    5
 Final particle energy                  =   40.0 MEV
 Ion source                             :   Sputter Cone
 Stripper                               :   Foil
                                            10.0 micro-gr/cm**2
 Charge state selected                  =   4
 Beam line                              :   L4
 Initial beam: rx_max, rz_max           =    6.5,  5.0 mm
               drx_max, drz_max         =    6.0,  6.0 mrad
               ex, ez                   =   30.0, 30.0 mm-mrad
 Initial energy                         =   25.0 KEV
 Pre-acceleration voltage               =  200.0  KV
 Voltage limit / column module          =    0.90 MV
 Short-circuited column modules         :  8, 9,10,11,12,13,14,15

***************************** CUTPUT ******************************

 Terminal Voltage                       =   9.116 MV
 Voltage per column module              =   0.760 MV
 Energy loss  (due to the stripper)     =   56.8 KeV

 DS-01-1                  Gap-X         =    4.00 mm
                          Gap-Z         =    6.00 mm
 DS-02-1                  Gap-X         =    4.00 mm
                          Gap-Z         =    6.00 mm
 DS-03-1                  Gap-X         =    3.00 mm
                          Gap-Z         =    4.00 mm
 VA-I1-1                  Apt-rad       =    6.50 mm
 VA-CB-1                  Apt-rad       =    1.50 mm
 VA-TL-1                  Apt-rad       =    3.00 mm
 VA-D2-2                  Apt-rad       =    3.00 mm
 EQ-01-1                  Element 1,3   =    5.56 KV
                             "     2    =    5.69 KV
 EQ-02-1                  Element 1,3   =    5.74 KV
                             "     2    =    5.85 KV
 EQ-D1-1                  Element 1,3   =   23.78 KV
                             "     2    =   26.35 KV
 EQ-TL-1                  Element 1,3   =    6.88 KV
                             "     2    =    7.21 KV
 EQ-TH-1                  Element 1,3   =    5.53 KV
                             "     2    =    5.92 KV
 EQ-TH-2                  Element 1,3   =    0.00 KV
                             "     2    =    0.00 KV
 EQ-D1-2                  Element 1,3   =   15.28 KV
                             "     2    =   17.03 KV
 MQ-03-1                  Element 1,3   =  754.1 A-T
                             "     2    =  457.7 A-T
 MQ-04-1                  Element 1,3   =  251.3 A-T
                             "     2    =  238.6 A-T
 MQ-L4-1                  Element 1,3   =  293.8 A-T
                             "     2    =  273.6 A-T
 BM-01-1                Field strength  =  3.5436 KG
 BM-TL-1                Field strength  =  3.0096 KG
 BM-04-1                Field strength  =  4.0033 KG
 BM-04-2                Field strength  =  4.0347 KG
```

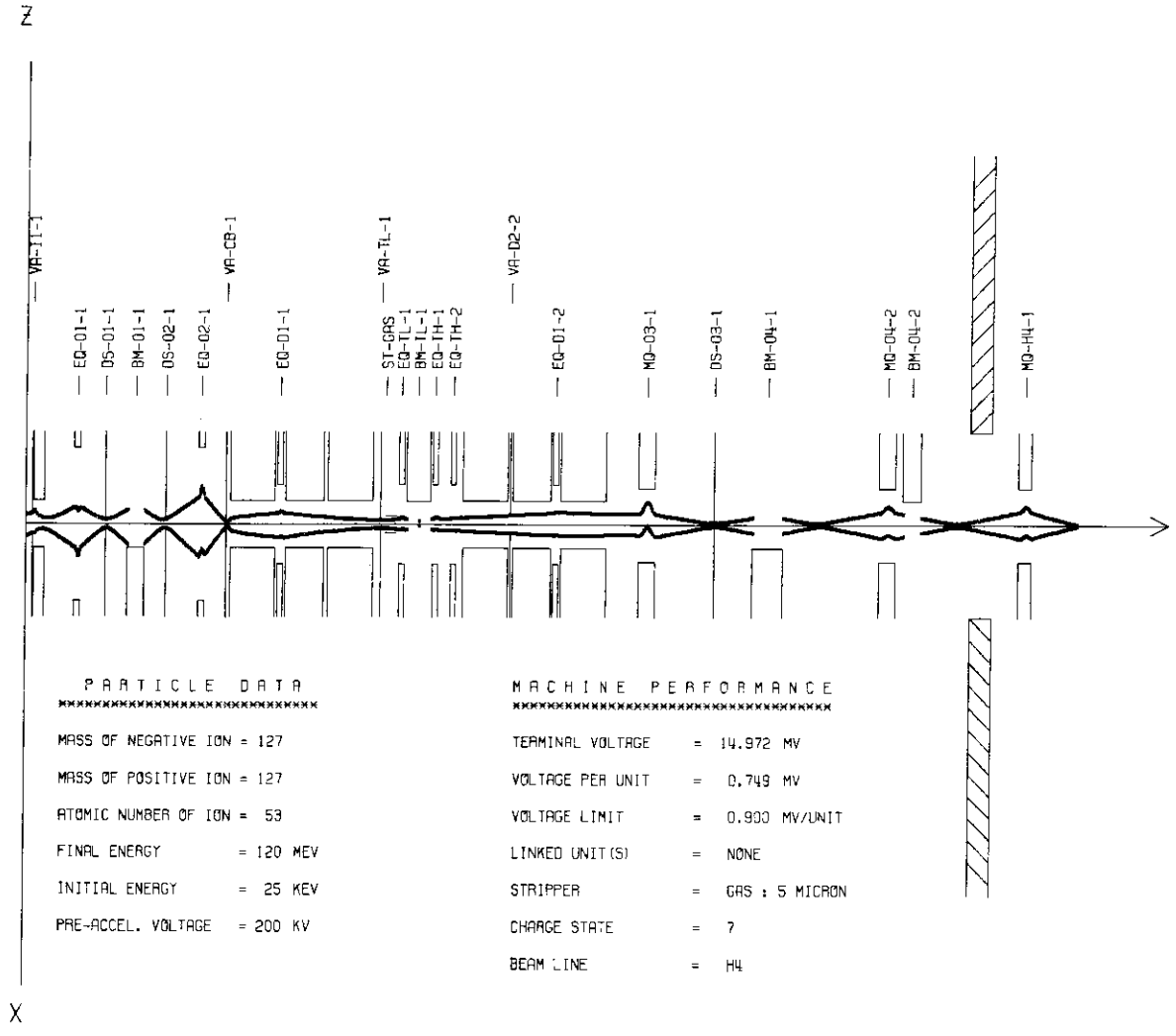

Fig. 38 The resultant trajectory of ^{127}I ions with the final energy of 120 MeV.

```
$ RUN BEAM
      Do you display trajectory ?      [Y/N]    :  Y
      Given final energy ?             [Y/N]    :  N
      Given Terminal Voltage ?         [Y/N]    :  Y
      Given Q_lens parameters ?        [Y/N]    :  Y

      Which ion-source do you use ?
            Enter  1. for Heinicke Penning,
                   2. for Duoplasmatron,
                   3. for Lithium Exchange or
                   4. for Sputter Cone.        :  4

 1.   Enter negative_particle_mass (amu).      :  58
 2.   Enter positive_particle_mass (amu).      :  58
 3.   Enter atomic number of the particle.     :  28
 4.   Enter terminal voltage (MV)              :  16
 5.   Which beam line ?
          L1,L2,L3,L4,H1,H2,H3,H4,H5,
                        R1,R2,N1, or N2        :  H2
 6.   Enter initial energy (in KEV).           :  25
 7.   Enter pre-acceleration voltage (in KV).: 200
 8.   Foil stripper or Gas stripper ?  [F/G] :  G
                  Enter gas pressure (micron): 5
 9.   Any short-circuited units ?  [Y/N]     :  N
10.   Any devices unnecessary ?          [Y/N] :  Y
                  How many devices ?          :  1
                  Enter device name.          :  EQ-TH-2

      Any correction for these input ? [Y/N] :  N

      CHARGE STATE INFORMATION (for Gas  stripper)
      --------------------------------------------

                          Charge state        Fraction
      ------------------------------------------------------------
                              4               0.0309
                              5               0.1052
                              6               0.2189
        Most probable =====>  7               0.2792
                              8               0.2182
                              9               0.1045
                             10               0.0307

      Which charge state do you choose ?   8

      Now calculation begins.

       EQ-01-1          V1 and V3 (in KV) = 5.56
                        V2 (in KV)        = 5.69
       EQ-02-1          V1 and V3 (in KV) = 5.74
                        V2 (in KV)        = 5.85
       EQ-D1-1          V1 and V3 (in KV) = 23.42
                        V2 (in KV)        = 25.97
       EQ-TL-1          V1 and V3 (in KV) = 14.60
                        V2 (in KV)        = 15.30
       EQ-TH-1          V1 and V3 (in KV) = 13.24
                        V2 (in KV)        = 14.02
       EQ-D1-2          V1 and V3 (in KV) = 31.61
                        V2 (in KV)        = 35.43
       MQ-03-1          (I-N)1 and (I-N)3 (in  Amp-turn) = 1719.9
                        (I-N)2            (in  Amp-turn) = 1044.8
       MQ-04-2          (I-N)1 and (I-N)3 (in  Amp-turn) = 609.6
                        (I-N)2            (in  Amp-turn) = 572.9
       MQ-H2-1          (I-N)1 and (I-N)3 (in  Amp-turn) = 877.7
                        (I-N)2            (in  Amp-turn) = 894.5

      Now, trajectory calculation completed.
```

Fig. 39 An example of the data input process where the terminal voltage and the Q-lens parameters are given as the input data.

9. Conclusion

The execution of the present code not only gives the parameters of the optical devices for the optimum beam transport, but also shows the aspect of the beam envelope trajectory along the beam line visually.

The latter function is useful for the accelerator operation to realize the situation of the beam focusing, especially that in the acceleration tube units. The appearance of the beam dispersion due to the stripper, or the weak beam focusing due to the weak field gradient in case of the low energy acceleration, can be recognized at a glance through such visual information. In virtue of this recognition, the selection of the stripper, foil or gas, to avoid the large beam dispersion, or the decision of the configuration of the tube units, namely, the choice of the column modules that should be short-circuited to strengthen the field gradient, can be made easily.

This code is available to electrostatic accelerators other than JAERI's, if their data files are provided. Furthermore, it can be utilized for constructing a new accelerator facility to decide the optimum setup of the beam transport system composed of many optical devices.

References

1) Steffen K.G. : "High Energy Beam Optics", Interscience Publishers, New York, 1965.
2) Lichtenberg A.J. : "Phase-Space Dynamics of Particles", John Wiley and Sons, Inc., New York, 1969.
3) Rose P.H. and Galejs A. :"Progress in Nuclear Techniques and Instrumentation", Vol.2, ed. by Forley F.J.M., North-Holland Publishing Company, Amsterdam, 1967.
4) Wilson R.G. and Brewer G.R. : "Ion Beams with Application to Ion Implantation", Robert E. Krieger Publishing Company, Huntington, New York, 1979.
5) Zworykin V.K., Morton G.A., Ramberg E.G., Hillier J. and Vance A.W. : "Electron Optics and the Electron Microscope", John Wiley and Sons, Inc., New York, 1945.
6) Fert C. : J. Phys. Radium, 13, 83A (1952).
7) Timm U. : Z. Naturforsch. 10a, 593 (1955).
8) Klemperer O. and Bernet M.E. : "Electron Optics", Cambridge University Press, Cambridge, 1955.
9) Pierce J.R. : "Theory and Design of Electron Beams", D. Van Nostrand Company, Inc., New York, 1949.
10) Elkind M.M. : Rev. Sci. Instrum. 24, 129 (1953).
11) Stenning P.J. and Trowbridge C.W. : Reading University/Rutherford Laboratory Report RU/RL-1 1968.
12) Sturrock P.A. : "Static and Dynamic Electron Optics", Cambridge University Press, Cambridge, 1955.
13) Betz H.D. :Rev. Mod. Phys. 44, 465 (1972).
14) Nikolaev V.S. and Dmitriev I.S. : Phys. Lett. 28A, 277 (1968).
15) Dmitriev I.S. and Nikolaev V.S. : Sov. Phtys.-JETP, 20, 409 (1965).
16) Ziegler J.F. : "Stopping Cross-Sections for Energetic Ions in All Elements", Vol.5, Pergamon Press, New York, 1980.
17) Joy T. : Nucl. Instrum. Methods, 106, 237 (1973).
18) Hamilton W.C. : "Statistics in Physical Science", The Ronald Press Co., New York, 1964.
19) Fermi E. : "Nuclear Physics", The University of Chicago Press, Chicago, 1953, p.53.
20) Takeuchi S., Minehara E. and Kikuchi S. : JAERI-memo 7285 (1977) (in Japanese).
21) Kikuchi S. : Private communication.

4. ま と め

現在，日本で使用されているNaI(Tℓ)シンチレーション検出器の大部分はJIS規格に従った検出器であり，ここに表したデータは，NaI(Tℓ)シンチレーション検出器を用いてガンマ線測定を行おうとする者たちに有用な情報である．また，NaI(Tℓ)シンチレーション検出器に関するJIS規格Z−4321は，国際電気標準会議（IEC；International Electrotechnical Commission）の規格412を参考に作成されていることを考慮すれば，諸外国で使用されている検出器にたいしても，この応答関数は充分適用できるものであり，今後，広く参照されることが期待される．

謝 辞

本論文の構成に関して有益な助言を頂いた環境安全研究部前部長岩本多實氏（現東海研究所副所長）ならびに環境第2研究室室長笠井篤氏に深く感謝いたします．

参 考 文 献

1) K. Saito and S. Moriuchi, Nucl. Instr. Meth. 185, 299 (1981).
2) K. Saito and S. Moriuchi, JAERI-M 9741 (1981).
3) K. Saito and S. Moriuchi, Nucl. Instr. Meth. 226, 449 (1984).
4) T. Miura, K. Takeuchi and M. Kinno, Proceeding of the Sixth International Conference on Radiation Shielding, p.787, Tokyo (1983).
5) T. Miura, Nucl. Instr. Meth. 221, 603 (1984).
6) R.L. Heath, AEC Report IDO-16880-1 (1964).
7) R.M. Green and R.J. Finn, Nucl. Instr. Meth. 34, 72 (1965).
8) K.L. Coop and H.A. Grench, Nucl. Instr. Meth. 36, 339 (1965).
9) H. Leutz and G. Schultz, Nucl. Instr. Meth. 40, 257 (1966).
10) B. Chinaglia and R. Malvano, Nucl. Instr. Meth. 45, 125 (1966).
11) U.C. Mishra and S. Sadasivan Nucl. Instr. Meth. 69, 330 (1969).
12) W.F. Miller and W.J. Snow, Rev. Sci. Instr. 31, 39 (1960).
13) C.D. Zerby and H.S. Moran, Nucl. Instr. Meth. 14, 115 (1961); ORNL-3169 (1962).
14) C. Weitkamp, Nucl. Instr. Meth. 23, 13 (1963).
15) B.J. Snyder and G.F. Knoll, Nucl. Instr. Meth. 40, 261 (1966).
16) M. Giannini, P.R. Oliva and M.C. Ramorino, RT/FI (69) 15 (1969); Nucl. Instr. Meth. 81, 104 (1970).
17) E. Nardi. Nucl. Instr. Meth. 83, 331 (1970).
18) M.J. Berger and S.M. Seltzer, Nucl. Instr. and Meth. 104, 317 (1972).
19) J.J. Steyn and R. Huang, Nucl. Instr. Meth. 107, 465 (1973).
20) M. Belluscio, R. De Leo, A. Pantaleo and A. Vox, Nucl. Instr. Meth. 118, 553 (1974).
21) B. Grosswendt and E. Waibel, Nucl. Instr. Meth. 133, 25 (1976).
22) E. Storm and H.I. Israel, LA-3753 (1967).
23) J.H. Hubbell, Int. J. Appl. Radiat. Isot. 33, 1269 (1982).
24) J.H. Hubbell, NBS Publ. NSRDS-NBS-29 (1969).
25) E. Storm and H.I. Israel, Nucl. Data Tables A7, 565 (1970).
26) W.W. Managan, in Applied Gamma-ray Spectrometry, Pergmon Press, New York (1960).
27) D. Engelkemeir, Rev. Sci. Instr. 27, 589 (1956).
28) C.D. Zerby, A. Meyer and R.B. Murray, Nucl. Instr. Meth. 12, 115 (1961).
29) A. Bisi and L. Zappa, Nucl. Instr. 3, 17 (1958).